Mississippi State University
Scholars Junction

Theses and Dissertations | Theses and Dissertations

1-1-2014

# Stochastic and Robust Optimal Operation of Energy-Efficient Building with Combined Heat and Power Systems

Ping Liu

Follow this and additional works at: https://scholarsjunction.msstate.edu/td

Recommended Citation
Liu, Ping, "Stochastic and Robust Optimal Operation of Energy-Efficient Building with Combined Heat and Power Systems" (2014). *Theses and Dissertations*. 4062.
https://scholarsjunction.msstate.edu/td/4062

This Dissertation - Open Access is brought to you for free and open access by the Theses and Dissertations at Scholars Junction. It has been accepted for inclusion in Theses and Dissertations by an authorized administrator of Scholars Junction. For more information, please contact scholcomm@msstate.libanswers.com.

www.manaraa.com

# Stochastic and robust optimal operation of energy-efficient building with combined heat and power systems

By

Ping Liu

A Dissertation
Submitted to the Faculty of
Mississippi State University
in Partial Fulfillment of the Requirements
for the Degree of Doctor of Philosophy
in Electrical Engineering
in the Department of Electrical and Computer Engineering

Mississippi State, Mississippi

December 2014

www.manaraa.com

Copyright by

Ping Liu

2014

www.manaraa.com

Stochastic and robust optimal operation of energy-efficient building

with combined heat and power systems

By

Ping Liu

Approved:

_____

Yong Fu
(Major Professor)

_____

Stanislaw Grzybowski
(Committee Member)

_____

Pan Li
(Committee Member)

_____

Mengqi Hu
(Committee Member)

_____

James E. Fowler
(Graduate Coordinator)

_____

Jason M. Keith
Interim Dean
Bagley College of Engineering

www.manaraa.com

Name: Ping Liu

Date of Degree:December 13, 2014

Institution: Mississippi State University

Major Field: Electrical Engineering

Major Professor: Dr. Yong Fu

Title of Study: Stochastic and robust optimal operation of energy-efficient building with combined heat and power systems

Pages in Study:147

Candidate for Degree of Doctor of Philosophy

Energy efficiency and renewable energy become more attractive in smart grid. In order to efficiently reduce global energy usage in building energy systems and to improve local environmental sustainability, it is essential to optimize the operation and the performance of combined heat and power (CHP) systems. In addition, intermittent renewable energy and imprecisely predicted customer loads have introduced great challenges in energy-efficient buildings' optimal operation.

In the deterministic optimal operation, we study the modeling of components in building energy systems, including the power grid interface, CHP and boiler units, energy storage devices, and appliances. The mixed energy resources are applied to collaboratively supply both electric and thermal loads. The results show that CHP can effectively improve overall energy efficiency by coordinating electric and thermal power supplies. Through the optimal operation of all power sources, the daily operation cost of building energy system for generating energy can be significantly reduced.

In order to address the risk due to energy consumption and renewable energy production volatility, we conduct studies on both stochastic programming and robust

www.manaraa.com

optimizations to operate energy-efficient building systems under uncertainty. The multi-stage stochastic programming model is introduced so that the reliable operation of building energy systems would be probabilistically guaranteed with stochastic decisions. The simulation results show that the stochastic operation of building systems is a promising strategy to account for the impact of uncertainties on power dispatch decisions of energy-efficient buildings.

In order to provide absolute guarantee for the reliable operation of building energy systems, a robust energy supply to electric and thermal loads is studied by exploring the influence of energy storage on energy supply and accounting for uncertainties in the energy-efficient building. The robustness can be adjusted to control the conservativeness of the proposed robust operation model.

For the purpose of achieving adaptability in the robust optimal operation and attaining robustness in the stochastic optimal operation of building energy systems, we also develop an innovative robust stochastic optimization (RSO) model. The proposed RSO model not only overcomes the conservativeness in the robust operation model, but also circumvents the curse of dimensionality in the stochastic operation model.

www.manaraa.com

DEDICATION

To my dear parents

Shaode Liu and Shue Chen

And my young brothers

Hai Liu and Wang Liu

And my lovely son

Daniel Xu



www.manaraa.com

ACKNOWLEDGEMENTS

It is a great opportunity for me to express my thanks to those who helped me with various aspects of conducting research and the writing of this dissertation. Firstly, I would like to take this opportunity to give my sincere thanks to my advisor Dr. Yong Fu, for drawing my attention to the complex optimization problem of electric power systems during the period from January 2011 to December 2014 of my PhD study.

I would like also to thank Dr. Stanislaw Grzybowski, Dr. Pan Li, and Dr. Mengqi Hu, to be my dissertation committee members.

This dissertation is impossible without the love from my parents and brothers. My gratitude to them is beyond what I can express in words. In addition, I want to thank my husband for his love and support. Last but not least, I would like to thank my friends, who have always been there for me, and who have made my experience at MSU an unforgettable one.



www.manaraa.com

TABLE OF CONTENTS





www.manaraa.com

www.manaraa.com

www.manaraa.com

LIST OF TABLES





www.manaraa.com

LIST OF FIGURES





www.manaraa.com

www.manaraa.com

www.manaraa.com

www.manaraa.com

www.manaraa.com

CHAPTER I

INTRODUCTION

## 1.1 Background

In recent years, the energy industry has experienced the transformation from traditional electric grid to smart grid. The advanced electric technologies in smart grid play a significant role in improving the efficiency of power generation and transformation [1]. In the renewable energy industry, distributed generation (DG) is applied at the individual consumer level as one of environment friendly energy resources.

In smart grid, buildings are powered by a hybrid energy supply system integrated with on-site electricity generation from solar, combined heat and power system (CHP). Figure 1.1 shows the various energy resources of an energy-efficient building system in smart grid.



www.manaraa.com

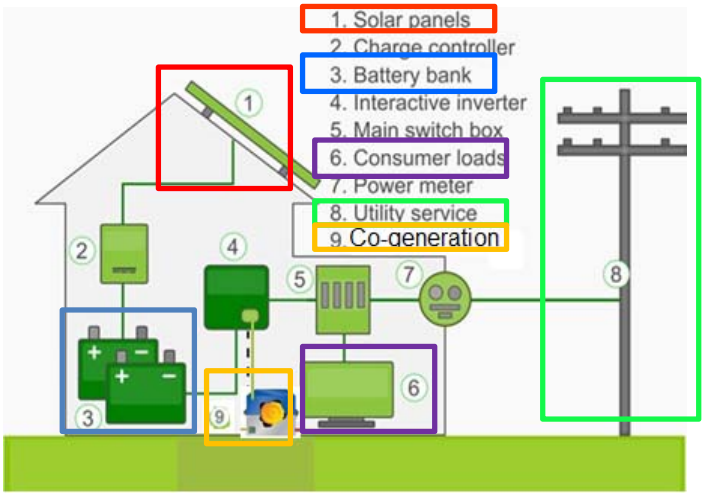


Figure 1.1 Smart building energy systems [2]

Solar energy is so far the most popular renewable energy technology at the individual customer level. While keeping home comforts without having to pay the increased fees for these comforts, customers only pay for the amount of energy that the photovoltaic (PV) system is unable to supply. Solar power is successfully and widely used in buildings around the world. The reason that PV is popular in Europe is partially because of the creative and practical use of PV by integrating it into a building, namely Building Integrated Photovoltaics (BIPV) [3]. Plugging renewable energy into home buildings is a smart strategy to save energy usage. Solar increases the energy efficiency in buildings by reducing the energy consumption at home. BIPV will potentially become one of the main uses of PV next to utility scale power generation because it can be dynamically used in almost any building design.

Energy efficiency technologies have been promising in improving the energy consumption performance of buildings. CHP, known as self-production facility or



www.manaraa.com

cogeneration unit, generate power and thermal energy at the same time. It is an approach for conventional power generation systems to recover the heat remaining in exhaust gases, cooling system. CHP systems are useful to overcome the drawback of intermittent power supply from renewable energy and unpredictable energy consumption, and have proven to be beneficial for energy performance of utility grid in many industrial situations through increasing the total thermal efficiency, reducing the overall power demand, and providing higher quality as well as more reliable power [4]. Therefore, applying CHP technology to utility grid is an attractive option [5]-[9].

## 1.2 Objectives and approaches

With the integration of renewable energy resources, smart grid has introduced great challenges in building energy systems. Despite the significant capital cost reductions for renewables, the volatile power generation of the solar PV system is the most critiqued of solar technologies [10]. The existing balance between energy production and consumption is significantly affected by these new sources [11]. These uncertainties may result in increased risk in energy supply for power systems. The system operators should consider the uncertainties from power produced by renewable energy sources in building energy systems.

Building energy consumption is not only impacted by intermittent solar power generation but also by the fluctuating energy consumption [12]. Accurate load forecasting technique is essential to achieve efficient load management in buildings. Trustworthy power demand forecasting method (energy demand forecast) must be provided to achieve reliable power generation. However, the forecastability of demand is largely dependent on the demand volatility. The actual demand of individual buildings varies over time,



www.manaraa.com

depending on the outside temperature seasons and end-user behavior. Load forecasting technique, which has been studied for decades [13], is still a big concern for the operation of buildings because of the inaccurate prediction of non-controllable electric and thermal loads.

In summation, these uncertain factors from the integration of renewable energy and random energy consumption are the major sources of disturbance for the optimal operation of building systems, including non-controllable electric and thermal loads, as well as solar power generation. In order to minimize energy import/export expenses under uncertainty, it is necessary to determine the power production for the utility grid from various energy sources including electric grid, battery, and CHP with boiler unit.

Energy-efficient building systems with the integration of renewable generation are becoming more and more popular worldwide. In order to address the risk due to energy consumption and renewable energy production volatility, the optimal operation problem of building systems integrated with CHP units will be modeled through both stochastic programming and robust optimization. The models incorporated the uncertain characteristics of solar energy as well as electric and thermal demand to predict CHP systems operation and performance.

Firstly, taking into account the randomness of future non-controllable electric and thermal load as well as solar power production through the multi-stage scenario tree, a multi-stage mixed-integer stochastic programming model for optimal operation of energy-efficient buildings is presented. The simulation results can offer a set of adaptive decision solutions within the scheduling horizon.



www.manaraa.com

To account for the effect of variable solar power and imprecise energy consumption, the case studies for stochastic operation of building energy systems are designed to

- Build a multi-stage stochastic model for the energy-efficient building system with CHP systems under uncertainties;
- Generate the multivariate stochastic scenario tree by backward reduction technology;
- Compare the load supply due to the impact of CHP systems;
- Investigate the operation and performance of CHP systems due to the impact of battery devices and controllable loads;
- Explore the impact of interruptible and non-interruptible loads on the optimal energy management of building energy systems.

Secondly, a robust energy supply to electric and thermal loads is studied by exploring the influence of energy storage on energy supply and accounting for uncertainties in the energy-efficient building. The tasks of robust operation of energy-efficient buildings are to

- Establish the robust optimization model for the operation problem of energy-efficient building system with CHP under uncertainties;
- Conduct robust case studies to investigate the effectiveness of the CHP unit and battery in alleviating the influence of uncertainties;
- Adjust the robustness parameter of the robust optimal operation model against the conservativeness of the robust solution on the energy supply.



www.manaraa.com

Thirdly, to improve the robustness of stochastic solutions and to reduce the computation burden at the same time, a robust stochastic optimization (RSO) technique differing from those two methods is needed.

This RSO model minimizes the expected operating cost of worst-case scenarios at each time stage. The tasks of robust stochastic operation of energy-efficiency buildings are to

- Formulate the robust stochastic optimization model by introducing penalty terms in constraints, which in turn reflects the cost volatility due to the uncertain solar power generations, electric and thermal loads;
- Establish the multiband uncertainty set through the multi-stage scenario tree so that the combination of all the individual uncertainty sub-bands can cover the complete uncertainty set;
- Compare the building energy solutions of the robust stochastic model with those obtained from both the stochastic and robust models.

## 1.3 Literature review of demand-side management

At the individual consumer side, demand side management (DSM) is to control energy consumption and reduce the cost of purchasing electrical energy for consumers [14]. It can be realized through a set of effective measures shown in Figure 1.2. For example, in the smart grid industry, Honeywell has been developed advanced electric devices to reduce the US's energy consumption at demand side (Figure 1.3).



www.manaraa.com

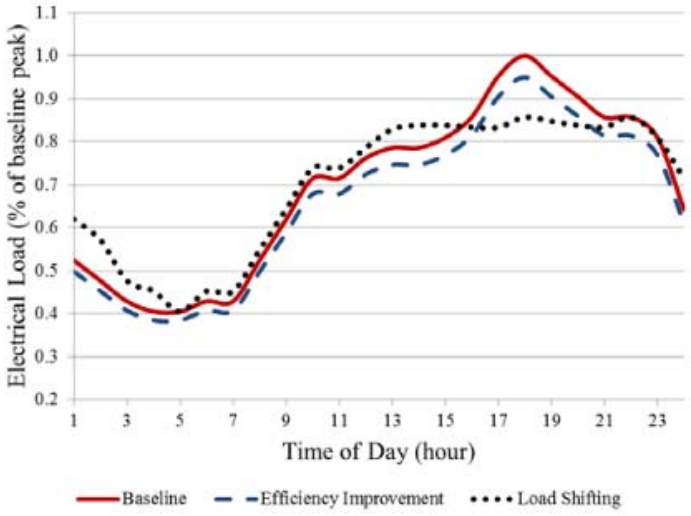


Figure 1.2 Demand side management for residential electrical loads profile [15]

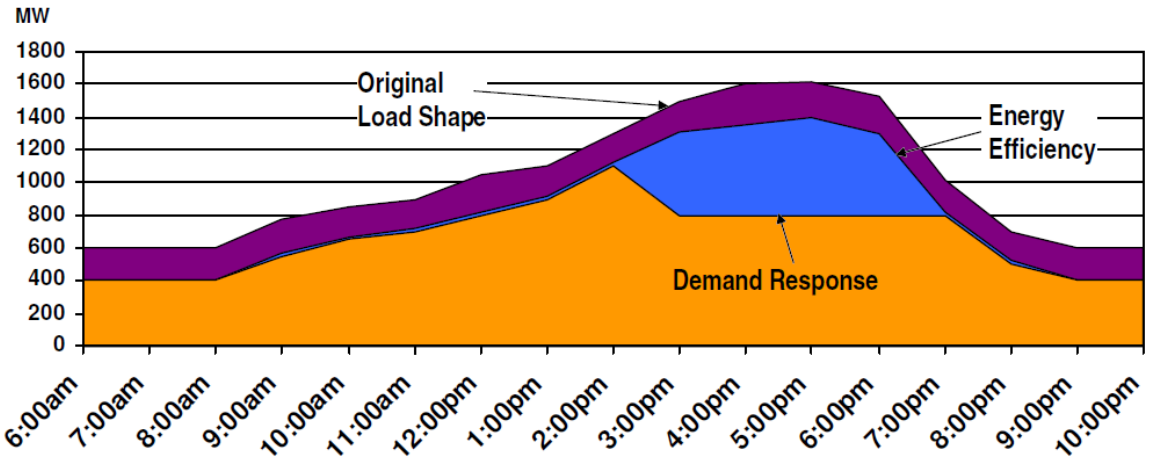


Figure 1.3 Honeywell's strategy in solving today's smart grid problem [16]

Based on the customers' priorities and the energy consumption profiles of individual building appliances, Z. Zhu etc. [1] proposed an optimization mechanism for the scheduling of power-shiftable and time-shiftable appliances at the demand side. The



www.manaraa.com

proposed approach was achieved through the minimization of the hourly peak load with integer linear programming algorithm.

T. T. Kim etc. [17] solved the scheduling power consumption problem at the consumer's side. The uncertain price of electricity was considered through a Markov decision process. The decisions were the optimal scheduling for both non-interruptible and interruptible loads. The real time data from Commonwealth Edison (ComEd) was demonstrated to show the effectiveness of the proposed method.

To maximize the utilization of energy from the electric grid and a distributed energy resource (DER), M. Rahimiyan etc. [18] proposed an energy management algorithm for a cluster of interconnected price-responsive demands. The robust optimization was presented to account for the uncertainty from the electricity price from the grid and the intermittent renewable power generation.

Hai-Yun Helen Xing [19] aimed to reduce building loads while maintaining an acceptable level of comfort through a variety of simulation and optimization methods in a multi-objective optimization problem. The load shedding method was introduced to increase thermostats in a single building, which can lead to about $10W/m^2$ peak load reduction. Thermostat-based and night-cooling-based load control strategies are optimized as well. To reduce the total peak demand or the total cost in a small pool of two or three buildings, the effectiveness of load aggregation was also investigated. At last, the multi-building optimization problem was solved with a model-based approach.

Z. Chen etc. [20] considered the real-time price uncertainty in the DSM at residential side. The price-based DR management is realized through smart meters. Both deferrable/non-deferrable and interruptible/non-interruptible appliances are considered in



www.manaraa.com

the stochastic and robust models. They concluded that both stochastic and robust models reduce electricity bill cost compared with the flat rate electricity price.

To schedule the Controllable Thermostatically Controlled Appliances (C-TCAs) loads in consumer level, Pengwei Du [21] presented a two-step appliance commitment algorithm. The proposed algorithm is adjustable to the optimal schedule taking into account thermal dynamics, random price, hot water consumption, and consumer comfort.

P. Samadi etc. [22] proposed an optimal residential load control algorithm for demand side management in presence of load uncertainty. The purpose is to minimize the electricity bill of the users with the estimate of the future demand. The study results show that users are encouraged to participate in DSM due to the reduction of the energy cost. Meanwhile, Real-Time Pricing (RTP) tariffs introduce lower Peak-to-Average Ratio (PAR) of the aggregate load demand, which in turn encourage utilities to support the proposed algorithm.

Through the optimal scheduling of building energy resources, X. Guan etc. [23] minimizes the overall energy cost of buildings. This method used the average performance over 100 scenarios for solar power generation, electrical, and cooling demands.

B. Sun etc. [24] developed a Lagrangian relaxation methodology combined with stochastic dynamic programming. The proposed approach coordinated the control for building appliances and satisfied the requirements of energy reduction and human comfort.

C. Chang etc. [25] solved the stochastic multi-objective optimization problem for CHP dispatch. The uncertainty from the electric power and thermal demands was taken



www.manaraa.com

into account. The problem was solved by the goal attainment method with fuzzy logic and genetic algorithm.

### 1.3.1 Energy efficiency and energy conservation

Energy efficiency and energy conservation are two alternative ways to reduce both energy consumption and energy bills at the same time. Energy efficiency is defined as the need for rationalization of energy consumption without any loss in value or comfort [17]. The investment in technologies or building improvements will be paid back in the long term during the operation of the energy-efficient appliances.

Energy conservation is to encourage customers to give up some comfort in exchange for saving money. The measures include setting the thermostat a few degrees higher in the summer or lower in the winter to reduce air conditioning use and costs. Energy conservation is more related to behavioral changes than technical improvements. For example, people could wash clothes only with cold water.

### 1.3.2 Demand response

Demand response (DR) is electrical energy management initiated by the supply side. Consumers take actions on the demand side but do not benefit directly from the supply side management which is designed specifically for the power supply company [14]. The time of electricity consumption and the peak duration are extremely relevant for determining the efficiency of the utilization of electrical equipments. In smart grid, demand response programs aim to adjust the timing and quantity of end-users' electricity consumption, which are elicited on the basis of variable electricity prices depending on the time of use and the load level [26]. DR benefits consumers and utility companies



www.manaraa.com

from intelligent resource scheduling [27], integration of intermittent renewable solar generation sources and reduction of the peak load for buildings [28]-[35]. It can be realized through the utility control or energy management systems at the end-users' facility.

Load shifting transfers the energy consumption of building appliances from a certain period to another. It can be realized with a cost minimization strategy by providing customers with the information of time-of-use prices. Customers are penalized or rewarded by adjusting short-term episodes of energy consumption, which is essential to demand response programs. For example, consumers can run the clothes washer only at night with low energy price.

The amount of bill reduction through load shifting depends on the rate structure [36]-[38]. Time of use (TOU) rates are predefined to respond on three levels, including off-peak, mid-peak, and on-peak, which is not flexible enough. Critical peak pricing (CPP) rates address the critical events during emergency periods or high wholesale market prices [39]. Peak-time rebates (PTR) rates include super peak periods as well, but customers are rewarded with a rebate on the basis of the usage reduction.

The Residential Real Time Pricing (RRTP) program launched by ComEd-An Exelon Company, allows consumers to pay the hourly, wholesale price for electricity rather than a fixed price, taking advantage of lower prices during off-peak times [40]. Air conditioner cutout program permits participants select a price threshold (like 0.10 $/kWh) in order for the central air conditioner to be cycled in the scheduling period. Both programs would in turn lower the cost of delivering electricity for the utility.



www.manaraa.com

However, not every facility is suitable to join in the demand response program even though it does introduce bill reduction in some cases [41]-[42]. For example, it is impossible for health care facilities to reduce their electrical loads without interfering with patient comfort or safety. Large information-technology centers are also unable to reduce sufficient loads without putting equipment at risk. Retail facilities may not be able to shut down air conditioning loads without compromising customer comfort.

### 1.3.3 Smart metering

In smart grid, advanced meters are used to provide real-time information for users to control their energy consumption patterns [43]. It allows homes to connect to data on usage and price. As shown in Figure 1.4, the smart meter offers the end user near-real time information from the supply side, which facilitates the demand-side energy management. It interacts dynamically with the utility grid in two ways, responds with information on usage and diagnostics.



www.manaraa.com


Figure 1.4 A smart meter at a residence [15]

PJM has two hourly pricing markets: real-time (RT) and day-ahead (DA) [44]. When less efficient (and often higher polluting) plants are needed to meet the demand, the real-time rates raise accordingly. The day-ahead pricing market is often a good indicator for the next-day real-time prices, as can be seen from Figure 1.5. From Figure 1.6, the extra 5-minute pricing feed also provide customers with the most appropriate information to reflect the current hour's potential price. The "current hour average" price reflects the real-time average of the current hour's 5-minute prices.



www.manaraa.com


Figure 1.5 Real-time hourly prices for September 10th, 2014 [45]

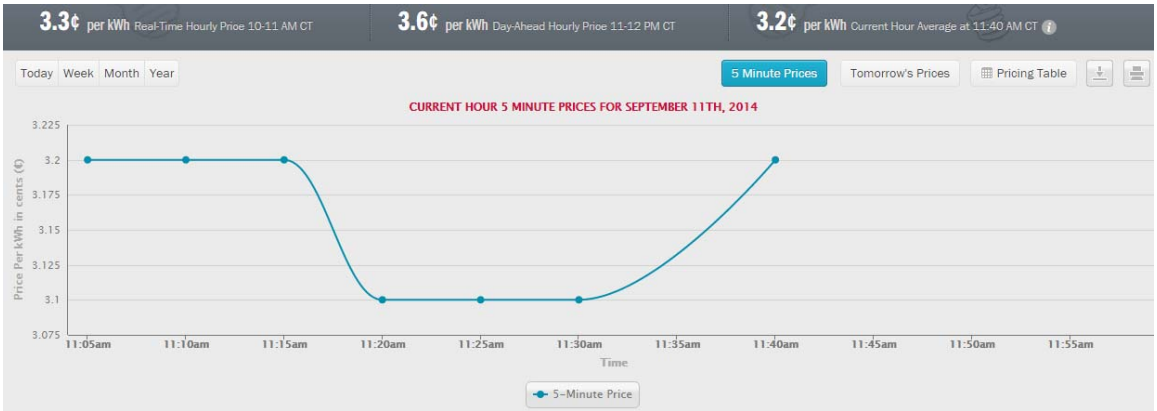


Figure 1.6 Current hour 5 minute prices for September 11th, 2014 [46]

The decision on whether to go with smart metering depends on the size of the building, the flexibility of the end users' in shifting electricity use, the intensity the customers use the electricity. For the average homeowner, a smart meter will increase the bill slightly, around a couple of percent.

## 1.4 Contribution

The main contributions of this dissertation are summarized as follows:

- Introduce an optimization tool to economically schedule operation for all components in building energy systems under the utility grid



www.manaraa.com

interconnection through a hybrid energy supply system integrated with onsite electricity generation from solar PV and CHP while satisfying a variety of end-use energy demands;

- Propose both the multi-stage mixed-integer stochastic programming model and robust optimization model for the optimal operation of energy-efficient building systems taking into account the random characteristics of non-controllable electric and thermal loads, and solar power generations.
- Develop a robust stochastic optimization model, which not only possesses the scenario features of stochastic programming, but also introduces the idea of robustness by constructing a multiband uncertainty set for each random variable. The partition of the uncertain feasible region makes the solution robust and adaptive at the same time.

## 1.5 Organization of the dissertation

The rest of this dissertation is organized as follows: Chapter 2 describes stochastic programming and robust optimization to address optimization problems associated with uncertainties, Chapter 3 introduces the deterministic optimal operation of energy-efficient building systems, Chapter 4 discusses the stochastic optimal operation of energy-efficient building considering controllable electric and thermal loads, Chapter 5 addresses the optimal operation of energy-efficient building systems from the robust perspective, Chapter 6 proposes a robust stochastic optimization model for the optimal operation of building energy systems, Chapter 7 provides conclusions and suggestions for the future work.



www.manaraa.com

# CHAPTER II

# MATHEMATICAL BACKGROUND FOR OPTIMIZATION UNDER UNCERTAINTY

This chapter presents the mathematical background for the optimal operation of energy-efficient building system. It starts with the formulation of two-stage and multi-stage stochastic programming, then moves forward to the forecast and modeling of uncertainty. Moreover, the static and two-stage robust optimization are introduced, together with the proof of the equivalence of the static robust model and the two-stage robust model in the case of constraint-wise robust optimization.

Uncertainties are mostly involved in decision-making problems. In general, the optimal operation of building systems is associated with uncertainty from electric loads, thermal loads and solar power generation. The evolution of each uncertainty is determined by several factors. For example, electric loads in buildings are influenced by the level of consumers' activities, energy savings in general and electricity providers' rate policies; the randomness of thermal loads is affected by the weather surrounding the building; the power output of a solar panel can be impacted by the radiation of the sun and the ambient weather [47].

In order to maximize the utilization of solar power production, we assume that the customer would take all available solar energy. This assumption benefits the customer from lower-price or no cost energy than that from the electric grid.



www.manaraa.com

The characteristics of solar power generation and non-controllable loads for a 24-hour horizon are shown in Figure 2.1, which are obtained from historic data.

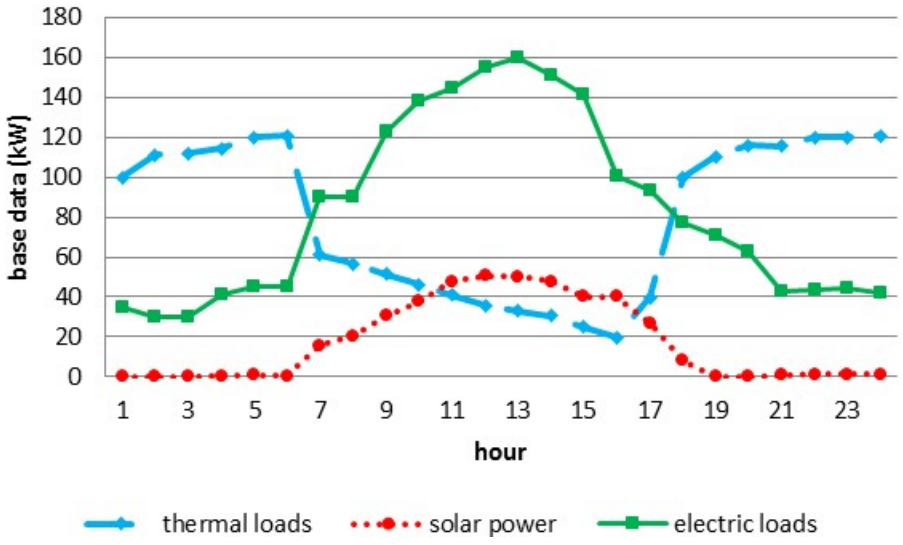


Figure 2.1 Daily non-controllable loads and solar power generation

## 2.1 Stochastic mathematical programming techniques

Stochastic programming studies the processes of decision making under uncertainty within a specific time period [48]. The solution to the stochastic programming problem provides probabilistic guarantee for the reliable operation of building energy systems under each realization of the uncertainty.

Assume $\omega_r$ is the random event to be realized at stage $r$ with the total $J_r$ scenarios, $\upsilon_{rj}$ indicates possible outcomes for $K$ uncertain variables, which consists of the uncertainty $y_{krj}$ at scenario $j$. The multivariate discrete random event $\xi_R$ made up to stage $r$ can be expressed as

$$\xi_R = (\xi_{R-1}, \omega_r) = (\omega_1, \omega_2, \ldots, \omega_r) \tag{2.1}$$



www.manaraa.com

Where $$\omega_r = \{\upsilon_{rj} \mid j = 1,\ldots, J_r\} \tag{2.2}$$

$$\upsilon_{rj} = (y_{1rj},\ldots, y_{krj},\ldots, y_{Krj}), k = 1,\ldots, K \tag{2.3}$$

We view the sequence of $\omega_r$ of data vectors as a stage-wise independent process if $\omega_r$ is stochastically independent of $\omega_{r-1}, r = 2, \ldots, T$.

Consequently, by considering certain time stages $1 \le t \le r$, the scenario $\xi_R$ is defined by (2.4) as a sequence of nodes $y_{ktj}$. Similarly, $\varsigma_R$ includes the scenarios to be realized between time stage $r$ and $T$ as shown in (2.5).

$$\xi_R = \{y_{ktj} \mid t = 1,\cdots, r; k = 1,\ldots, K; j = 1,\ldots, J_t\} \tag{2.4}$$

$$\varsigma_R = \{y_{ktj} \mid t = r,\cdots, T; k = 1,\ldots, K; j = 1,\ldots, J_t\} \tag{2.5}$$

### 2.1.1 Two-stage stochastic model

Generally, two-stage stochastic programing models have a structural part which is fixed at the first stage and independent of the uncertainty, and a recourse part dependent on the uncertainty at the second stage [49]. The two-stage stochastic programming problems are with the following form

$$Min \quad J = c_1 x_1 + E_{\varsigma_2}[Q_2(\xi_2, x_1)] \tag{2.6}$$

s.t. $$W_1 x_1 = h_1,\ x_1 \ge 0 \tag{2.7}$$

Where $\xi_2$ is viewed as a random vector. The expected function at the problem (2.6)-(2.7) depends on the probability distribution of $\xi_2$. $Q_2(\xi_2, x_1)$ is the optimal value of the second-stage sub-problem, which can be represented by the model (2.8)-(2.9).

$$Min\ c_2(\xi_2) x_2 \tag{2.8}$$



www.manaraa.com

s.t. $$T_1 x_1 + W_2 x_2 = h_2(\xi_2),\ x_2 \geq 0 \tag{2.9}$$

We are considering now the expected value function

$$\phi(x_1) := E_{\varsigma_2}[Q_2(\xi_2, x_1)] \tag{2.10}$$

Assume that $\xi_2$ has a limited number of realizations associated with corresponding probabilities $\rho_k, k = 1, \ldots, K$. Then

$$E_{\varsigma_2}[Q_2(\xi_2, x_1)] = \sum_{k=1}^{K} \rho_k Q_2(\xi_{2,k}, x_1) \tag{2.11}$$

For a given $x_1$, the expectation $E_{\varsigma_2}[Q_2(\xi_2, x_1)]$ is defined as the optimal value of the linear programming problem

$$Min \sum_{k=1}^{K} \rho_k \cdot c_2(\xi_{2,k}) x_{2,k} \tag{2.12}$$

s.t. $$T_{1,k} x_1 + W_{2,k} x_{2,k} = h_{2,k}(\xi_{2,k}) \tag{2.13}$$

$$x_{2,k} \geq 0, k = 1, \ldots, K \tag{2.14}$$

The two-stage stochastic problem (2.6)-(2.7) is equivalent to the following deterministic problem:

$$Min \quad J = c_1 x_1 + \sum_{k=1}^{K} \rho_k \cdot c_2(\xi_{2,k}) x_{2,k} \tag{2.15}$$

s.t. $$W_1 x_1 = h_1 \tag{2.16}$$

$$T_{1,k} x_1 + W_{2,k} x_{2,k} = h_{2,k}(\xi_{2,k}) \tag{2.17}$$

$$x_{2,k} \geq 0, k = 1, \ldots, K \tag{2.18}$$



www.manaraa.com

### 2.1.2 Multi-stage stochastic model

We now focus our attention on the multi-stage stochastic problem. Based on the historical event $\xi_R$ and the future occurrence $\varsigma_R$, the general multi-stage linear SP model is shown below [50],

*Stochastic (LP)*:

$$Min \quad J = c_1 x_1 + E_{\varsigma_2}[c_2(\xi_2)x_2 + ... + E_{\varsigma_T}[c_T(\xi_T)x_T]] \tag{2.19}$$

*s.t.*

$$W_1 x_1 = h_1 \tag{2.20}$$

$$Ax_r \le b_r, r = 2,...,T \tag{2.21}$$

$$T_{r-1}x_{r-1} + W_r x_r = h_r(\xi_R)\ , R = 1,...,r, r = 2,...,T \tag{2.22}$$

$$x_r \in X_r\ , r = 1,...,T \tag{2.23}$$

where $r$ are the stages, each of which represents the beginning of each hour. $X_r$ refers to deterministic, static linear constraints at stage $r$. $\xi_R$ enters into the optimization model (2.19)-(2.23) through the costs $c_r$ and the right-hand sides $h_r$. The vector $x_r$ includes both "here-and-now" and "wait-and-see" decision variables at stage $r$. (2.21) represents intra-period constraints, which is the basic requirement of non-anticipativity. Non-anticipative here-and-now decisions do not depend on the revealing of the uncertainty. The inter-period constraints (2.22) describe the random and time-coupling requirements.

Multi-stage stochastic optimization looks for optimal solutions for problems with correlated dynamic and stochastic elements [51]. Typically, multi-stage stochastic programs minimize the expected cost value from first-stage variables and probable



www.manaraa.com

recourse decisions [52]. From the dynamic programming viewpoint, the problem (2.19)-(2.23) could be reformulated with a group of recourse function as.

$$Q_r(x_{r-1},\xi_R)=Min \quad c_r x_r + E_{\omega_{r+1}}[Q_{r+1}(x_r,\xi_{R+1})] \tag{2.24}$$

s.t. $$W_r x_r = h_r(\xi_R) - T_{r-1}x_{r-1}, x_r \in X_r, r<T \tag{2.25}$$

The terminal condition is

$$Q_T(x_{T-1},\xi_T)=Min \quad c_T x_T \tag{2.26}$$

*s.t.* $$T_{T-1}x_{T-1}+W_T x_T = h_T(\xi_T), x_T \in X_T \tag{2.27}$$

With the recursive equations (2.24)-(2.27), the dynamic form of the standard SP formulation (2.19)-(2.23) can be written as,

$$Min \quad E[\sum_{t=1}^{r} c_{t-1}(\xi_{t-1})x_{t-1} + Q_r(x_{r-1},\xi_R)] \tag{2.28}$$

s.t. $$T_{r-1}x_{r-1}+W_r x_r = h_r(\xi_R), x_r \in X_r \tag{2.29}$$

### 2.1.3 Auto-regressive moving average model

In the following, the stochastic processes for the forecast error are generated by multivariate auto-regressive moving average (ARMA) time series model [53]-[61]. The aim is then to simulate realistic possible outcomes, which have the correct statistical behavior concerning forecast errors and correlation between different forecast errors. The time series in the ARMA (n, m) model is defined as

$$v_0^j = 0 \tag{2.30}$$

$$z_0^j = 0 \tag{2.31}$$



www.manaraa.com

$$v_t^j = \alpha_1 v_{t-1}^j + \alpha_2 v_{t-2}^j + \ldots + \alpha_n v_{t-n}^j + z_t^j + \beta_1 z_{t-1}^j + \beta_2 z_{t-2}^j + \ldots + \beta_m z_{t-m}^j \qquad (2.32)$$

Where $v_t^j$ is the forecast error in $t$-hour forecast; $z_t^j$ is the normal white noise process with standard deviation $\sigma_z$; $\alpha_i$ for i=1,2,…,n is auto-regressive parameter; $\beta_i$ for i=1, 2, …,m is moving average parameter. This approach simulates forecast errors. The forecast data takes into account of the correlation among the magnitude of forecast errors in consecutive time periods [62].

### 2.1.4 Multi-stage scenario tree

Within a specified forecast period, the scenarios of possible events are defined as a series of outcomes associated with probabilities. At this point, the multiple input scenarios with a probability tree were captured in Figure 2.2 [63], which represents hourly forecasts in the optimization period. Because the data forecast may be reliable till hour 1, so the process for the first stage is deterministic.

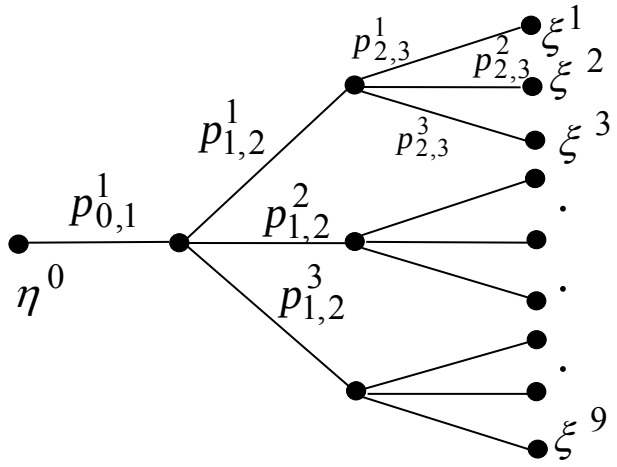


Figure 2.2 Multi-stage scenario tree with probability



www.manaraa.com

The scenario $\xi_t^j$ is defined as a sequence of nodes $\eta_t^j$.

$$\xi_t^j = (\eta_0, \eta_1^j, \ldots, \eta_{T_t}^j), j = 1, \ldots, J_t \tag{2.33}$$

Where $\eta^0$ is the root of all scenarios, $J_t$ is the number of scenarios at stage $t$, $T_t$ is the terminal time at stage $t$. Therefore, each node $\eta_t^j$ has a vector parameter $v_t^j$ at different stages. $J_t = 1, T_t = 1$ when $t = 1; J_t = 3, T_t = 6$ when $t = 2; J_S = 9, T_t = 24$ when $t = 3$.

Due to the large size of the resulting problem, it is usually impossible to explicitly consider the full scenario tree in the problem [49]. The multi-stage scenario tree generation consists of two major procedures [64]. The one-stage scenario tree generation involves the reduction of the pure number of scenarios. For the process of multi-stage scenario tree generation, both inner nodes will be deleted and branching will be created within the scenario tree. The process of one-stage scenario tree generation will be briefly described here.

Step 1: Determine the scenario to be deleted.

The scenario reduction for multiple variables can be reached by calculating the distance between different scenarios.

$$d(\xi_R^j, \xi_R^k) = (\sum_{t=0}^{T_r} (\left\| V_t^j - V_t^k \right\|)^2)^{1/2} \tag{2.34}$$

If the probability for scenario $\xi_t^j$ is given by $p_t^j$, $p_{t,t+1}^j$ is the transition probability from the ancestor of scenario $\xi_{t+1}^j$ to $\xi_{t+1}^j$.



www.manaraa.com

$$p_s^j = \prod_{m=0}^{T_s-1} p_{m,m+1}^j \tag{2.35}$$

The scenario $\xi_t^{q^*}$ $(q^* = 1, \ldots, J_t)$ to be deleted can then be determined if satisfying

$$p_s^{q^*} \cdot \min_{\substack{q=1,\ldots,J_s, \\ q\neq q^*}} d_s(\xi_s^q, \xi_s^{q^*}) = \underset{j=1,\ldots,J_s}{Min} (p_s^j \cdot \min_{\substack{k=1,\ldots,J_s, \\ k\neq j}} d_s(\xi_s^j, \xi_s^k)) \tag{2.36}$$

Step 2: Renew the probability of the scenario $\xi_s^{\bar{q}}$ nearest to the deleted one.

$$d_s(\xi_s^{\bar{q}}, \xi_s^{q^*}) = \underset{q=1,\ldots,J_s, q\neq q^*}{Min} d_s(\xi_s^q, \xi_s^{q^*}) \tag{2.37}$$

$$p_{0,1}^{\bar{q}} = p_{0,1}^{\bar{q}} + p_{0,1}^{q^*} \tag{2.38}$$

Step 3: Change the number of scenarios.

$$J_t := J_t - 1 \tag{2.39}$$

For the second procedure, steps for creation of a multi-stage scenario tree include

1) Set s to be the actual stage with the terminal time $T_s$ ;

2) Determine the series of admissible nodes $q^*$ whose inner nodes have to be deleted;

$$\{\prod_{k=0}^{s-1} p_{k,k+1}^{q^*}\} \underset{q=1,\ldots,J_{s-1}, q\neq q^*}{Min} d_{s-1}(\xi_{s-1}^q, \xi_{s-1}^{q^*}) = \underset{j=1,\ldots,J_{s-1}}{Min} \{\{\prod_{k=0}^{s-1} p_{k,k+1}^j\} \min_{k=1,\ldots,J_{s-1}, k\neq j} d_{s-1}(\xi_{s-1}^j, \xi_{s-1}^k)\} \tag{2.40}$$

3) Delete the inner nodes from the set of nodes on each stage of the tree;

4) Determine the new predecessors $\bar{q}$ of the last node with two branches;



www.manaraa.com

$$d_{s-1}(\xi_{s-1}^{\bar{q}}, \xi_{s-1}^{q^*}) = \underset{q=1,\ldots,J_{s-1}, q\neq q^*}{Min} \{d_{s-1}(\xi_{s-1}^{q}, \xi_{s-1}^{q^*}) : s(\eta_{s-1}^{q}) < 2\} \tag{2.41}$$

5) The deleted nodes $q^*$ on the stages 1, 2, 3 are then changed to equal the corresponding nodes $\bar{q}$ in the predecessor;

6) Change the probabilities;

$$p_{s-1,s}^{\bar{q}} := p_{0,1}^{\bar{q}} \Big/ (p_{0,1}^{\bar{q}} + p_{0,1}^{q^*}) \tag{2.42}$$

$$p_{s-1,s}^{q^*} := p_{0,1}^{q^*} \Big/ (p_{0,1}^{\bar{q}} + p_{0,1}^{q^*}) \tag{2.43}$$

7) Set s:=s-1 and return to 2) until more inner nodes have to be deleted at the actual stage.

## 2.2 Robust optimization

### 2.2.1 Interval uncertainty set model

Let's consider the following nominal linear optimization problem (2.44)-(2.46) subject to data uncertainty

$$Min \quad f(x) = cx \tag{2.44}$$

s.t. $$g(x) = Ax \le b \tag{2.45}$$

$$l \le x \le u \tag{2.46}$$

The uncertainty may reside in a particular row $i$ of the matrix $A$, or in the objective function $c$ or the right hand side $b$. Different from the modeling of uncertainty in stochastic programming, the uncertainty model in robust optimization is usually depicted as an uncertainty range. The scaled deviation $\eta_{ij}$ is defined as the relative value of the forecast



www.manaraa.com

error and the realization of the uncertainty. Furthermore, with the introduction of a budget of uncertainty $\Gamma_i$ with values in the interval $[0, |J_i|]$, the $\eta_{ij}$ is constrained as:

$$\sum_{j \in J_i} |\eta_{ij}| \leq \Gamma_i \tag{2.47}$$

### 2.2.2 Static robust model

Static robust optimization formulation looks for optimal solutions that optimize the objective function and meet the problem requirements for all possible revealing of the uncertainty in constraint coefficients. Hence, the variables are independent of the uncertain parameters. For a worst case analysis when taking into account the uncertainty, we consider the following problem (2.48)-(2.50):

$$Min \quad cx \tag{2.48}$$

s.t.
$$\sum_{j=1}^{n} a_{ij} x_j + Max \sum_{j \in J_i} \hat{a}_{ij} \eta_{ij} x_j \leq b_j \tag{2.49}$$

$$l \leq x \leq u \tag{2.50}$$

For the $i$ th constraint, the auxiliary problem (2.51)-(2.53) is shown as following:

$$Max \sum_{j \in J_i} \hat{a}_{ij} \eta_{ij} |x_j| \tag{2.51}$$

s.t.
$$\sum_{j \in J_i} \eta_{ij} \leq \Gamma_i \tag{2.52}$$

$$0 \leq \eta_{ij} \leq 1 \tag{2.53}$$

Accordingly, the dual of problem (2.51)-(2.53) is shown as problem (2.54)-(2.57).



www.manaraa.com

$$Min \quad z_i\Gamma_i + \sum_{j\in J_i} p_{ij} \tag{2.54}$$

s.t. $$z_i + p_{ij} \geq \hat{a}_{ij} y_j, \forall i, j \in J_i \tag{2.55}$$

$$\left|x_j\right| \leq y_j \tag{2.56}$$

$$z_i,\ p_{ij}, y_j \geq 0 \tag{2.57}$$

Where $z_i$, $p_{ij}$ are the dual decision variables for constraints (2.52)-(2.53) of the auxiliary problem .

Incorporating model (2.54)-(2.57) into the original problem (2.48)-(2.50), the robust linear counterpart is formulated as:

$$Min \quad cx \tag{2.58}$$

s.t. $$\sum_{j=1}^{n} a_{ij} x_j + z_i\Gamma_i + \sum_{j\in J_i} p_{ij} \leq b_i \tag{2.59}$$

$$l_j \leq x_j \leq u_j \tag{2.60}$$

$$z_i + p_{ij} \geq \hat{a}_{ij} y_j, \forall i, j \in J_i \tag{2.61}$$

$$-y_j \leq x_j \leq y_j \tag{2.62}$$

$$z_i,\ p_{ij}, y_j \geq 0 \tag{2.63}$$

### 2.2.3 Two-stage robust optimization

It is proved that the two-stage robust optimization with constraint-wise uncertainty is equivalent to the static robust optimization [65]. In particular, the assumption of constraint-wise uncertainty means that the uncertainty in a specific



www.manaraa.com

constraint does not exist in the other constraints [66]. The proof is shown in detail as following.

With the uncertainty $b$ bore in the right-hand side of the equality constraint, a two-stage robust optimization problem can generally be formulated as follows:

$$\underset{x^1}{Min} \quad (c^T x^1 + \underset{b}{Max}\, \underset{x^2}{Min} \quad d^T x^2) \tag{2.64}$$

s.t. $$Ax^1 + Bx^2 = b, \; x^1, x^2 \geq 0 \tag{2.65}$$

Where uncertainty $b$ is modeled as

$$b = \left\{ b_i \middle| b_i = \bar{b}_i + \hat{b}_i z_i, \middle| z_{ij} \middle| \leq 1, \sum\nolimits_j \middle| z_{ij} \middle| \leq \Gamma_i \right\} \tag{2.66}$$

In order to solve the above two-stage robust optimization problem with Benders' Decomposition algorithm [67]-[68], the following second-stage problem is usually generated:

$$\underset{b}{Max}\, \underset{x^2}{Min}\, d^T x^2 \tag{2.67}$$

s.t. $$Bx^2 = b - Ax^1, \; x^1, x^2 \geq 0 \tag{2.68}$$

The first-stage and second-stage variables interact with each other through the dual problem of the second-stage problem as below, where the first-stage variables are passed through the main problem.

$$\underset{b}{Max}\, \underset{p}{Max} \quad (b - Ax^1)^T p = \underset{b,p}{Max} \quad (b - Ax^1)^T p = \underset{p}{Max} \quad (\underset{b}{Max}\, b - Ax^1)^T p \tag{2.69}$$

s.t. $$B^T p \leq d^T \tag{2.70}$$



www.manaraa.com

Where $p$ is the dual variable introduced for the equality constraint with uncertainty $b$.

Therefore, the optimal solutions for $x^1, x^2$ correspond to the maximum value of the interval for the uncertainty $b$. And in the two-stage model, the optimal solution for $x^1$ is feasible for every possible realization of the uncertainty $b$.

While the static robust optimization is proposed so that a set of robust solutions can be provided against the realization of the uncertainty, which is shown below.

$$\underset{x^1}{Min} \quad (c^T x^1 + \underset{x^2}{Min}\, d^T x^2) \tag{2.71}$$

s.t. $$Ax^1 + Bx^2 = \underset{b}{Max}\, b\,, x^1, x^2 \geq 0 \tag{2.72}$$

Similarly, the original second-stage problem of the static robust model is

$$\underset{x^2}{Min} \quad d^T x^2 \tag{2.73}$$

s.t. $$Bx^2 \geq \underset{b}{Max}\, b - Ax^1\,, x^1, x^2 \geq 0 \tag{2.74}$$

Therefore, we can obtain the corresponding dual problem for (2.73)-(2.74):

$$\underset{p}{Max} \quad (\underset{b}{Max}\, b - Ax^1)^T\, p \tag{2.75}$$

s.t. $$B^T p \leq d^T \tag{2.76}$$

It can be seen that (2.69)-(2.70) is equivalent to (2.75)-(2.76).

Since the solution for $x^2$ is the same in both the static and the adaptive robust model, the solution for $x^1$ in the static robust model is also feasible for every realization



www.manaraa.com

of the uncertainty $b$, which means $x^2$ in the static robust optimization is adjustable according to the uncertainty. Under such situation, the static robust optimization is equivalent to the adaptive robust optimization.

## 2.3 Conclusions

This chapter summarizes two different optimization models under uncertainty, including stochastic programming and robust optimization. The process for the generation of multi-stage scenario tree is described in detail. It is also addressed how to build the uncertainty models for both the SP and RO models respectively. Moreover, it is proved that static robust optimization is equivalent to the two-stage robust optimization with constraint-wise uncertainty



www.manaraa.com

# CHAPTER III

# DETERMINISTIC OPTIMAL OPERATION OF ENERGY-EFFICIENT BUILDINGS

This chapter presents the components of the building energy systems, including electric grid integration, rooftop solar PV system, energy storage, as well as building appliances. Based on the description of the various components, the mathematical modeling of building system components is introduced. Furthermore, the building optimization problem is modeled as to minimize the daily operation cost for energy exchange and purchase. Case studies are conducted to show the effectiveness of the integration of combined heat and power system in reducing the energy dependence on electric grid while increasing the energy efficiency for the building energy systems.

## 3.1 Components of building energy systems

Running infrastructure of buildings more efficiently would lead to minimal capital investment and results in little or no disruption for occupants. From the economic perspective, this should make it the preferred starting point for increased energy efficiency in a real building system [69].

In general, a building energy system is integrated with a mix of energy resources as well as energy storage units and a variety of energy consumption devices, which is shown in Figure 3.1. The detailed description for each component will be discussed in the following sections.



www.manaraa.com

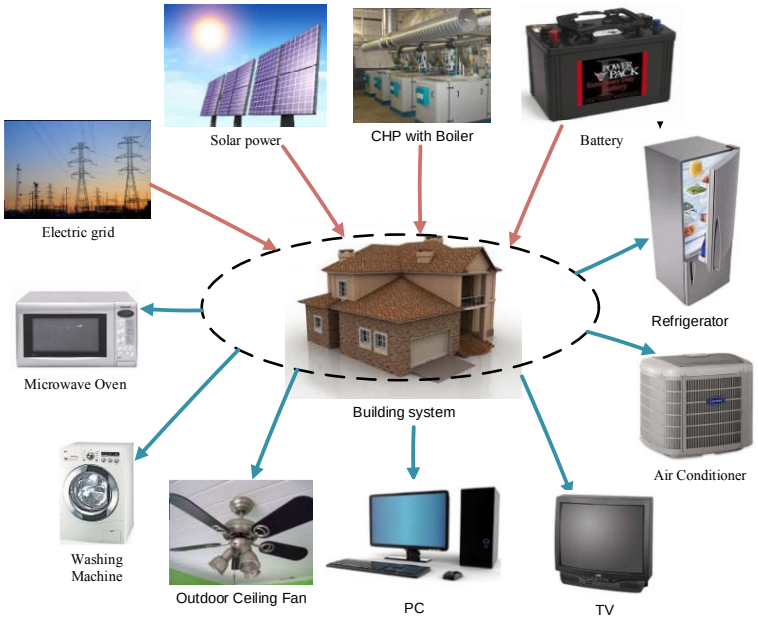


Figure 3.1 Typical components of a building energy system

### 3.1.1 Electric grid

The grid acts as a battery in the grid-integrated building energy system [70]. The whole energy efficiency of a hybrid building energy supply system is usually higher than that of an independent system, as the storage capacity of the grid is supposed to be unlimited. The electricity generated by distributed generators can always be sold to the grid, and the additional produced electricity will not be wasted.

### 3.1.2 Combined heat and power system

The integration of CHP system is driven by the problems in electricity generation and distribution with respect to the availability and cost of electricity as well as by the inefficiencies in the traditional generation systems. These factors led to the great interest in onsite generation and simultaneous generation of heat and electricity.



www.manaraa.com

In Figure 3.2, a typical CHP system produces electricity onsite while recovering the waste heat from power generation for heating or cooling purpose in a close building. The integration of CHP system benefits the consumers at the demand side to a great extent. It reduces the dependence of building energy systems on the electric power grid, which is especially in times of natural disasters or grid black outs. Meanwhile, CHP systems are capable of powering electric facilities during a disaster. Moreover, it meets both the electricity demand and the cooling and heating requirement for the building.

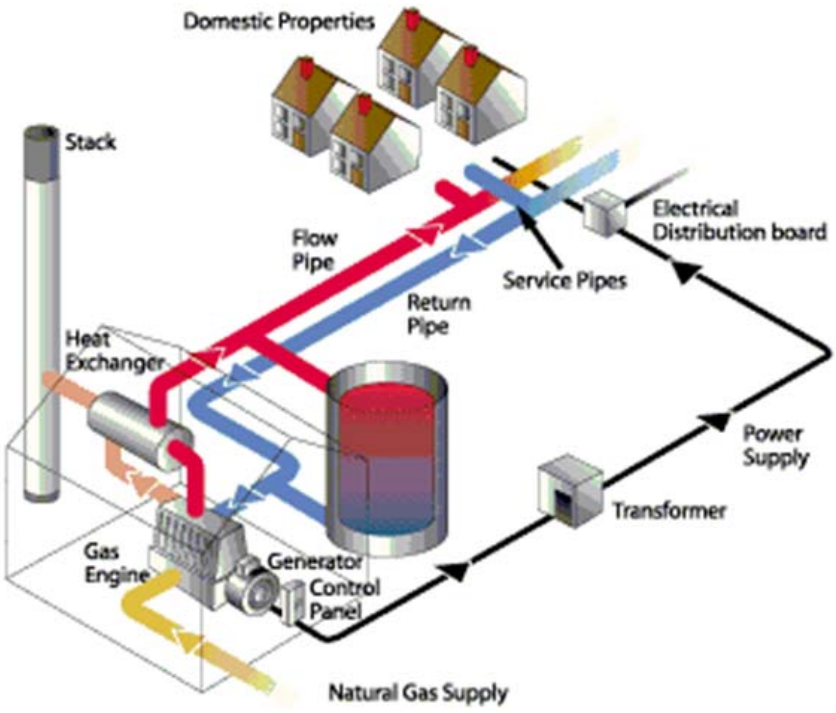


Figure 3.2 Typical CHP system [71]

### 3.1.3 Solar PV

Despite of the technical problems for both the utility and the PV system [72], the ratio of grid-connected building systems with solar PV is increasing greatly [73]-[74].



www.manaraa.com

There are several reasons for this [75]: 1) Grid-connected BIPV delivers electricity at cheaper cost than the power grid to end users because power can be generated at the point of consumption without transmission or distribution; 2) The building owners can benefit a lot from selling surplus solar electricity back to the utility grid. 3) It is rare that PV panels fail or malfunction. Therefore, utilities have generated great interest in investing in PV.

### 3.1.4 Battery units

The building is supposed to be supplied with certain amounts of energy at certain times. With the battery storage device, it is more likely and economic to meet the load demands in different time periods. The availability of the battery depends on the amount of electricity charged and discharged in the different time periods, and it is influenced by the building demand and solar output. Battery technology is paired with the photovoltaic technologies to supply maximum flexibility to control diverse systems. Because solar power generation is occasional during a day, a season or a year, the battery system is a good choice to postpone the use of renewable energy at home. A battery backup system can help provide power to the system's owners during an outage or at evening.

The role of battery technologies is different depending on the amount of storage deployed in short and long terms. For flywheel and super-capacitor type of batteries, the frequency and stability control is provided in the short term. For electrical batteries, hydrogen-chemical batteries, and pumped storage with water or air, they are acting as peak load shifting or shaping in the long term.



www.manaraa.com

### 3.1.5 Building appliances

As reported by the United States Department of Energy (DOE), the buildings consume up to 40.7% of the nation's primary energy in 2013, among them residential buildings take around 22% and commercial ones for 18.7% [76]. Buildings in Hong Kong contributed about 40% toward the total energy consumption [77]. In addition, buildings are contributing mostly to global carbon emissions, which have a surprisingly profound influence on the natural environment around our corporation or industry, health, economy, and productivity [78].

The types of residential and commercial end uses are examined in Figure 3.3. It can be observed that the major energy consumption is from lighting, refrigerator and HVAC.

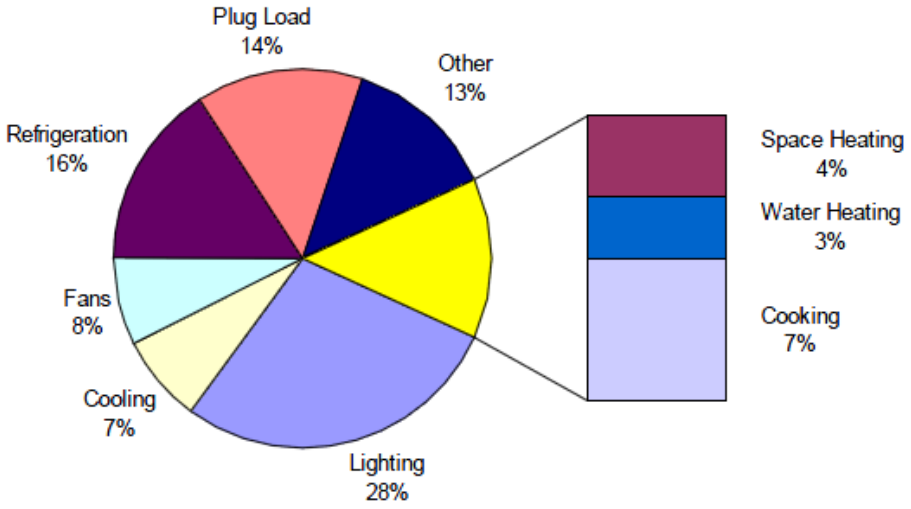


Figure 3.3 Overall electricity consumption by end use [10]

Based on the demand requirements of the customer, each appliance can be set as either controllable or non-controllable. For controllable loads at the consumer side,



www.manaraa.com

building appliances could be delayed or interrupted if necessary by the end user through a control system located at home or on internet [79]. In contrast, the operation of non-controllable appliances need to start working immediately without the interference of the end user. The control strategies reflect the needs for the end users by minimizing energy costs over time instead of the regulatory and reserving benefits for the utility provider at the supply side. These strategies are achievable through local area networks (LAN) or home area network (HAN) network devices.

## 3.2 Modeling of building energy system

A typical energy-efficient building system is shown in Figure 3.4, where various energy sources including the electric grid, solar panel, battery, and CHP with boiler unit are utilized to supply both electric and thermal loads in the building. The building loads are classified into two main categories: non-controllable and controllable electric and thermal loads.

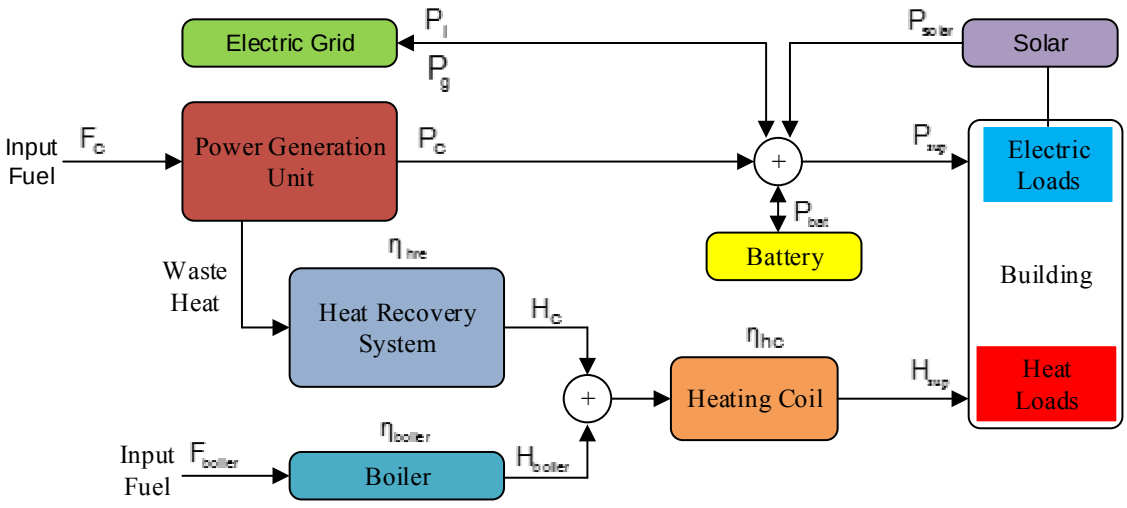


Figure 3.4 Building integrated with various energy sources and loads



www.manaraa.com

### 3.2.1 Integration with the grid

In order to properly operate the building energy system under the integration of utility distribution system, the operating constraints include the grid interface capacity limits for the electric power (3.1)-(3.3). The scheduling variables for the power grid in each time period are the amount of grid electricity supplied to the building ($P_{gf}$), and the building electricity injected to the grid ($P_{gt}$) in each period, and the corresponding status of electricity flowing to the building ($x_{gf}$) and/or to the electric grid ($x_{gt}$). Constraint (3.3) determines the energy flow direction of the electric grid.

$$0 \le P_{gf,t} \le M_{gf} \cdot x_{gf,t} \tag{3.1}$$

$$0 \le P_{gt,t} \le M_{gt} \cdot x_{gt,t} \tag{3.2}$$

$$x_{gf,t} + x_{gt,t} \le 1 \tag{3.3}$$

where $P_{gf,t}, P_{gt,t}$ are the electric power supplied from or fed into the electric grid (kW), respectively. $M_{gf}$ and $M_{gt}$ are assumed to be the upper limits for the electricity exchanged between the building and the grid; the binary variable $x_{gf,t} = 1$ indicates that the grid power is supplying electric loads for the building; otherwise, $x_{gf,t} = 0$; the binary variable $x_{gt,t} = 1$ indicates that the excess power is fed into the electric grid, otherwise, $x_{gt,t} = 0$.



www.manaraa.com

### 3.2.2 Combined heat and power system

For the CHP with boiler unit, the control variables are their operating status ($x_{chp}$) as well as the power and thermal output ($F_{chp}, P_{chp}$). Power and thermal generation limits are shown in (3.4)-(3.6) for the CHP unit, and in (3.7)-(3.8) for the boiler. In (3.4), when CHP is in operation, it consumes the natural gas with the amount of at least $b$ even without any power generation; when CHP generates power with natural gas, the additional operation cost will be proportional to the power it produces with the coefficient $a$. Equation (3.5) describes the relationship between the thermal and electric power output from the CHP. Moreover, equation (3.6) limits its electric power output.

$$F_{chp,t} = a \cdot p_{chp,t} + b \cdot x_{chp,t} \tag{3.4}$$

$$H_{chp,t} = \eta_{hre}(F_{chp,t} - P_{chp,t}) \tag{3.5}$$

$$P_{chp}^{\min} \cdot x_{chp,t} \le P_{chp,t} \le P_{chp}^{\max} \cdot x_{chp,t} \tag{3.6}$$

where $F_{chp,t}$ is the fuel power consumed by the CHP (kW); $p_{chp}^{t}$ is the power production from the CHP; $H_{chp,t}$ is the thermal output supplied by the CHP unit; $p_{chp}^{max}, p_{chp}^{min}$ are the electric power capacity limits of the CHP; $x_{chp,t}$ is the operating status of the CHP; $\eta_{hre}$ is the heat recovery efficiency of the CHP.

The boiler can supply the thermal loads of the building as in (3.7). The thermal supply from the boiler is bounded by constraint (3.8).

$$H_{boi,t} = \eta_{boi} \cdot F_{boi,t} \tag{3.7}$$

$$H_{boi}^{\min} \cdot x_{boi,t} \le H_{boi,t} \le H_{boi}^{\max} \cdot x_{boi,t} \tag{3.8}$$



www.manaraa.com

where $F_{boi,t}$ is the fuel power consumed by the boiler unit (kW); $H_{boi,t}$ is the thermal output supplied by the boiler unit; $H_{boi}^{max}, H_{boi}^{min}$ are the thermal capacity limits of the boiler; $x_{boi,t}$ is the operating status of the boiler; $\eta_{boi}$ is the efficiency of the boiler.

According to (3.4)-(3.8), when the marginal fuel consumption parameter$a$ in (3.4) for electricity production is set to a certain value, the minimum fuel consumption parameter $b$ should meet the requirement (3.9).

$$b \geq H_{nc}^{\min} / \eta_{hc}\eta_{hre} - (a-1) \cdot P_{chp}^{\min} - H_{boi}^{\min} / \eta_{hre} \tag{3.9}$$

### 3.2.3 Battery energy storage

The decision variables for the battery are status of charge/discharge ($x_{bc}, x_{bd}$), and its charging/discharging rates ($P_{bc}, P_{bd}$). The dynamics of the charging level of the battery is modeled by (3.10), which creates a link between the charging rate of the battery in a given time period $t$and the successive state at $t+1$. Because of the energy loss in the storage device [80], the energy efficiency of the battery is considered in the storage transition constraint (3.10). Meanwhile, the limits of the state of charge (SOC) are bounded in (3.11). By defining as a boundary value problem [81], both the initial and the final SOC of the battery are specified as the same predefined value in (3.12), so that the battery can meet the requirement during the next day.

$$s_{bat,t+1} = s_{bat,t} + (\eta_{bc} \cdot P_{bc,t+1} - P_{bd,t+1} / \eta_{bd}) \cdot T_d / c_{bat}^{\max} \tag{3.10}$$

$$s_{bat}^{\min} \leq s_{bat,t} \leq s_{bat}^{\max} \tag{3.11}$$

$$S_{bat}^{0} = S_{bat}^{T} = \hat{S}_{bat} \tag{3.12}$$



www.manaraa.com

$$s_{bat}^{\min} = c_{bat}^{\min} / c_{bat}^{\max} \tag{3.13}$$

Where $p_{bc}^{t}, p_{bd}^{t}$ are the charging and discharging power of battery; $s_{bat}^{max}, s_{bat}^{min}$ are the bounds of SOC; $c_{bat}^{max}, c_{bat}^{min}$ are the capacity limits.

The upper and lower limits for the charging level are imposed by (3.14)-(3.15) to keep sufficient amount of energy in the battery to feed the building during emergency circumstances. The energy flow direction of the battery is defined by (3.16).

$$P_{bd}^{\min} \cdot x_{bd,t} \le P_{bd,t} \le P_{bd}^{\max} \cdot x_{bd,t} \tag{3.14}$$

$$P_{bc}^{\min} \cdot x_{bc,t} \le P_{bc,t} \le P_{bc}^{\max} \cdot x_{bc,t} \tag{3.15}$$

$$0 \le x_{bd,t} + x_{bc,t} \le 1 \tag{3.16}$$

where $p_{bc}^{max}, p_{bc}^{min}, p_{bd}^{max}, p_{bd}^{min}$ are the upper and lower limits of charging/ discharging power of the battery; $x_{bc,t}, x_{bd,t}$ indicate the charging and discharging status, respectively.

### 3.2.4 Building appliances

Response characteristics of smart loads will be modeled as controllable and non-controllable types. In addition, operating characteristics of controllable loads including energy consumption pattern and preferences will be incorporated into the proposed model. For controllable electric and thermal loads, the major constraints include that 1) the loads must run for $T_{ON}$ hours for each scenario during the whole time horizon in (3.17); 2)the total energy consumption requirement in (3.18); 3) the required ON/OFF state at specific time periods in (3.19).



www.manaraa.com

$$\sum_{t=k}^{k+T_{ON}-1} x_{cntr,t} \geq T_{ON} \cdot (x_{cntr,k} - x_{cntr,k-1}), k = 1:(T - T_{ON} + 1) \tag{3.17}$$

$$E_{cntr,t}^{\min} \leq \sum_{t=1}^{T} P_{eh\_cntr,t} \cdot x_{cntr,t} \leq E_{cntr,t}^{\max} \tag{3.18}$$

$$x_{cntr,t} = \hat{x}_{cntr,t} \tag{3.19}$$

## 3.3 Deterministic formulation

Opposite of global optimization which optimizes home energy use with regard to constraints from the grid or micro-grid system within which the home is integrated [82]-[83], local optimization considers the building as a fully self-contained system and takes into account local criteria only [84]. In our research, local optimization is taken into account to manage all energy consumption, generation and storage components at the building level.

In general, the goal for the operation of the energy-efficient building is to minimize the total net cost for operating CHP with boiler and exchanging electricity between electric grid and the building over the entire time horizon while satisfying the operational requirements of the building energy system. As shown in Figure 3.5, the problem is going to find the optimal scheduling decisions for all electric power and thermal units in the system.



www.manaraa.com

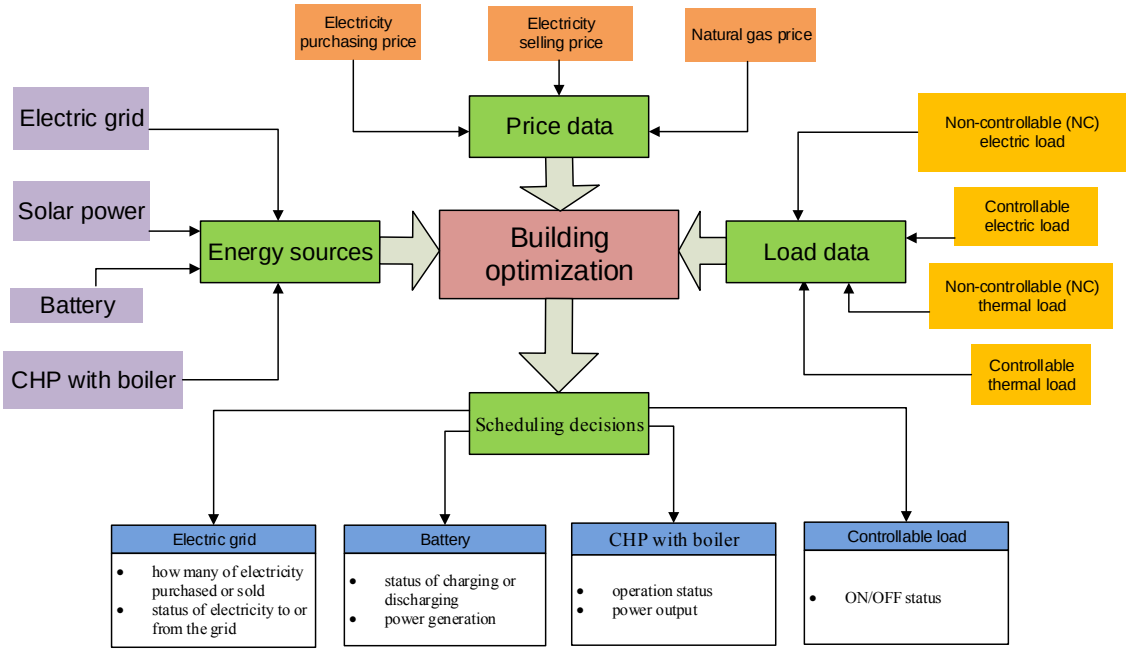


Figure 3.5 Building optimization problem

In order to focus on the improvement of energy consumption efficiency of building energy systems, there are several assumptions made here: 1) Solar power production and energy consumption are considered as exactly known; 2) Interruptible and non-interruptible demands are all considered as controllable loads directly; 3) Thermal supply is supposed to just meet the thermal loads sufficiently, and no extra thermal power is wasted for the building system.

The objective function (3.20) consists of the cost of grid electricity and energy supplied by the CHP with boiler unit, and the revenue obtained from selling energy to the electric grid for 24 hours. No costs are incurred by the operation of solar PV panels and battery storages.



www.manaraa.com

$$Min \quad \sum_{t=1}^{T}[c_{gf,t} \cdot P_{gf,t} - c_{gt,t} \cdot P_{gt,t} + c_{gas,t} \cdot (F_{chp,t} + F_{boi,t})] \cdot T_d \tag{3.20}$$

where the superscript $t$ is time index; $T_d$ is the time interval (one hour here); $c_{gf,t}$, $c_{gt,t}$ are the energy prices supplied from or fed into the electric grid ($/kWh); $c_{gas,t}$ is the natural gas price for the CHP and boiler unit ($/kWh).

The price of purchasing energy from the grid at different hours is depicted in Figure 3.6. This time-of-use electricity prices are labeled with three levels, including off-peak price (5.1 cent/ kWh), mid-peak price (7.1 cent/ kWh), and on-peak price (11.9 cent/ kWh). As described in chapter 1, this kind of rate structure is not flexible enough since it is fixed far in advance. The price for building electricity injected into the grid is 6.7 cent/ kWh. And the price of natural gas is assumed to be 3.1 cent/ kWh.

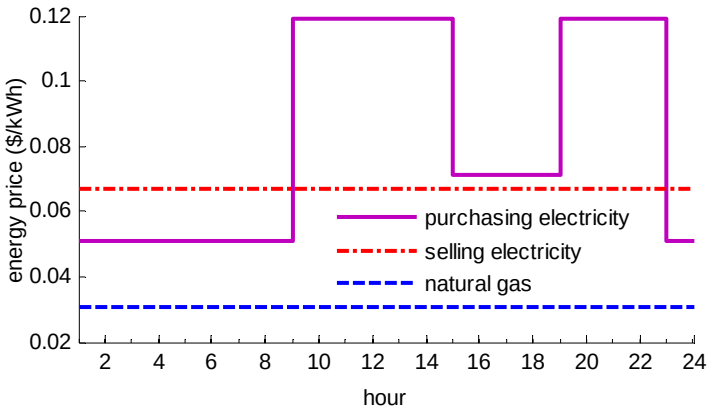


Figure 3.6 Energy prices

In the grid-connected building energy system integrated with renewable solar power generation, the required amount of energy should be provided for both electric and



www.manaraa.com

thermal loads. In the deterministic model, the electric loads are fed by power from the grid, battery, solar PV, and CHP in (3.21).

$$P_{gf,t} - P_{gt,t} + P_{chp,t} - P_{bc,t} + P_{bd,t} + P_{sol,t} = P_{nc,t} + P_{cntr,t} \cdot x_{e\_cntr,t} \tag{3.21}$$

Where $p_{sol}^{t}$ is the solar power production; $P_{nc,t}, P_{cntr,t}$ is the must-on and controllable electric loads, respectively; $x_{e\_cntr,t}$ is the status of controllable electric loads.

The CHP and boiler unit should satisfy the demand of controllable and non-controllable thermal loads as in (3.22).

$$\eta_{hc}(H_{chp,t} + H_{boi,t}) = H_{nc,t} + H_{loss,t} \tag{3.22}$$

Where $H_{nc,t}, H_{cntr,t}$is the must-on and controllable thermal loads, respectively; $\eta_{hc}$is the thermal coil efficiency; $x_{h\_cntr,t}$ is the status of controllable thermal loads.

### 3.4 Case study

As shown in Table 3.1, 5 cases are conducted for the deterministic analysis. From Cases 1 to 5, the solar power productions and non-controllable loads are considered to be deterministic parameters. The goal of these cases is to show the effect of solar power sources and loads on the total daily production cost of electricity and the amount of natural gas required for producing electric and thermal power. In Case 1, the grid is the sole power source to supply electric loads of the building. In Case 2, the solar power is added to the building as a free distribution generation source for electric loads. The battery is considered as an alternative power source in Case 3. From Cases 1 to 3, the controllable electric loads are fixed at hours 11-13 and 17; and there are no thermal loads.



www.manaraa.com

Thermal loads and the boiler are considered in Case 4; and the CHP is taken into account to supply the loads in Case 5.

Table 3.1 Cases with a variety of mix of energy sources

| Cases | | 1 | 2 | 3 | 4 | 5 |
|---|---|---|---|---|---|---|
| Power Generation | Electric grid | ✓ | ✓ | ✓ | ✓ | ✓ |
| | Solar | × | ✓ | ✓ | ✓ | ✓ |
| | Battery | × | × | ✓ | ✓ | ✓ |
| | CHP | × | × | × | × | ✓ |
| | Boiler | × | × | × | ✓ | ✓ |
| Loads | Non-controllable electric loads | ✓ | ✓ | ✓ | ✓ | ✓ |
| | Controllable electric loads | - | - | - | … | … |
| | Non-controllable thermal loads | × | × | × | ✓ | ✓ |
| | Controllable thermal loads | × | × | × | … | … |

Note: '✓'means candidate; '×'means non-candidate; '-'means fixed status; '…' means unfixed status

The operating cost is shown in Table 3.2. Compared with Case 1, the operating cost is reduced by 20.9 % after integration of solar power to the building. The coordination of the battery can further reduce the cost to 96.56% of that in Case 2. Note that the thermal loads are not taken into account in Cases 1-3 but considered from Cases 4-5. The operating cost of Case 5 with the CHP is 11.57% less than Case 4.



www.manaraa.com

Table 3.2 Daily production cost for Cases 1-5

| Case | 1 | 2 | 3 | 4 | 5 |
|---|---|---|---|---|---|
| Cost ($) | 196.80 | 155.67 | 150.32 | 221.08 | 195.49 |

### 3.4.1 Electric power supply

The power exchanged between the grid and building over the time horizon is shown in Figure 3.7, where the negative value means that the building feeds the electric power back to the grid. There is no solar power generation at hours 1-6 and 19-24, therefore the power supplied by the grid has the same curve during these periods for Cases 1 and 2. In Case 3, the battery charges when the price of power provided by the grid is low (e.g. hours 1, 4-5, 7-8, 15, 17-18), and it discharges to supply the loads during the hours (e.g. hours 19-22) when the electricity price is high. In Case 5, in order to obtain the optimal operating point of the building, the building utilizes its own generating units in hours 1-3, 5, 22, and 24, and provides excessive power to the electric grid.



www.manaraa.com

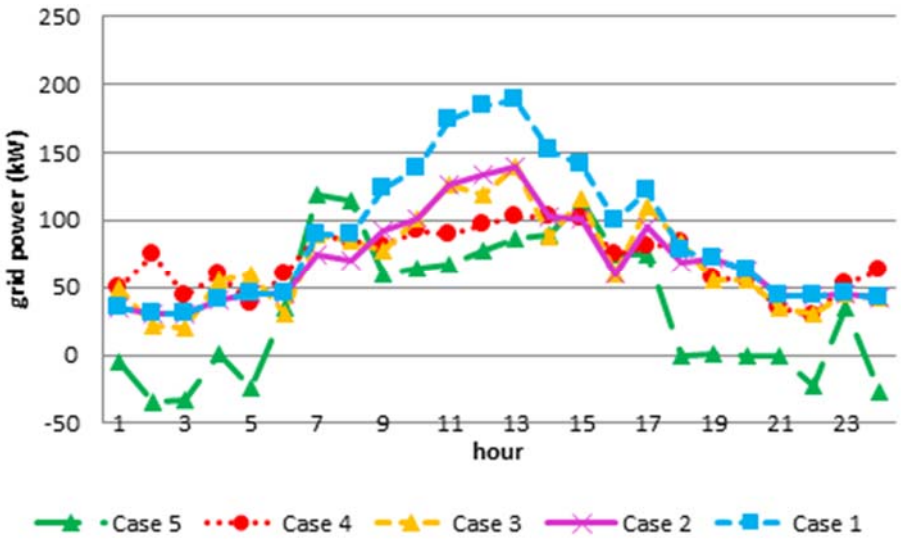


Figure 3.7 Power exchange between the grid and building

### 3.4.2 Impact of controllable electric loads

For Case 3 shown in Figure 3.8, the controllable electric loads are not shiftable and should be supplied in hours 11-13 and 17; but for Case 4 in Figure 3.9, the controllable loads are scheduled to optimally operate in hours 2-4 and 24. This flexibility of the scheduling of controllable electric loads improves the energy-efficiency performance for the building and reduces the operating cost for the electric loads from $150.32 in Case 3 to $143.83 in Case 4.



www.manaraa.com

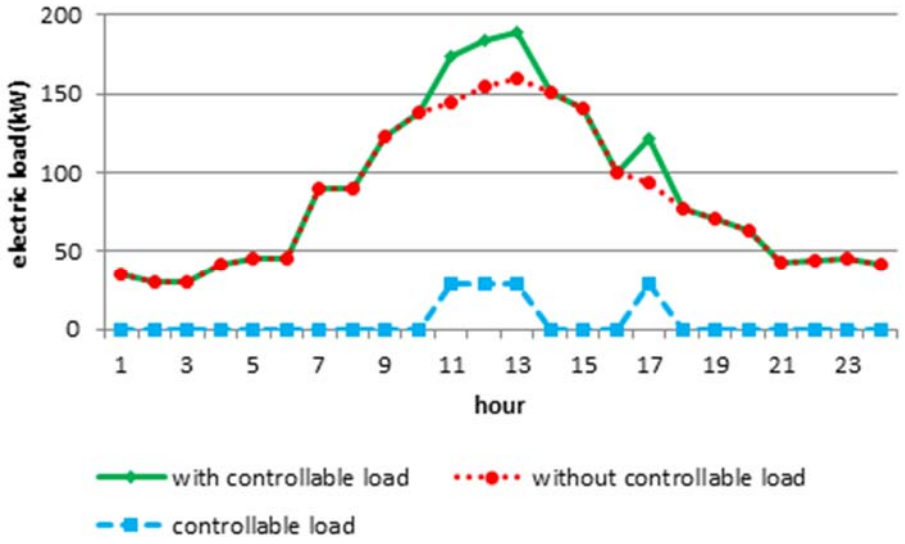


Figure 3.8 Scheduling of controllable electric loads (Case 3: fixed)

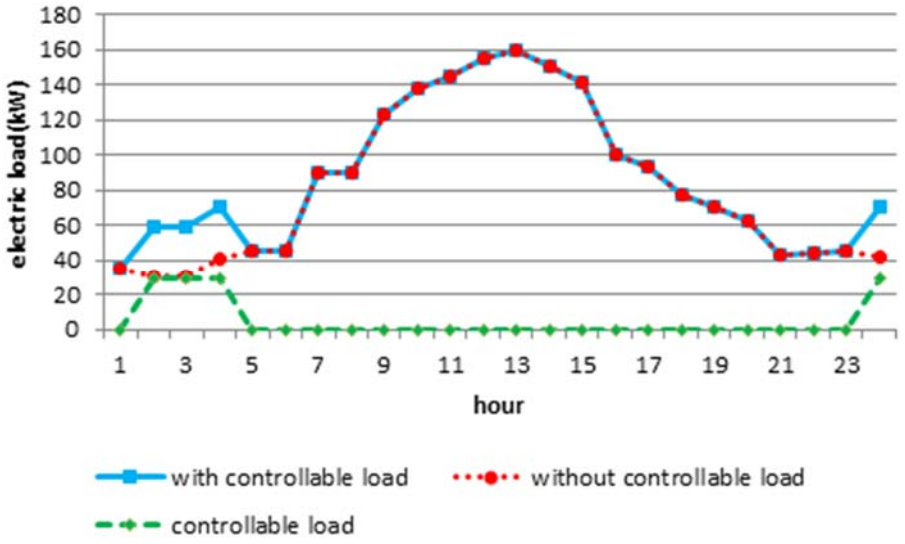


Figure 3.9 Scheduling of controllable electric loads (Case 4: unfixed)

Under the impact of controllable electric loads, the electric power from different power sources is compared in Case 3 (Figure 3.10) and Case 4 (Figure 3.11).



www.manaraa.com

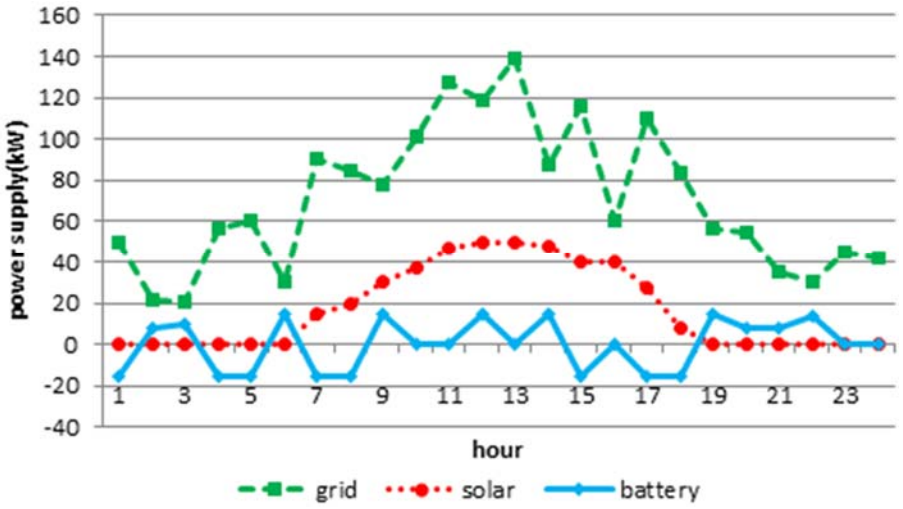


Figure 3.10 Power supply (Case 3: fixed)

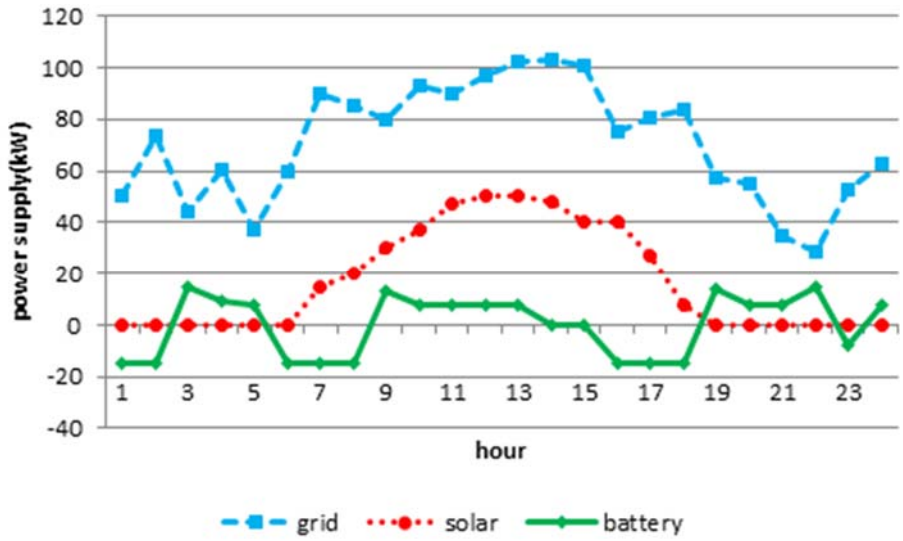


Figure 3.11 Power supply (Case 4: unfixed)

In Case 5 (Figure 3.12), the controllable electric loads operate at hours 6-8 and 23. In Figure 3.13, due to the lower energy price and high energy efficiency of the CHP, electric grid supplies to electric loads almost zero or negative power during hours 1-6 and



www.manaraa.com

18-24 when thermal loads are higher than electric loads, and the CHP constantly produces maximum power of 55 kW. For hours 7-17, the CHP has lower power output to meet the decreasing demand of thermal loads. As a result, electric grid power increases to pick up the electric loads in the building.

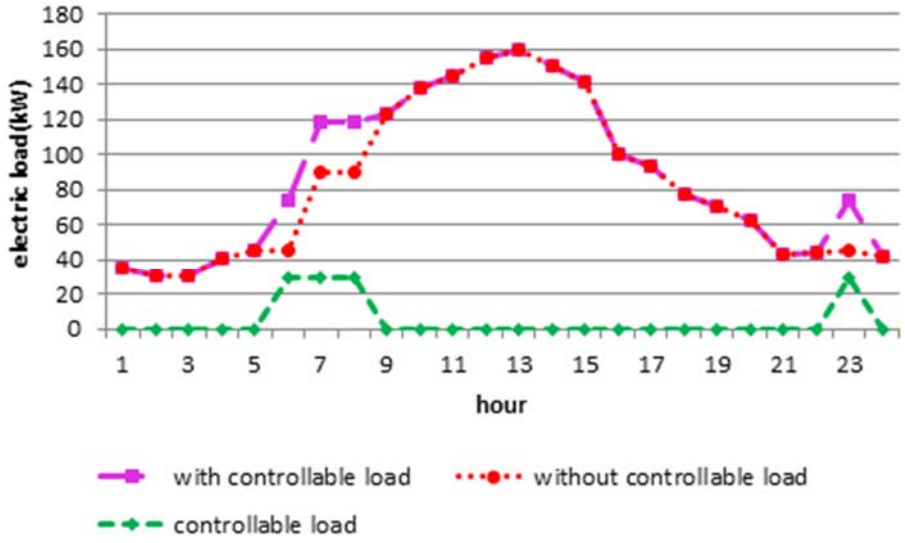


Figure 3.12 Scheduling of controllable electric loads (Case 5)



www.manaraa.com

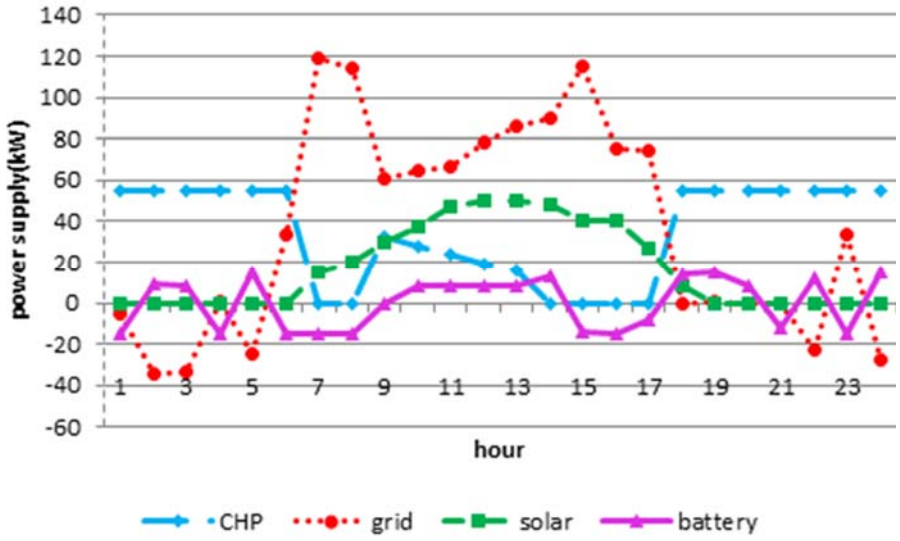


Figure 3.13 Electric power supply (Case 5)

### 3.4.3 Impact of controllable thermal loads

In Case 4, the controllable thermal loads are operated at hour 1-5. Figure 3.14 depicts the power supplied by the boiler for both controllable and non-controllable thermal loads.



www.manaraa.com

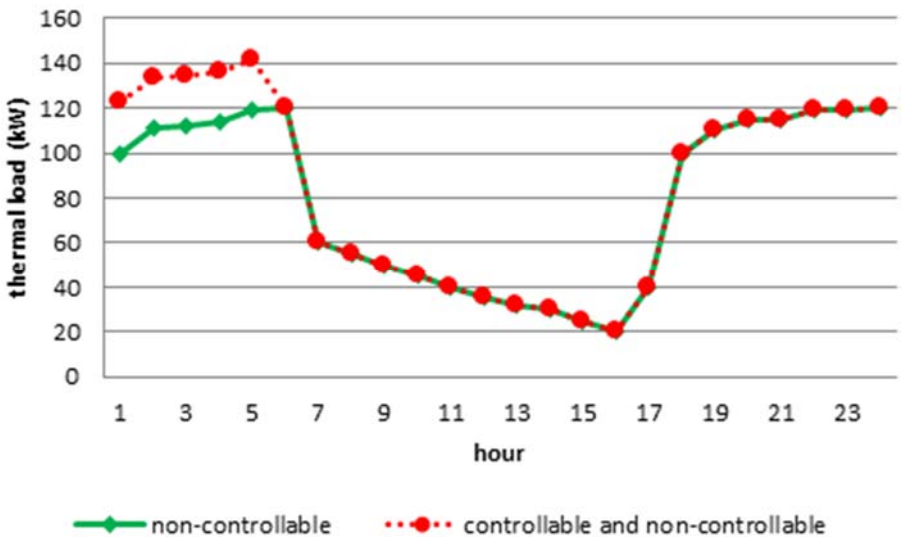


Figure 3.14 Scheduling of controllable thermal loads without CHP (Case 4)

In Case 5, due to the higher thermal loads than electric loads for hours 1-6, 18-24 as in Figure 2.1, it is noticed from Figure 3.15 that the CHP has higher power output than the boiler while contributing to the electric loads. It is also observed from Figure 3.16 that the CHP supplies the total power required by controllable thermal loads during hours 9-13. This is because of the cheaper cost of natural gas compared with the energy price from the electric grid as listed in Figure 3.6.



www.manaraa.com

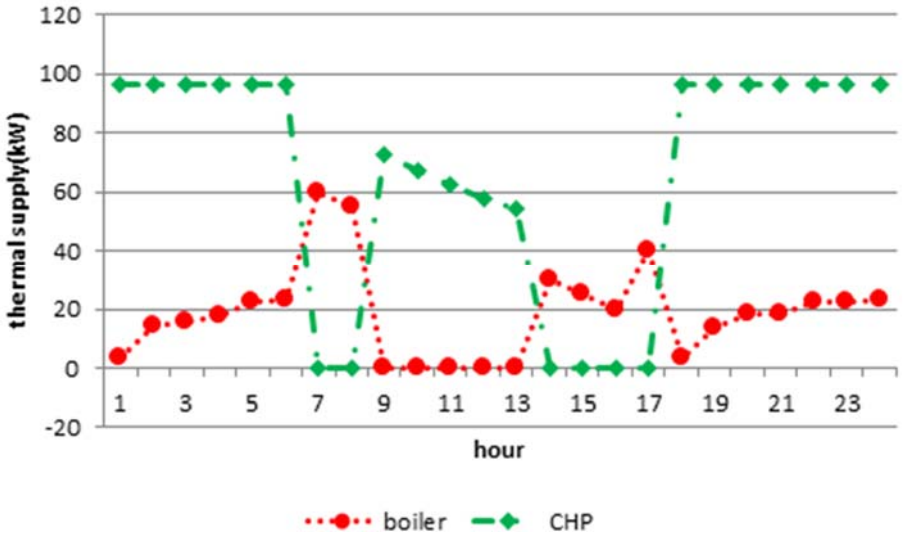


Figure 3.15 Thermal power supply from CHP and boiler (Case 5)

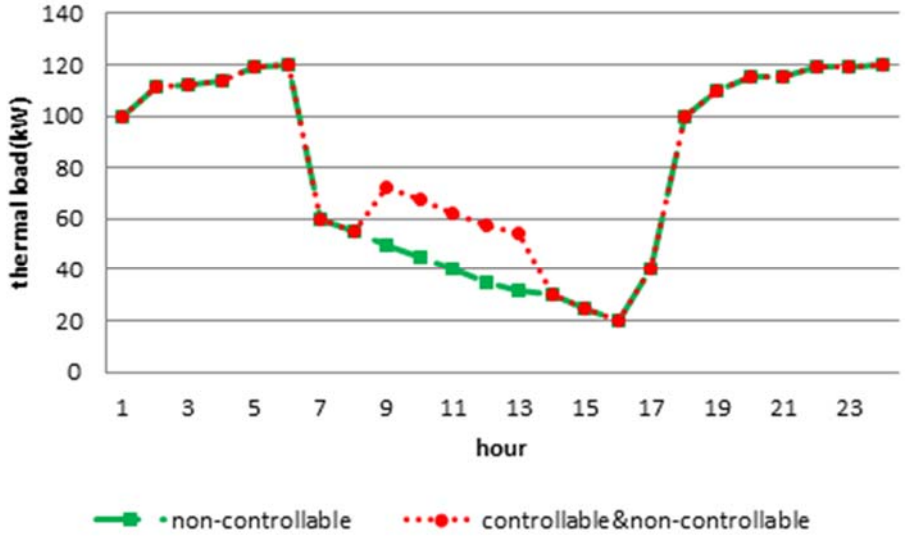


Figure 3.16 Scheduling of controllable thermal loads with CHP (Case 5)

## 3.5 Conclusion

In sum, a CHP system's energy consumption model is developed to simulate the energy consumption pattern of CHP systems. The system component characteristics and



www.manaraa.com

building energy demand are incorporated to optimize CHP systems' operation and performance. The optimization problem of building systems is introduced through the modeling of all components in energy-efficient building systems under the utility grid interconnection, including the power grid interface, CHP units, energy storage devices, and building appliances. The mixed energy sources are applied to collaboratively supply both electric and thermal loads.

The results of these case studies show the economically scheduling operation of the grid, battery devices, CHP and boiler units can provide a set of optimal solutions for the grid-tied energy-efficient building in order to fulfill the energy demand requirement while keeping the operating cost minimum.



www.manaraa.com

# CHAPTER IV

# STOCHASTIC OPTIMAL OPERATION OF ENERGY-EFFICIENT BUILDINGS

This chapter presents a multi-stage mixed integer stochastic programming model for the optimal operation of energy-efficient building systems considering controllable electric and thermal loads. In order to minimize energy usage expenses under uncertainty, the randomness with solar power production, non-controllable loads is incorporated in the optimization model with a multi-stage scenario tree, which represents hourly forecasts in the optimization period. The simulation results to the multi-stage stochastic programming problem offer a set of adaptive decision solutions within the scheduling horizon, which provides the optimal strategy of energy dispatch from various energy resources for each realization of the uncertainty. Hence, the operation of energy-efficient buildings will be more robust against changes in uncertain variables.

## 4.1 Stochastic formulation

An uncertain future requires that we consider multiple solutions to deliver cost-effective and reliable energy. The stochastic modeling addresses the risk due to energy consumption and renewable energy production volatility. Moreover, the optimal operation of building energy systems involves the decision-making under uncertainty. In order to minimize the daily production cost of the building energy systems under uncertainty from the energy consumption and renewable energy generation, the multi-



www.manaraa.com

stage stochastic programming is a promising approach to mathematically represent the stochastic decision-making problem accounting for the impact of the uncertainty on power dispatch decisions of energy-efficient buildings.

With the consideration of uncertainties ($P_{sol}$, $P_{nc}$, $H_{nc}$), a multi-stage SP model is designed where a set of decisions ($P_{gf}, P_{gt}, F_{chp}, F_{boi}$) are to be made sequentially using the partial revealed information. Assume that there are several scenarios to model the uncertain variables in the problem, and the probability of each scenario is $\rho_{tj}$ with $\sum_{j=1}^{J_t} \rho_{tj} = 1$ for $t = 2, \cdots, T$. The objective function is shown as follows.

$$\begin{aligned} Min \quad & C_{gf,1} \cdot P_{gf,1} - C_{gt,1} \cdot P_{gt,1} + C_{gas,1} \cdot (F_{chp,1} + F_{boi,1}) \\ & + \sum_{t=2}^{T} \sum_{j=1}^{J_t} \rho_{tj} [C_{gf,t} \cdot P_{gf,tj} - C_{gt,t} \cdot P_{gt,tj} + C_{gas,t} \cdot (F_{chp,tj} + F_{boi,tj})] \end{aligned} \tag{4.1}$$

In the above model, the first-stage variables consist of the electric outputs ($P_{gf}, P_{gt}, P_{chp}, P_{bc}, P_{bd}$) and thermal outputs ($F_{chp}$, $F_{boi}$) decisions at hour 1, which should be made irrelevant of the actual loads ($P_{nc}, H_{nc}$) and the solar power generation ($P_{sol}$). In contrast, at the following stages $t \geq 2$, the future operation status and energy outputs of the electric grid, battery, and CHP with boiler unit are taken as wait-and-see variables, which are dependent on the uncovering of the uncertainty.

The basic system requirement is to continuously supply the non-controllable loads while optimally scheduling the controllable electric and thermal loads. Further operating constraints include the capacity limits for electricity from and to the electric grid, charging and discharging capacity of battery devices, power generation limits of CHP with boiler units.



www.manaraa.com

$$P_{gf,tj} - P_{gt,tj} + P_{chp,tj} + P_{bd,tj} - P_{bc,tj} + P_{sol,tj} = P_{nc,tj} + P_{cntr,t} \cdot x_{e\_cntr,tj} \tag{4.2}$$

$$\eta_{hc}(H_{chp,tj} + H_{boi,tj}) = H_{nc,tj} + H_{cntr,t} \cdot x_{h\_cntr,tj} + H_{exh,tj} \tag{4.3}$$

$$0 \le P_{gf,tj} \le M_{gf} \cdot x_{gf,tj} \tag{4.4}$$

$$0 \le P_{gt,tj} \le M_{gt} \cdot x_{gt,tj} \tag{4.5}$$

$$S_{bat,t+1,j} = S_{bat,tj} + (\eta_{bc} \cdot P_{bc,t+1,j} - P_{bd,t+1,j} / \eta_{bd}) \cdot T_d / C_{bat}^{\max} \tag{4.6}$$

$$S_{bat}^{\min} \le S_{bat,tj} \le S_{bat}^{\max} \tag{4.7}$$

$$S_{bat,tj}^{0} = S_{bat,tj}^{T} = \hat{S}_{bat} \tag{4.8}$$

$$P_{bd}^{\min} \cdot x_{bd,tj} \le P_{bd,tj} \le P_{bd}^{\max} \cdot x_{bd,tj} \tag{4.9}$$

$$P_{bc}^{\min} \cdot x_{bc,tj} \le P_{bc,tj} \le P_{bc}^{\max} \cdot x_{bc,tj} \tag{4.10}$$

$$F_{chp,tj} = a \cdot P_{chp,tj} + b \cdot x_{chp,tj} \tag{4.11}$$

$$H_{chp,tj} = \eta_{hre}(F_{chp,tj} - P_{chp,tj}) \tag{4.12}$$

$$P_{chp}^{\min} \cdot x_{chp,tj} \le P_{chp,tj} \le P_{chp}^{\max} \cdot x_{chp,tj} \tag{4.13}$$

$$H_{boi,tj} = \eta_{boi} \cdot F_{boi,tj} \tag{4.14}$$

$$H_{boi}^{\min} \cdot x_{boi,tj} \le H_{boi,tj} \le H_{boi}^{\max} \cdot x_{boi,tj} \tag{4.15}$$

$$x_{gf,tj} + x_{gt,tj} \le 1 \tag{4.16}$$

$$0 \le x_{bc,tj} + x_{bd,tj} \le 1 \tag{4.17}$$

$$0 \le x_{bc,tj}, x_{bd,tj}, x_{gf,tj}, x_{gt,tj}, x_{chp,tj}, x_{boi,tj} \le 1 \tag{4.18}$$

Where $P_{cntr,t}$ includes both interruptible and non-interruptible electrical loads; $H_{exh,tj}$



www.manaraa.com

represents the exhausted heat from the building; $H_{cntr,t}$ includes both interruptible and non-interruptible thermal loads. The electric power and thermal balance constraints are represented in (4.2)-(4.3), respectively. The electric grid interface operation for selling and purchasing power are constrained by (4.4)-(4.5). The state of charge of the battery is determined through (4.6)-(4.8), and both charging and discharging rate limits of the battery are formulated in (4.9)-(4.10). Electrical and thermal operation limits of CHP with boiler are listed in (4.11)-(4.15). The constraints for binary status variables consist of (4.16)-(4.18).

Finally, response characteristics of controllable loads will be modeled as interruptible and non-interruptible types. For interruptible electric loads, it includes PHEV; dishwasher, cloth dryer and washing machine belong to the type of non-interruptible electric loads; electrical water heater is either non-interruptible or interruptible thermal loads [85].

For interruptible loads, the minimum continuous operation period is 1 hour. The constraints for interruptible loads are the minimum and maximum power consumption requirements, as shown in (4.19) for electric loads and in (4.20) for thermal loads.

$$E_p^{\min} \le \sum_{t=1}^{T} P_{cntr,t} \cdot x_{e\_cntr,tj} \le E_p^{\max} \tag{4.19}$$

$$E_h^{\min} \le \sum_{t=1}^{T} H_{cntr,t} \cdot x_{h\_cntr,tj} \le E_h^{\max} \tag{4.20}$$

For non-interruptible electric and thermal loads, the minimum continuous operation requirements are formulated as in (4.21)-(4.22). Because of the non-



www.manaraa.com

interruptible nature of the loads, the minimum and maximum energy consumptions are therefore the same.

$$\sum_{t=k}^{k+T_{ele,ON}-1} x_{e\_cntr,tj} \geq T_{ele,ON} \cdot (x_{e\_cntr,kj} - x_{e\_cntr,k-1,j}), k = 1,\ldots,(T - T_{ele,ON} + 1) \quad (4.21)$$

$$\sum_{t=k}^{k+T_{heat,ON}-1} x_{h\_cntr,tj} \geq T_{heat,ON} \cdot (x_{h\_cntr,kj} - x_{h\_cntr,k-1,j}), k = 1,\ldots,(T - T_{heat,ON} + 1) \quad (4.22)$$

## 4.2 Multi-stage scenario tree generation and reduction

Assume that these three uncertainties are in normal distribution and independent from each other. In the multivariate ARMA (1, 1) time series model, the auto-regressive parameter $\alpha_i$ is 0.95, and the moving average parameter $\beta_i$ is 0.02. This approach means that forecast errors $v_{tj}$ in (4.23) are simulated for solar power generation and load demands through (2.30)-(2.32). The real solar power and energy consumption at time t is computed as the sum of the measured time series from the historic data and the forecast error from ARMA model as in (4.24).

$$v_{tj} = (\Delta P_{sol,tj}, \Delta P_{nc,tj}, \Delta H_{nc,tj})^T \quad (4.23)$$

$$\begin{bmatrix} \tilde{P}_{sol,tj} \\ \tilde{P}_{nc,tj} \\ \tilde{H}_{nc,tj} \end{bmatrix} = \begin{bmatrix} P_{sol,tj} \\ P_{nc,tj} \\ H_{nc,tj} \end{bmatrix} + \begin{bmatrix} \Delta P_{sol,tj} \\ \Delta P_{nc,tj} \\ \Delta H_{nc,tj} \end{bmatrix} \quad (4.24)$$

Figure 4.1 shows the 100 scenarios for the uncertainty from non-controllable electric and thermal loads, as well as solar power generation within 24 hours. In the ARMA time series model, the standard deviations are 0.2 for non-controllable electric loads, 0.3 for non-controllable thermal loads, and 0.5 for solar power generation,



www.manaraa.com

respectively. The generated scenarios will be used as the input of the scenario tree generation.

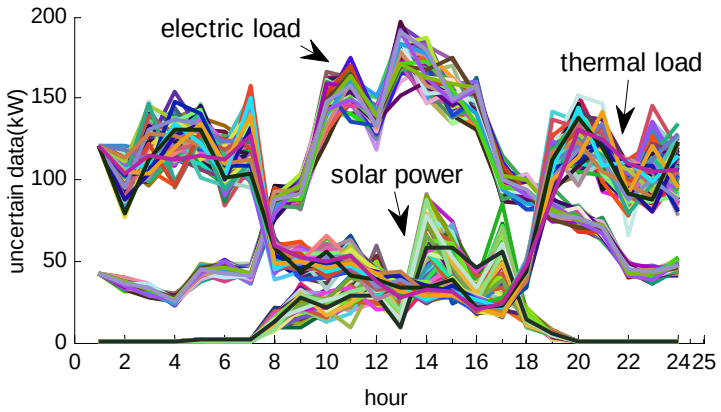


Figure 4.1 Scenarios generated for the uncertainty (100 groups)

A multi-stage scenario tree with hourly discretized data within one day is generated by conducting the scenario reduction algorithm, which is used as the input for the stochastic analysis. The scheduling horizon is hourly discretized into 3 stages, branching at hour 1 and 6. Through aggregating the 100 scenarios in Figure 4.1 into 9 reduced ones, the multi-stage scenario tree is shown in Figure 4.2. At each node, there are three data standing for the uncertainty from electric and thermal loads as well as solar power generation. The first stage is hour 1, the second stage is within hour 2 to hour 6, and the third stage starts from hour 7 to 24. Besides, the reduced scenarios are shown in Figure 4.3.



www.manaraa.com

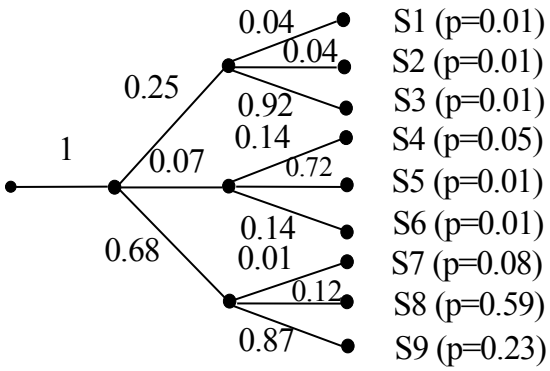


Figure 4.2 Scenario tree with probability

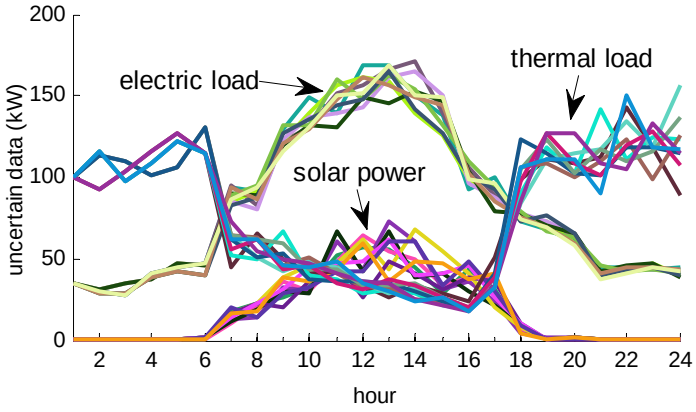


Figure 4.3 Reduced scenarios

## 4.3 Case Studies

The controllable loads are described in Table 4.1. For non- interruptible electric and thermal loads, their initial statuses are set to be OFF and OFF separately; the minimum ON hours are 4, 5 respectively; the power demands are 29 kW and 47 kW at the operating hour. The Maximum and minimum controllable energies are set to be the same, 116 kWh for non- interruptible electric loads, and 235 kWh for non- interruptible thermal loads. Hence, the total operating hours for non- interruptible loads are 4 hours for



www.manaraa.com

electric loads and 5 hours for thermal loads. The following analysis for stochastic cases is based on the 4th scenario ($S_4$) among 9 scenarios.

Table 4.1 Controllable loads data

| Controllable loads | | Initial state | Min. ON hours | Power demand per hour (kW) | Energy demand range (kWh) | Total operating hours |
|---|---|---|---|---|---|---|
| Electric loads | Interruptible | OFF | 1 | 18 | [50, 56] | 3 |
| | Non-interruptible | OFF | 4 | 29 | [116, 116] | 4 |
| Thermal loads | Interruptible | OFF | 1 | 30 | [80, 100] | 3 |
| | Non-interruptible | OFF | 5 | 47 | [235, 235] | 5 |

### 4.3.1 Impact of CHP on energy supply

We are going to discuss the operation decision under the impact of the commitment of CHP. In this case, only non-controllable loads are considered. Compared to the daily cost of $211.1 without the operation of CHP, it would be decreased to $173.8 when CHP is involved in the building system.

#### 4.3.1.1 Power supply

Without CHP as shown in Figure 4.4, most of the power will be supplied from electric grid. Battery takes the role of storage, it charges when there is extra power from



www.manaraa.com

electric grid and solar panel; and discharges when the power is not enough. Solar power has a big contribution during noon time.

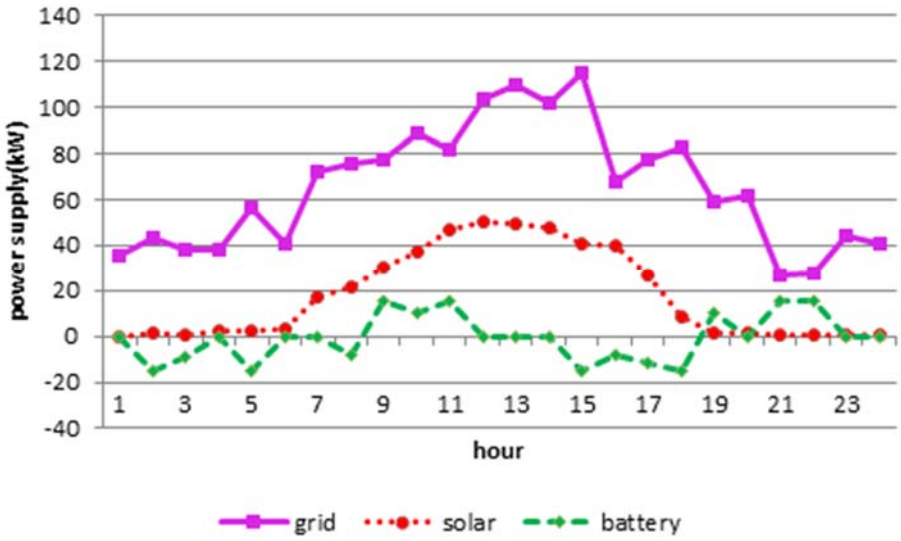


Figure 4.4 Power supply without CHP ($S_4$)

For hours 1-6, 21-24 in Figure 4.5, the electric loads are totally supplied by CHP. During this period, the extra power will be fed back to the electric grid except hour 5. During hours 7-19, there is no power fed back to the electric grid, it is supplying power to the building. It is noted that the CHP unit, battery and solar panel are collaboratively supplying power for the building and the grid at hour 20. Battery charges at hours 7-8, 17-18 while the solar power is contributing to energy production; also charges at hour 5 with the extra power from CHP. It discharges at hour 10-11 and 13-14 with high electric demands, and hour 19-20 with low solar power production.



www.manaraa.com

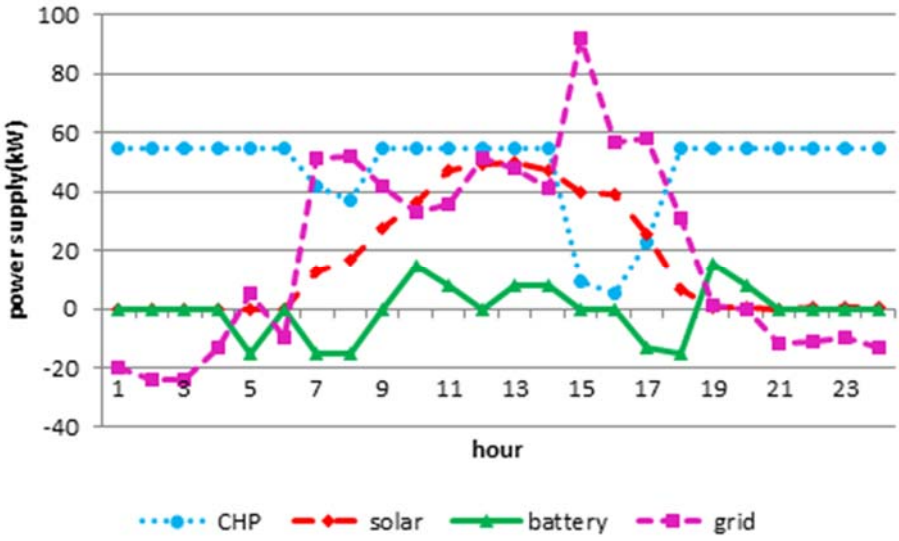


Figure 4.5 Power supply with CHP ($S_4$)

#### 4.3.1.2 Thermal supply

When the CHP is not committed, the boiler will take over the responsibility for providing the total thermal loads. However, when CHP is involved in the building system as shown in Figure 4.6, then the CHP system is supplying much more power for the thermal loads than the boiler unit does. The thermal supply from the CHP is constantly 74 kW when the electricity price from the electric grid is relatively high during hours 1-6, 9-14 &18-24. However, it decreases during hours 7-8 &15-17 as the thermal demands are decreasing. In addition, there will be extra thermal supply from the CHP during hours 9-14 with low thermal demands, which decreases the daily operation cost by 17.6%.



www.manaraa.com

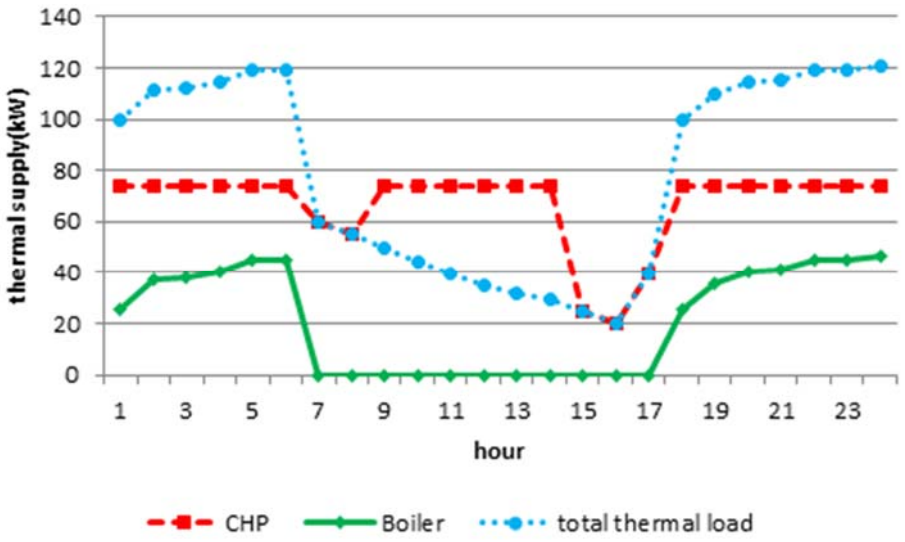


Figure 4.6 Thermal supply with CHP ($S_4$)

### 4.3.2 Impact of battery on energy supply

This case is designed in order to investigate the impact of battery on the operation of CHP and grid, where controllable loads are not considered either. Figure 4.7 shows the power supply from various energy sources except the battery. When the battery is considered in power supply (Figure 4.8), the operation of the grid is changed while the CHP unit doesn't because its thermal output is determined by the thermal demand. The change of power output from the grid is due to the charging and discharging effect of the battery. The operation of battery can decrease the daily cost from $176.5 to $173.8.



www.manaraa.com

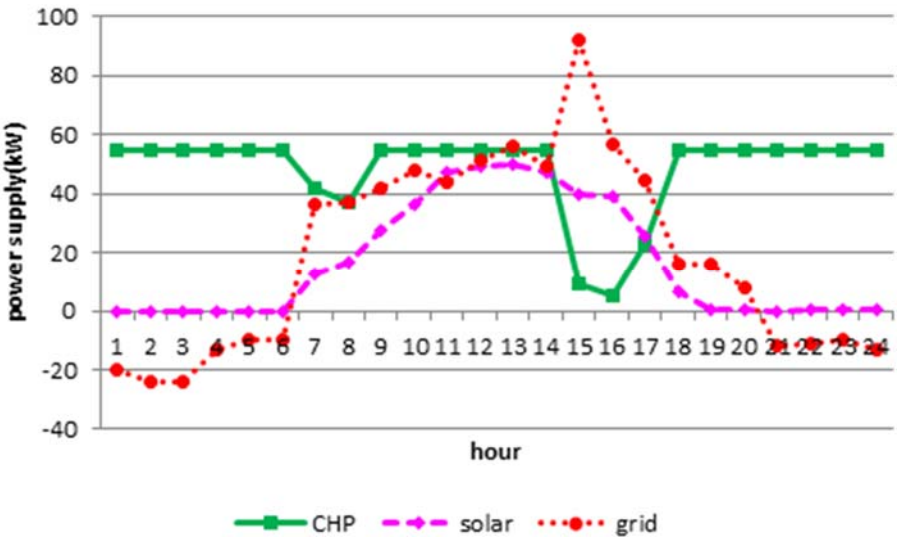


Figure 4.7 Power supply without battery ($S_4$)

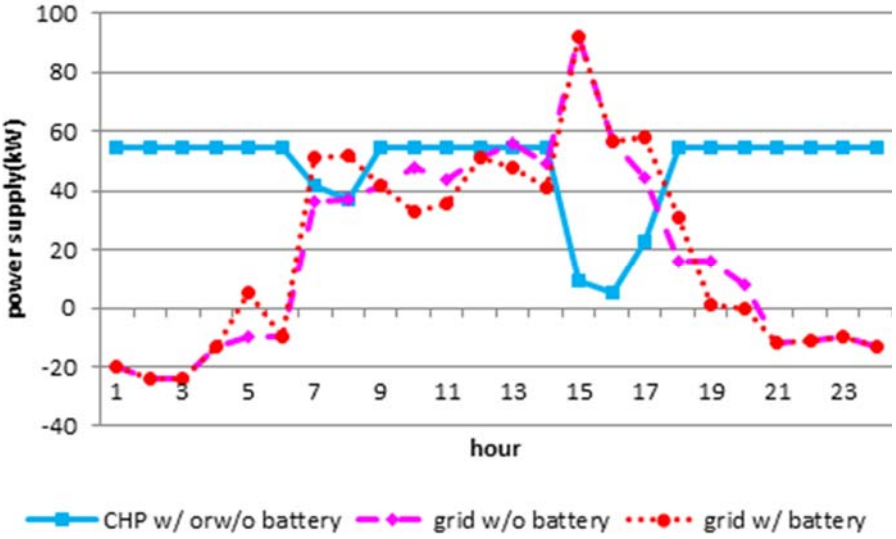


Figure 4.8 Power supply with battery ($S_4$)



www.manaraa.com

### 4.3.3 Impact of controllable loads on energy supply

#### 4.3.3.1 Controllable electric loads

From Figure 4.9, interruptible electric loads are operated at hours 1, 7, 8; non-interruptible electric loads are in operation from hour 1-4 due to the low energy price. Figure 4.10 shows the power supply with the consideration of controllable electric loads, which increases the daily operation cost from \$173.8 to \$183.6 compared with the case when no controllable electric loads are considered.

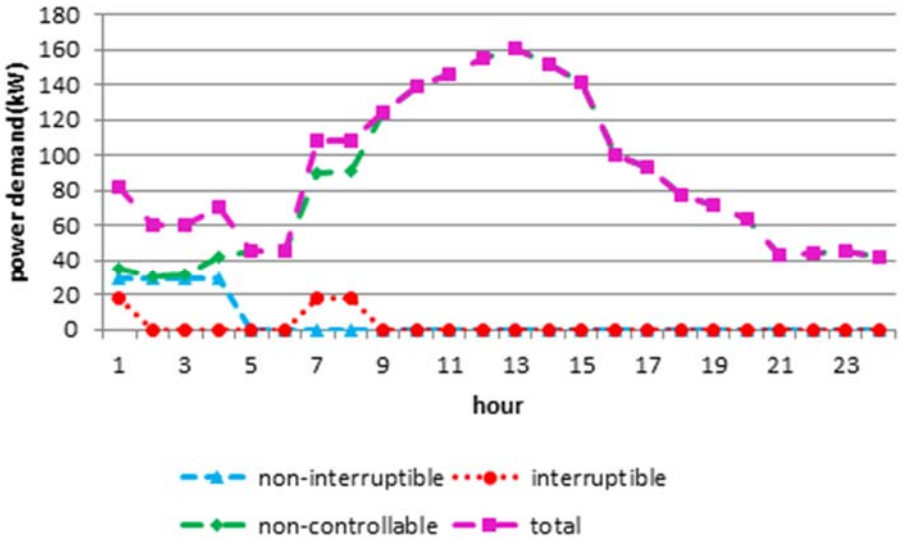


Figure 4.9 Power demand considering controllable electric loads ($S_4$)



www.manaraa.com

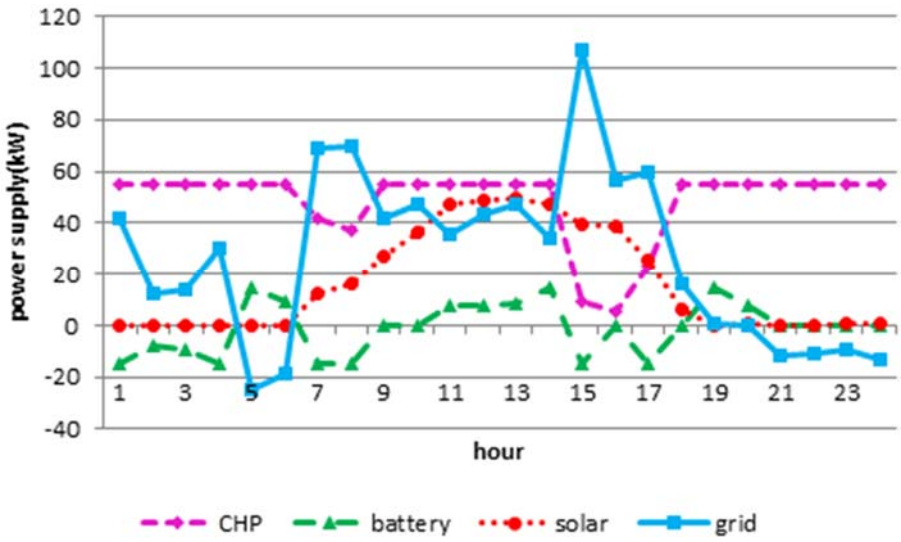


Figure 4.10 Power supply considering controllable electric loads ($S_4$)

The impact of the controllable electric loads on the power supply from the electric grid and the battery is compared respectively. The power output from the CHP has no change and is the same as shown in Figure 4.8. In Figure 4.11, there is energy exchanged from the building to the grid during hours 1-4 when no controllable electric loads are taken into account. In Figure 4.12, the operation of non-interruptible electric loads at hour 1-4 and the interruptible electric loads at hour 1 leads to the increased output from the electric grid and that the status of the battery changes from no power output to charging. No energy exchanges between the grid and the battery. It is observed that grid power increases during hour 7-8 in order to run the interruptible electric loads, but the battery has the same power output.



www.manaraa.com

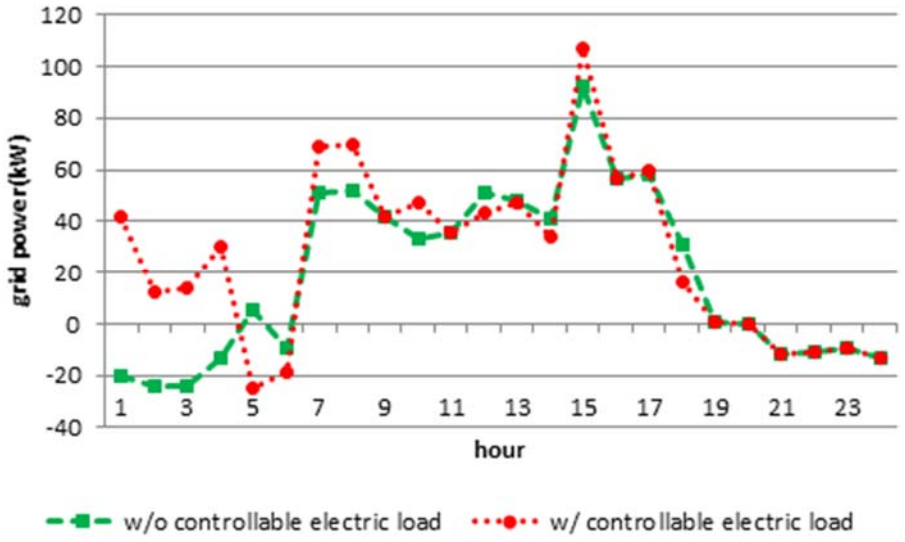


Figure 4.11 Impact of controllable electric loads on grid power supply ($S_4$)

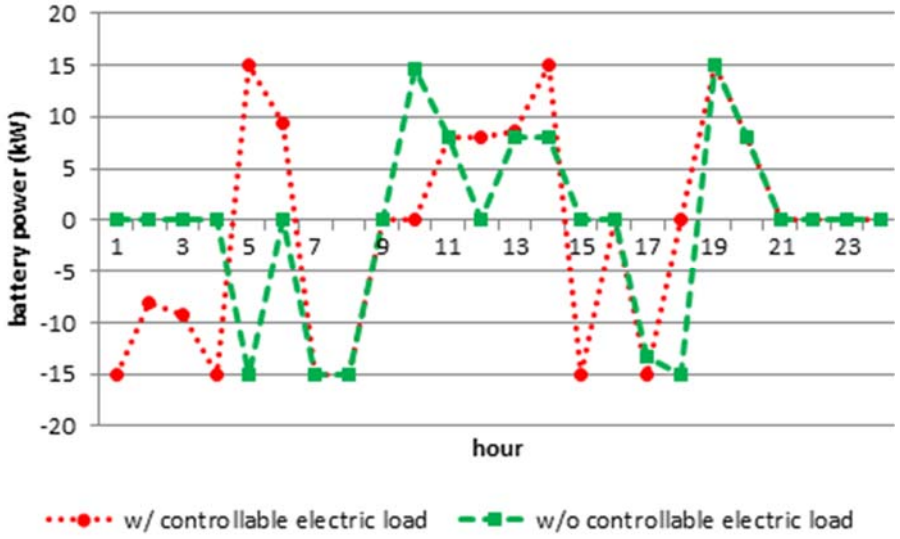


Figure 4.12 Impact of controllable electric loads on battery power supply ($S_4$)

#### 4.3.3.2 Controllable thermal loads

For interruptible thermal loads in Figure 4.13, they are operated at hours 1, 11, 13; while for non-interruptible thermal loads, they run from hours 1-5 when their initial status



www.manaraa.com

is ON. Therefore, the daily operation cost will be increased from $173.8 to $179.3. From hours 7-17 in Figure 4.14, the CHP is contributing due to the interruptible thermal loads and the high energy price from the electric grid.

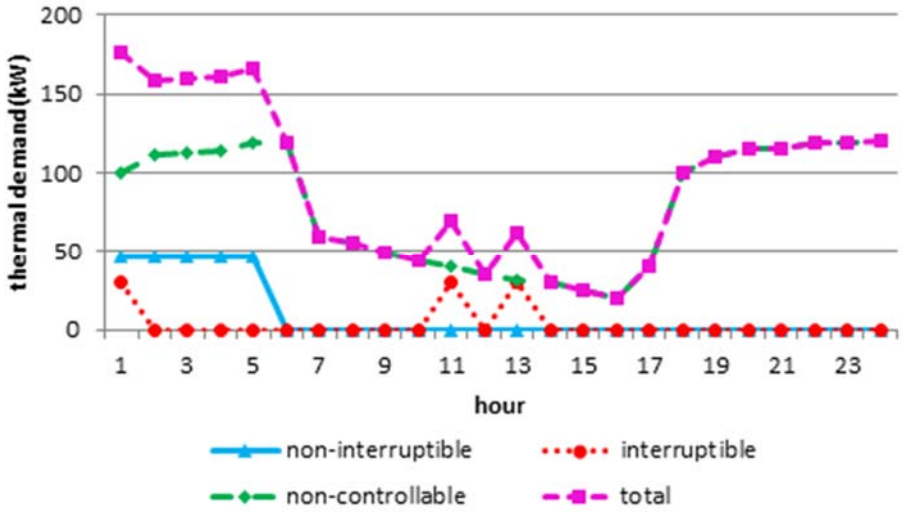


Figure 4.13 Thermal demand considering controllable thermal loads ($S_4$)

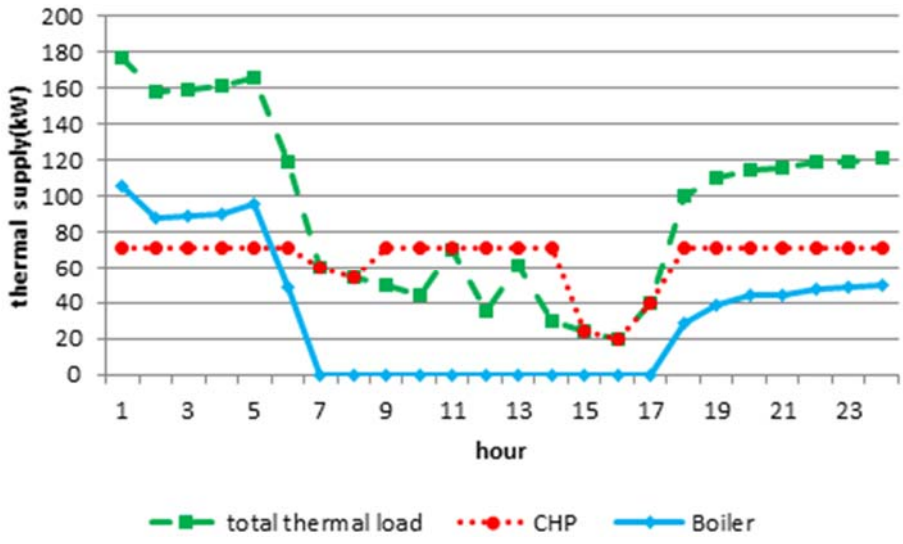


Figure 4.14 Thermal supply considering controllable thermal loads ($S_4$)



www.manaraa.com

The thermal output from the CHP unit will be slightly impacted by the operation of controllable thermal loads. With the consideration of controllable thermal loads, the thermal output from the CHP will be decreased from 74.1 kW to 70.8 kW (Figure 4.15) when the controllable thermal loads are running, including both interruptible loads at hour 1 and non-interruptible loads at hour 1-5 (Figure 4.13); while the boiler increases its thermal output in order to sufficiently supply thermal power to run the controllable thermal loads normally (Figure 4.16). At hour 6 without controllable thermal loads, the increased thermal power from the boiler supplements the reduced amount from the CHP. Even though the CHP lowers its thermal output during hour 9-14, the interruptible thermal loads at hour 11 and 13 are fulfilled by the CHP when the boiler has no any output. This can be explained by the fact that when no controllable loads are considered the extra thermal supply from the CHP is more than the amount the interruptible thermal loads require.



www.manaraa.com

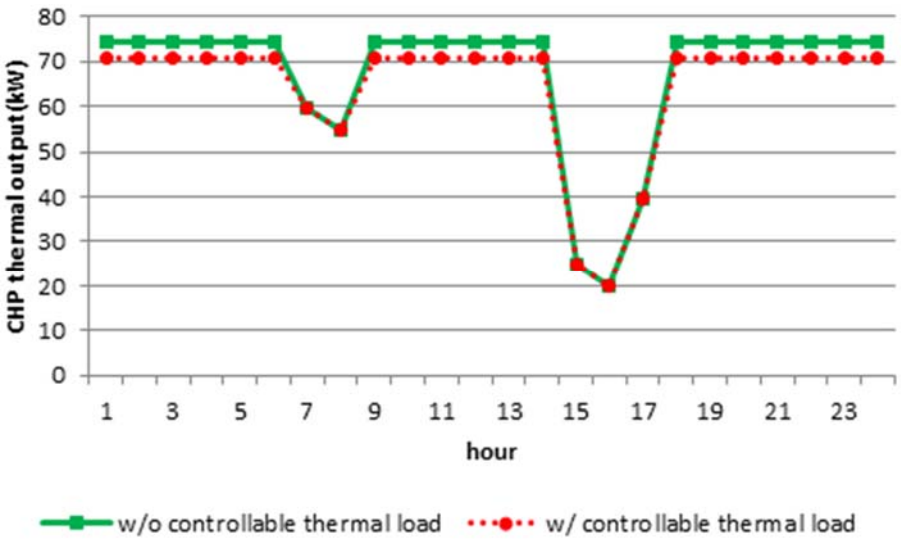


Figure 4.15 Impact of controllable thermal loads on CHP thermal supply ($S_4$)

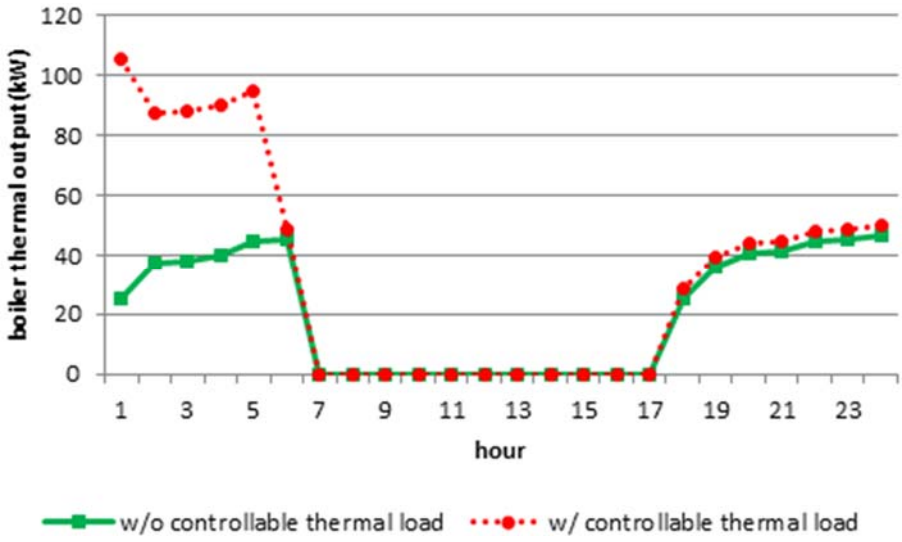


Figure 4.16 Impact of controllable thermal loads on boiler thermal supply ($S_4$)

## 4.4 Rolling stochastic optimal operation of building energy system

In practice, the scenarios in stochastic programming would deviate from the realized outcome of the uncertainty. In order to utilize the updated information of the



www.manaraa.com

uncertainty, the rolling stochastic strategy is proposed where hourly adjusted scenarios are considered. The stochastic optimization problem is solved for each hour to find the optimal solutions at the present and the future hours. The power dispatch decisions are supposed to be known for the past hours. However, only the current decisions would be taken into consideration. The benefit of considering the remaining hours is adaptability. Through this way the model would be less likely to jump into any possibly infeasible or hard-to-implement solution.

The decision structure is described in the left of Figure 4.17 which shows the scenario tree for several scheduling periods. The right of Figure 4.17 shows the flow chart for rolling scheduling purpose, where the multi-stage stochastic programming will be iterated until the max rolling horizon is met.

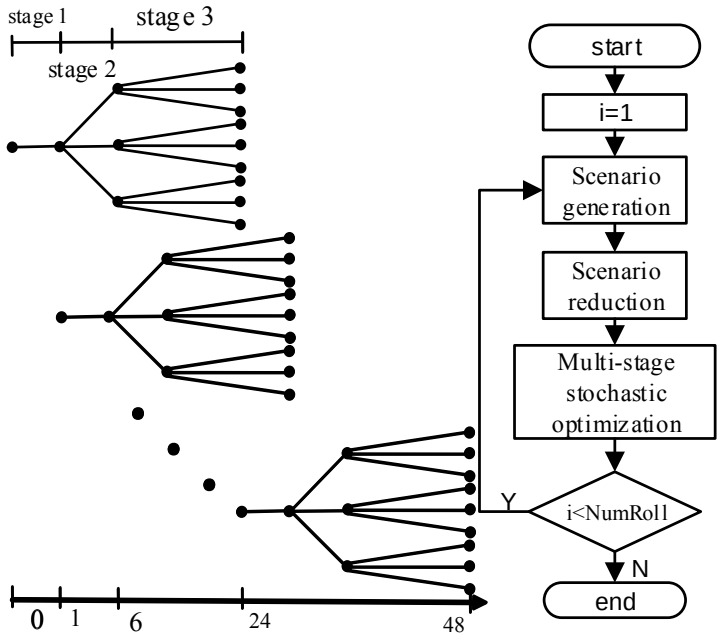


Figure 4.17 Diagram of rolling scheduling, left: decision structure, right: flow chart



www.manaraa.com

Table 4.2 lists the loads data. For controllable electric and thermal loads, their initial statuses are set to be OFF and ON separately; the minimum ON hours are 3, 4 respectively; the power demands are 29 kW and 22.5 kW at the operating hour. The Maximum and minimum controllable energies are set to be the same, 116 kWh for electric loads, and 112.5 kWh for thermal loads. Hence, the total operating hours under different cases are the same, 4 hours for electric loads and 5 hours for thermal loads.

Table 4.2 Loads data

| Loads | | Initial state | Min. ON hours | Power demand per hour (kW) | Energy demand range (kWh) | Total operating hours |
|---|---|---|---|---|---|---|
| Electric loads | Controllable | OFF | 3 | 29 | [116, 116] | 4 |
| | Non-controllable | -- | 1 | -- | -- | 24 |
| Thermal loads | Controllable | OFF | 4 | 22.5 | [112.5,112.5] | 5 |
| | Non-controllable | -- | 1 | -- | -- | 24 |

In order to analyze the effectiveness of the proposed algorithm, case studies are implemented to analyze the impact of uncertainties on the optimal operation of the energy-efficient buildings. It studies the stochastic behavior of the solar power source and loads with their hourly updated information.

During the test in rolling scheduling analysis, different scenarios for each uncertainty are generated at each hour. Figure 4.18 shows the difference of information between the updated and forecasted data during the 24 hours rolling period.



www.manaraa.com

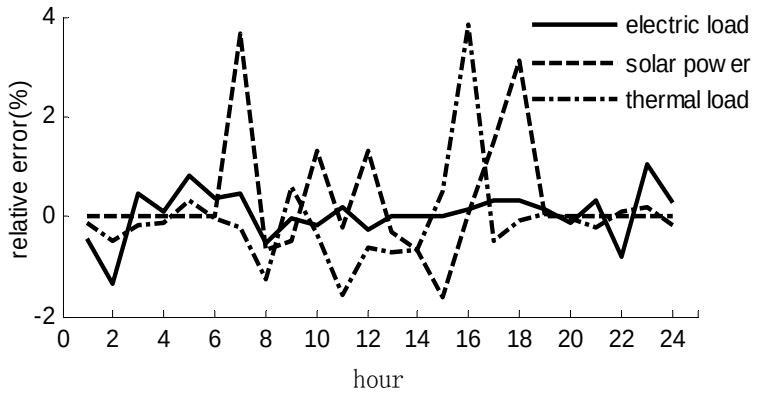


Figure 4.18 Relative errors of the uncertainty (rolling scheduling)

The operating cost of rolling stochastic method is $216.54, which is higher than the deterministic case. The case study shows that the random characteristics of these three uncertain variables increase the total operating cost by 10.76% compared with the deterministic case. The simulation results are shown in Figure 4.19-Figure 4.24. In Figure 4.19-Figure 4.20, due to the lower energy price and high energy efficiency of the CHP, electric grid supplies to electric loads almost zero or negative power during hours 1-6 and 18-24 when thermal loads are higher than electric loads, and CHP constantly produces maximum power of 55 kW. For hours 7-17, CHP has lower power output to meet the decreased demand of thermal loads. As a result, electric grid power increases to pick up the electric loads in the building. In the deterministic case, the controllable electric loads operate at hours 6-8 and 23. Due to the impact of uncertainties in the rolling stochastic case, the controllable electric loads are shifted to operate at hours 9-11 and 15.



www.manaraa.com

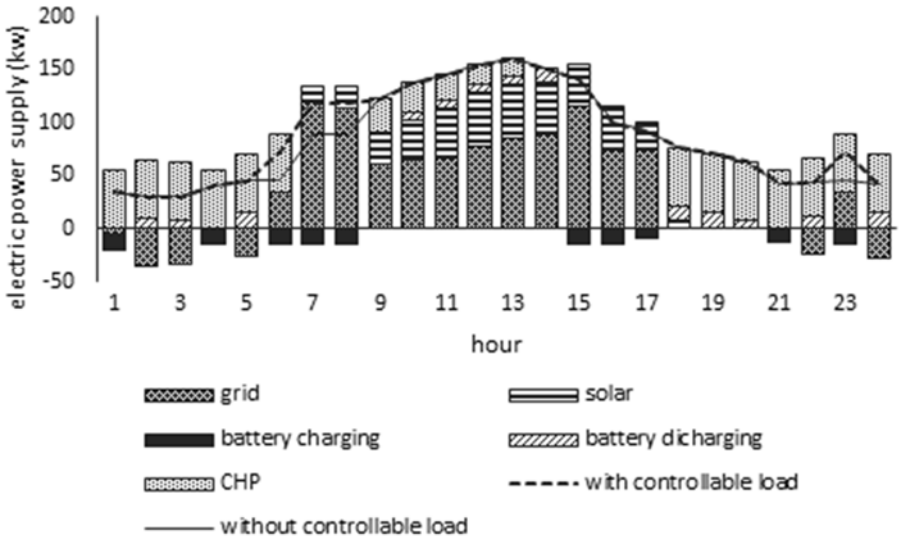


Figure 4.19 Electric power supply (deterministic)

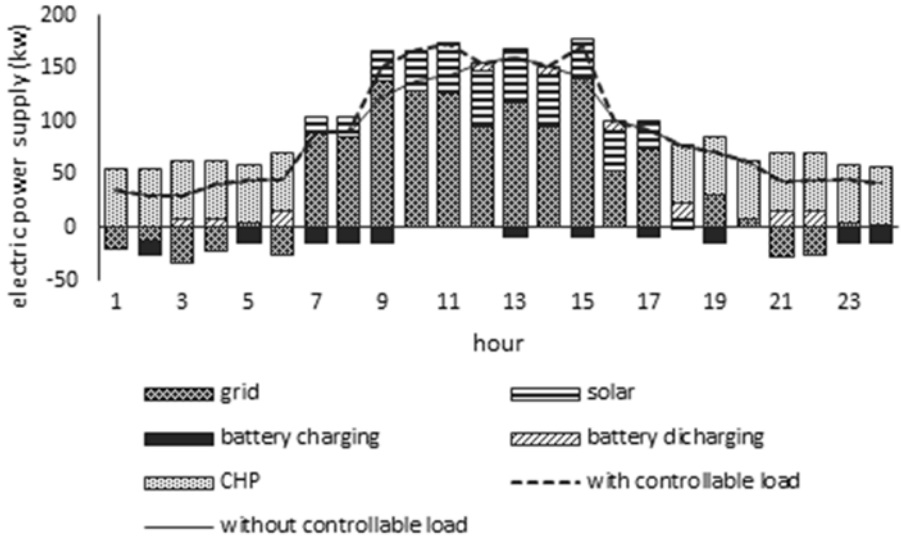


Figure 4.20 Electric power supply (stochastic)

Figure 4.21-Figure 4.24 illustrate the impact of uncertainties on the controllable thermal loads and thermal power supplied by the CHP with boiler unit. In deterministic case without uncertainty, due to the higher thermal loads than electric loads for hours 1-6,



www.manaraa.com

18-24 as shown in **Error! Reference source not found.**, the CHP has higher power output than the boiler while contributing to the electric loads. During hours 9-13 with the cheaper cost of natural gas compared with the energy price from the electric grid as listed in Figure 3.6, the CHP supplies the total power required by controllable thermal loads. In the rolling stochastic case, the controllable thermal loads are shifted to operate in hours 1-4 and 24, and they are supplied by both CHP and boiler.

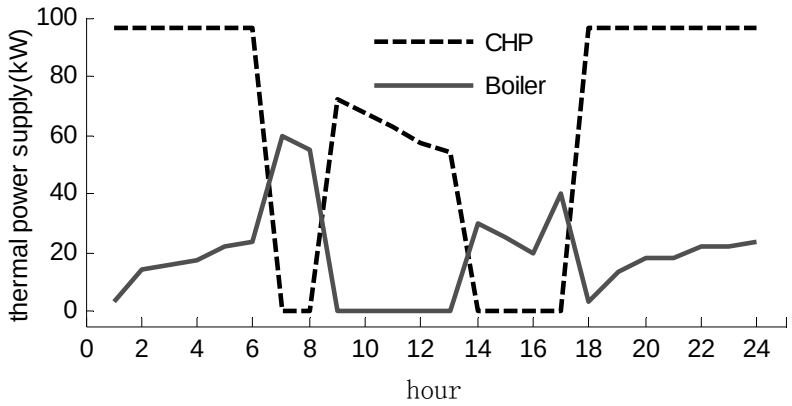


Figure 4.21 Thermal power supply (deterministic)

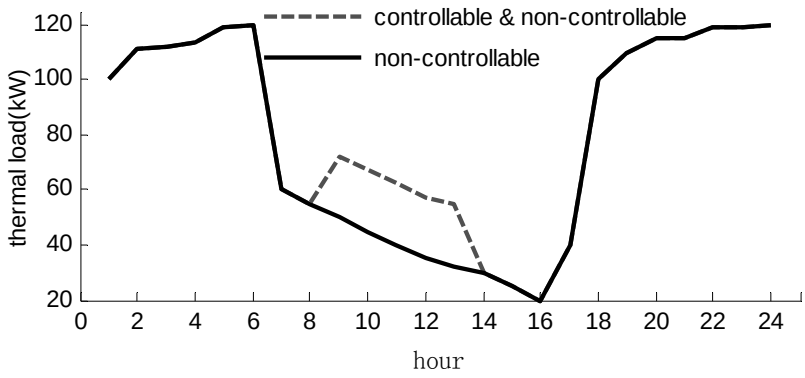


Figure 4.22 Thermal power demand (deterministic)



www.manaraa.com

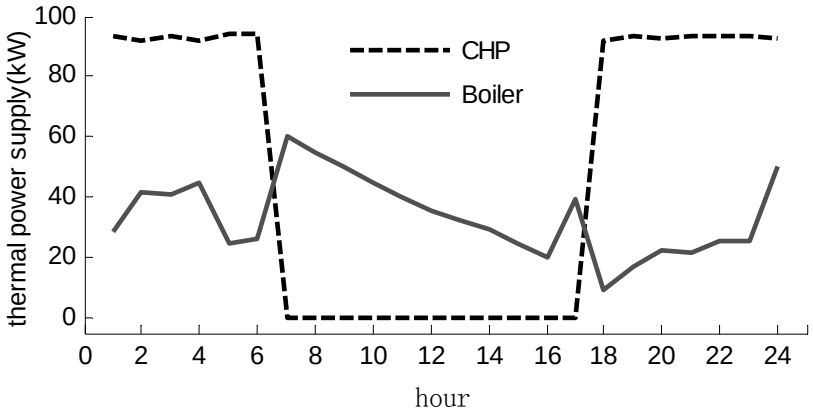


Figure 4.23 Thermal power supply (stochastic)

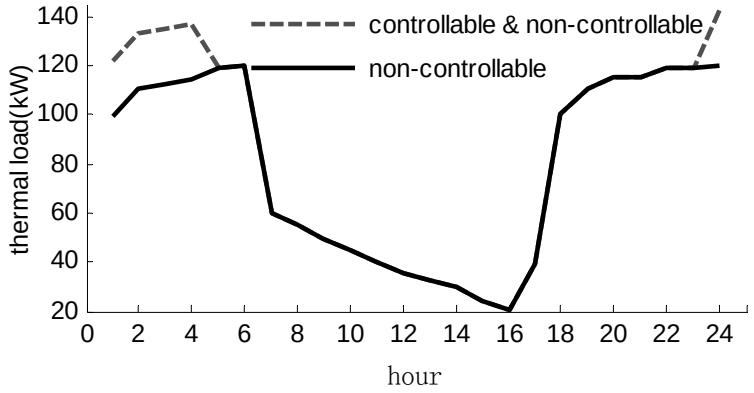


Figure 4.24 Thermal power demand (stochastic)

## 4.5 Conclusion

This chapter analyzes the optimal operation of energy-efficient building systems from the stochastic viewpoint. For the stochastic study, the impact of uncertainty on the operation for the building is taken into account. The multi-stage mixed-integer stochastic programming model is built for the optimal operation of energy-efficient building systems taking into account the random characteristics of non-controllable electric and thermal loads, and solar power generations. The CHP technology is proved to be



www.manaraa.com

effective in reducing the operating cost, and its operation is mainly determined by the thermal demands. The consideration of interruptible and non-interruptible loads can greatly impact the optimal decisions for the energy management of the grid, battery, and the CHP with boiler unit as well.



www.manaraa.com

CHAPTER V

ROBUST OPTIMAL OPERATION OF ENERGY-EFFICIENT BUILDINGS

This chapter proposes a robust optimization method for the optimal operation of energy-efficient building systems. Both of the CHP unit and battery are applied in the building energy system to overcome the drawbacks introduced by uncertainties. The effectiveness of the CHP and battery unit is investigated in alleviating the influence of intermittent solar power generation and variable customer loads. The proposed robust model is solved using mixed integer linear programming, and the model's robustness is adjusted against the level of conservatism of the solution.

## 5.1 Robust formulation

Assume that all the decision variables should be made before the revealing of the uncertainty from solar power generation, non-controllable electric and thermal loads. In both electric balance (3.21) and thermal balance (3.22), uncertainties $p_{solar}^t, p_{load}^t, H_{load}^t$ are modeled as asymmetric and bounded variables $\tilde{p}_{solar}^t, \tilde{p}_{load}^t, \tilde{H}_{load}^t$. None of controllable loads are considered in the robust optimal operation of the building energy systems. The uncertainty takes values in

$$\tilde{p}_{solar}^t = p_{solar}^t + \Delta p_{solar}^t, \hat{p}_{solar}^{lt} \le \Delta p_{solar}^t \le \hat{p}_{solar}^{ut} \tag{5.1}$$

$$\tilde{p}_{load}^t = p_{load}^t + \Delta p_{load}^t, \hat{p}_{load}^{lt} \le \Delta p_{load}^t \le \hat{p}_{load}^{ut} \tag{5.2}$$



www.manaraa.com

$$\tilde{H}^t_{load} = H^t_{load} + \Delta H^t_{load}, \hat{H}^{lt}_{load} \le \Delta H^t_{load} \le \hat{H}^{ut}_{load} \tag{5.3}$$

In the robust model, the objective function (5.4) is the same as (3.20) in the deterministic model. The electric power and thermal balances in the building should be met when the worst case of uncertainties occurs. For the electric loads balance in (5.5), the worst case would occur at the maximum increase in the electric loads and the maximum decrease in solar power generation. For the thermal loads balance in (5.6), the worst case would occur when the thermal loads reach the possible maximum value.

$$Min \quad \sum_{t=1}^{T} [c^t_{GF} \cdot p^t_{GF} - c^t_{GT} \cdot p^t_{GT} + c^t_{gas} \cdot (F^t_{CHP} + F^t_{boiler})] \cdot T_d \tag{5.4}$$

s.t.

$$\begin{aligned} & p^t_{GF} - p^t_{GT} + p^t_{CHP} - p^t_{BC} + p^t_{BD} + p^t_{solar} = p^t_{load} \\ & + Max \left\{ \hat{p}^{ut}_{load} \eta^{ut}_p + \hat{p}^{lt}_{load} \eta^{lt}_p - \hat{p}^{ut}_{solar} \eta^{ut}_{solar} - \hat{p}^{lt}_{solar} \eta^{lt}_{solar} \right\} \end{aligned} \tag{5.5}$$

$$\eta^{ut}_p + \eta^{lt}_p + \eta^{ut}_{solar} + \eta^{lt}_{solar} \le \Gamma^t_1 \tag{5.6}$$

$$0 \le \eta^{ut}_p, \eta^{lt}_p, \eta^{ut}_{solar}, \eta^{lt}_{solar} \le 1 \tag{5.7}$$

$$\eta_{hc} (H^t_{CHP} + H^t_{boiler}) = H^t_{load} + H^t_{exhausted} + Max \left\{ \hat{H}^{ut}_{load} \eta^{ut}_H + \hat{H}^{lt}_{load} \eta^{lt}_H \right\} \tag{5.8}$$

$$\eta^{ut}_H + \eta^{lt}_H \le \Gamma^t_2 \tag{5.9}$$

$$0 \le \eta^{ut}_H, \eta^{lt}_H \le 1 \tag{5.10}$$

and constraints (3.1)-(3.19).

Where $\eta^{ut}_p, \eta^{lt}_p, \eta^{ut}_{solar}, \eta^{lt}_{solar}$ are the scaled deviations for the random electric loads and solar power generation. Similarly, $\eta^{ut}_H, \eta^{lt}_H$ are the scaled deviations for the random thermal loads; $\Gamma^t_1, \Gamma^t_2$ are both the robust measurements for the adjustment of the robustness of the problem against the level of conservatism of the solution. $\Gamma^t_1$ is used to adjust the range of



www.manaraa.com

uncertainty set for electric loads and solar power generation at time *t*; $\Gamma_2^t$ is used for uncertain thermal loads at time *t*.

In order to make the above problem tractable, the following two sub-problems (5.11)-(5.13) and (5.14)-(5.16) need to be converted into the corresponding dual problems (5.17)-(5.20) and (5.21)-(5.23) by introducing dual variables $\lambda_1^t, \pi_{11}^{t+}, \pi_{11}^{t-}, \pi_{12}^{t+}, \pi_{12}^{t-}$ for constraints (5.12)-(5.13), and dual variables $\lambda_2^t, \pi_{21}^{t+}, \pi_{21}^{t-}$ for constraints (5.15)-(5.16), respectively.

Problem

$$Max\ \hat{p}_{load}^{ut}\eta_p^{ut} + \hat{p}_{load}^{lt}\eta_p^{lt} - \hat{p}_{solar}^{ut}\eta_{solar}^{ut} - \hat{p}_{solar}^{lt}\eta_{solar}^{lt} \tag{5.11}$$

s.t.
$$\eta_p^{ut} + \eta_p^{lt} + \eta_{solar}^{ut} + \eta_{solar}^{lt} \le \Gamma_1^t \tag{5.12}$$

$$0 \le \eta_p^{ut}, \eta_p^{lt}, \eta_{solar}^{ut}, \eta_{solar}^{lt} \le 1 \tag{5.13}$$

Problem

$$Max\ \hat{H}_{load}^{ut}\eta_H^{ut} + \hat{H}_{load}^{lt}\eta_H^{lt} \tag{5.14}$$

s.t.
$$\eta_H^{ut} + \eta_H^{lt} \le \Gamma_2^t \tag{5.15}$$

$$0 \le \eta_H^{ut}, \eta_H^{lt} \le 1 \tag{5.16}$$

Problem

$$Min\ \lambda_1^t\Gamma_1^t + \pi_{11}^{t+} + \pi_{11}^{t-} + \pi_{12}^{t+} + \pi_{12}^{t-} \tag{5.17}$$

s.t.
$$\lambda_1^t + \pi_{11}^{t+} \ge \hat{p}_{load}^{ut}, \lambda_1^t + \pi_{11}^{t-} \ge \hat{p}_{load}^{lt} \tag{5.18}$$

$$\lambda_1^t + \pi_{12}^{t+} \ge -\hat{p}_{solar}^{ut}, \lambda_1^t + \pi_{12}^{t-} \ge -\hat{p}_{solar}^{lt} \tag{5.19}$$



www.manaraa.com

$$\lambda_1^t, \pi_{11}^{t\pm}, \pi_{12}^{t\pm} \geq 0 \tag{5.20}$$

Problem

$$Min \quad \lambda_2^t \Gamma_2^t + \pi_{21}^{t+} + \pi_{21}^{t-} \tag{5.21}$$

s.t. $$\lambda_2^t + \pi_{21}^{t+} \geq \hat{H}_{load}^{ut}, \lambda_2^t + \pi_{21}^{t-} \geq \hat{H}_{load}^{lt} \tag{5.22}$$

$$\lambda_2^t, \pi_{21}^{t\pm} \geq 0 \tag{5.23}$$

Finally, a tractable robust model can be formulated as follows,

$$Min \sum_{t=1}^{T} [c_{GF}^t \cdot p_{GF}^t - c_{GT}^t \cdot p_{GT}^t + c_{gas}^t \cdot (F_{CHP}^t + F_{boiler}^t)] \cdot T_d \tag{5.24}$$

s.t. $$p_{GF}^t + p_{GT}^t + p_{CHP}^t - p_{BC}^t + p_{BD}^t = p_{load}^t - p_{solar}^t + \lambda_1^t \Gamma_1^t + \pi_{11}^{t+} + \pi_{11}^{t-} + \pi_{12}^{t+} + \pi_{12}^{t-} \tag{5.25}$$

$$\eta_{hc}(H_{CHP}^t + H_{boiler}^t) = H_{load}^t + H_{exhausted}^t + \lambda_2^t \Gamma_2^t + \pi_{21}^{t\pm} \tag{5.26}$$

And constraints (3.1)-(3.19), (5.18)-(5.20), and (5.22)-(5.23).

## 5.2 Case studies

As shown in Table 5.1, both deterministic and robust cases are conducted to investigate the energy supply under the influence of 1) uncertain electric loads and solar power generation; 2) the battery; 3) the CHP; 4) the budget of robustness. $\Delta p_{load}^t$ is set to be within the range of [-4%, 5%] of the nominal electric loads; $\Delta H_{load}^t$ lies in the range of [-9%, 10%] of the nominal thermal loads; $\Delta p_{solar}^t$ is within [-20%, 19%] of the nominal solar power generation. Table 5.2 summarizes the comparison of daily operating costs obtained for both deterministic and robust cases.



www.manaraa.com

Table 5.1 Cases for deterministic and robust models

| Cases | | 1 | 2 | 3 | 4 | 5 |
|---|---|---|---|---|---|---|
| Power generation | Electric grid | × | × | × | × | × |
| | Solar | | × | × | × | × |
| | Battery | | | × | × | × |
| | CHP | | | | | × |
| | Boiler | | | | × | × |
| Loads | Electric loads | × | × | × | × | × |
| | Thermal loads | | | | × | × |

Table 5.2 Operating cost in cases 1-5 ($)

| Case | 1 | 2 | 3 | 4 | 5 |
|---|---|---|---|---|---|
| Deterministic | 184.7 | 143.5 | 138.2 | 211.1 | 172.3 |
| Robust | 193.9 | 160.9 | 155.7 | 235.9 | 195.6 |
| Increase (%) | 4.98 | 12.13 | 12.66 | 11.75 | 13.52 |

### 5.2.1 Influence of electric loads and solar power generation

As shown in Figure 5.1, compared with the deterministic Case 1, the uncertain electric loads lead to a much higher grid power supply in the robust Case 1 with an increase in cost by 4.98%. In Case 2, the integration of solar energy contributes to provide a portion of the electric loads, which can be observed from the reduction of grid power supply compared with Case 1. However, the robust Case 2 has a lower reduction as the solar power generation is reduced due to its uncertainty. Moreover, the combined influence of uncertain electric loads and solar power generation results in the increase in operating cost by 12.13%.



www.manaraa.com

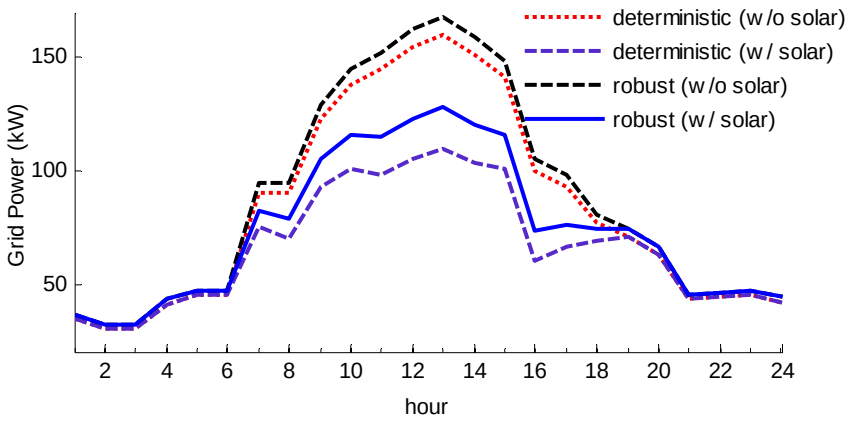


Figure 5.1 Grid power for cases 1 and 2

### 5.2.2 Effect of the battery

In Figure 5.2, the commitment of the battery causes the difference in grid power supply between Cases 2 and 3. As indicated in Figure 5.3, the battery is discharging during most of the hours with high energy purchasing price from the grid. Consequently, the grid power in Case 3 is lower than that in Case 2 (e.g. hours 9, 10, 12, 14, 19, 21, 22 in the deterministic Case 3, and hours 10, 11, 13, 14, 19, 21, 22 in the robust Case 3). While the energy purchasing price is low enough, the battery is charging during hours 1, 2, 7, 8, 15-18, 23 in the deterministic Case 3, and hours 1, 3, 5-8, 15, 17, 18, 23 in the robust Case 3. Therefore, the grid power in Case 3 is higher than the corresponding one in Case 2. There is no change in SOC at the remaining hours 3-5, 11, 20 in the deterministic Case 3 and at hours 9, 16, 20 in the robust Case 3. Due to the charging and discharging effect of the battery in Case 3, the total operating cost is reduced by 3.69% in deterministic Case 3 and by 3.23% in robust Case 3.

By comparing the robust Case 3 with the deterministic Case 2, we explore the effect of the battery in alleviating the influence of additional power demand caused by the



www.manaraa.com

uncertain electric loads and solar power generation. When the SOC of battery is increasing (which means the battery is charging) or keeps constant (which means the battery is idle) at hours 1, 3, 5-9, 12, 15-18, 20, 23 as shown in Figure 5.3, the additional power demand is totally supplied by the grid. When the SOC is decreasing (which means the battery is discharging) at hours 2, 4, 10, 11, 13, 14, 19, 21, 22, 24, the grid provides lower power and the battery not only supplies the additional power demand, but also covers a portion of normal building power. Therefore, the battery is effective in coordinating with the electric grid to meet the uncertain power demand.

Without the battery, the robust Case 2 always needs a higher grid power supply than the deterministic Case 2 due to the combined influence of uncertain electric loads and solar power generation. However, with the battery, it is possible that the grid power supply in the robust Case 3 is lower than that in the deterministic Case 3 due to the response of the battery to uncertainties. For robust Cases 2 and 3 in Table 5.1, it can be seen that the daily operating cost increases by 8.5% with the battery, while it has a higher increase of 12.13% without the battery. Therefore, the battery is an economic means to supply uncertain power demand.



www.manaraa.com

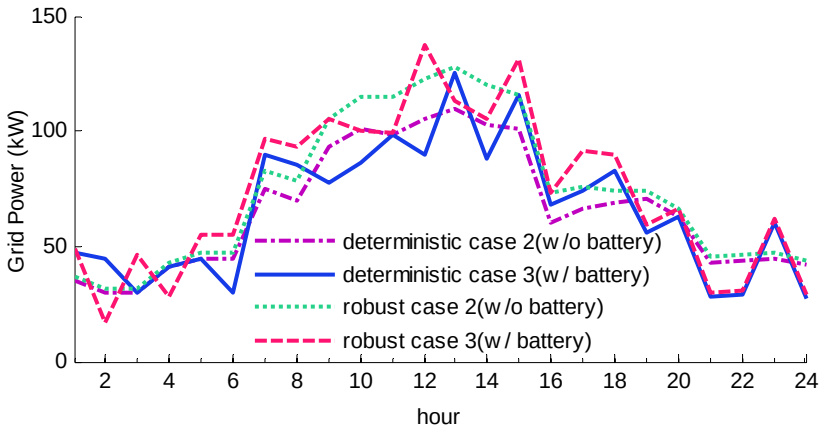


Figure 5.2 Effect of the battery on grid power (Cases 2 & 3)

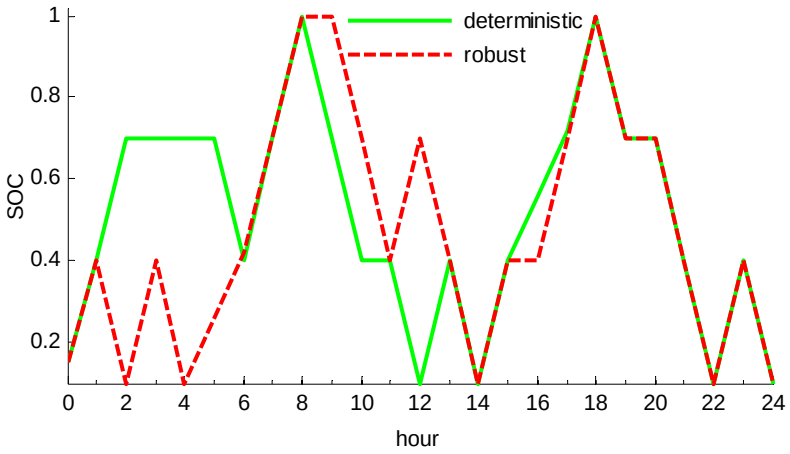


Figure 5.3 Effect of the battery on SOC of the battery (Case 3)

### 5.2.3 Effect of the CHP

In Figure 5.4, by coupling electric and thermal energy supply, the introduction of the CHP results in the reduction in the power supply from both the grid and battery in Case 5. Due to the response of the CHP to both uncertain electric and thermal energy



www.manaraa.com

requests, the total operating cost is reduced by 18.38% in deterministic Case 5 and by 17.08% in robust Case 5.

Compared with the deterministic Case 4, when there is lower power supply from both the grid and battery in the robust Case 5, the CHP supplies the additional power demand at hours 1-14,17-24. When there is higher power supply from both the grid and battery during hours 15 and 16, the grid, battery and CHP contribute to the additional power demand together. Thus, the CHP is effective in coordinating with the grid and battery in supplying uncertain power demand.

No matter whether the CHP is involved or not, the power supply from both the grid and battery in the robust Case is always higher than that in the corresponding deterministic Case because of the uncertain electric loads and solar generation. For robust Cases 4 and 5 in Table 5.1, it can be observed that the daily operating cost increases by 11.75% without the CHP, while it decreases by 7.34% with the CHP. Therefore, the CHP is also an economic way to meet the uncertain power demand.

In Figure 5.5, there is higher thermal supply in the robust Case 4 than in the deterministic Case 4 due to the uncertainty in the thermal loads. During hours 9-14 in the robust Case 5, the thermal supplied by the CHP is higher than the actual thermal demand which is the same as that in the robust Case 4. It means that the excess thermal supply from the CHP is exhausted when the energy purchasing price from the grid is relatively higher than the CHP generation cost.



www.manaraa.com

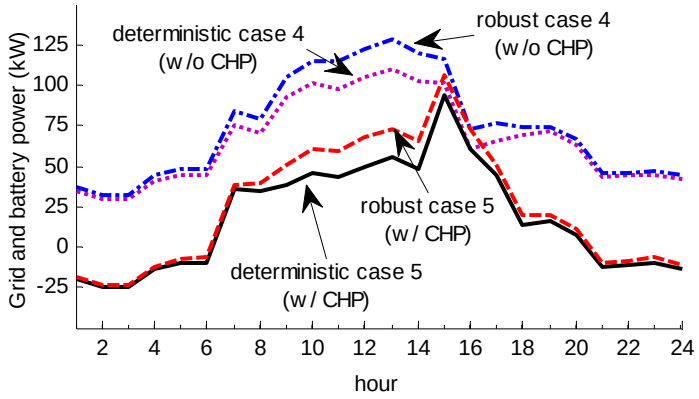


Figure 5.4 Effect of the CHP on electric power supply from the grid and battery

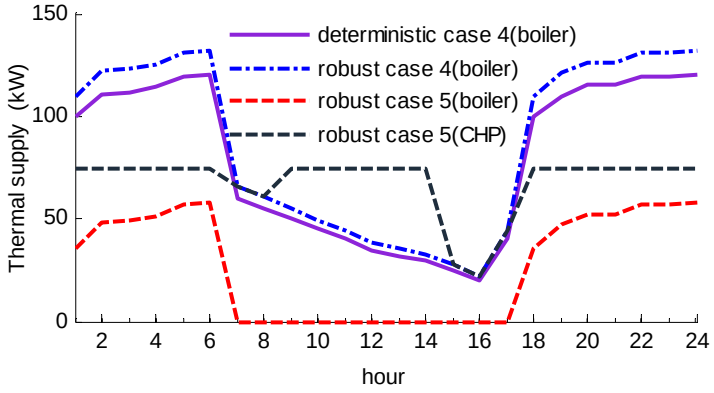


Figure 5.5 Effect of the CHP on thermal supply

### 5.2.4 Influence of budget of robustness on the energy supply

Figure 5.6 and Figure 5.7 shows the effect of budget of robustness in controlling the uncertain ranges of electric and thermal loads, and solar power generation. In Figure 5.6, $\Gamma_2$ is fixed at 1 to ensure the worst case thermal loads and $\Gamma_1$ is adjusted from 0 to 2. Here, $\Gamma_1$=0 means that no protection will be taken against uncertainties in the electric loads and solar power generation; $\Gamma_1$=2 means that the protection against uncertainties in the electric loads and solar power generation are fully ensured.



www.manaraa.com

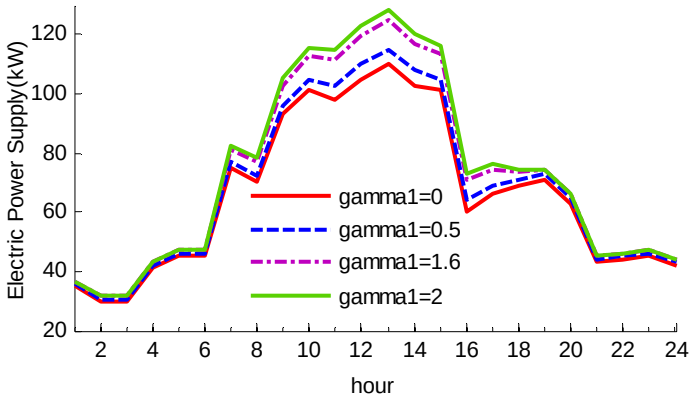


Figure 5.6 Effect of budget of robustness on electric power supply ($\Gamma_2$=1)

Table 5.3 summarizes the change of operating cost as the increase of budget of robustness $\Gamma_1$.

Table 5.3 Operating cost with various $\Gamma_1$ ($\Gamma_2$=1)

| $\Gamma_1$ | Cost ($) | Increase (%) |
|---|---|---|
| 0.0 | 172.3 | 0 |
| 0.5 | 183.5 | 6.5 |
| 0.8 | 186.6 | 8.3 |
| 1.0 | 188.7 | 9.52 |
| 1.3 | 190.8 | 10.74 |
| 1.6 | 192.8 | 11.90 |
| 1.8 | 194.2 | 12.71 |
| 2.0 | 195.6 | 13.52 |

In Figure 5.7, the worst case for the uncertain power demand caused by the uncertain electric loads and solar power generation is considered by fixing $\Gamma_1$ at 2; and the uncertainty set of the thermal loads is enlarged by increasing the robustness $\Gamma_2$ from 0 to 1. It is observed that the additional thermal loads will be supplied by the boiler during hours 1-6, 18-24 and by the CHP at hours 7 and 8. However, no change happens in the



www.manaraa.com

thermal output either from the CHP or from the boiler during hours 9-14, which means that the thermal supply during this period is enough to cover the uncertain thermal loads, and that the resulted excess thermal output is exhausted.

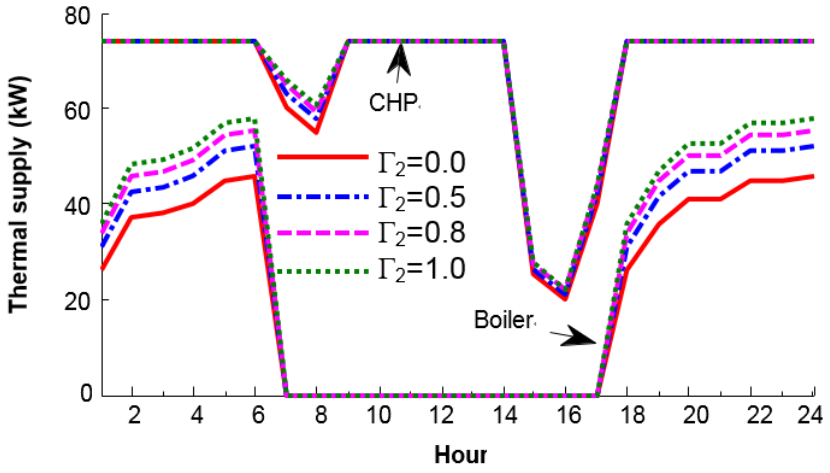


Figure 5.7 Effect of budget of robustness on thermal power supply ($\Gamma_1$=2)

## 5.3 Conclusion

This chapter presented a robust optimization model to coordinate the energy supplies from various energy sources including electric grid, battery, and CHP with boiler unit. The influence of the CHP unit and battery had been examined on energy supply against uncertainties in the energy-efficient building systems. The simulation results showed that the CHP unit and battery are indeed efficient and economical in alleviating the influence of uncertainties in the operation of the energy-efficient building. The robustness can also be adjusted to control the conservativeness of the proposed model.



www.manaraa.com

# CHAPTER VI

# ROBUST STOCHASTIC OPTIMAL OPERATION OF ENERGY-EFFICIENT BUILDINGS

This chapter presents the construction of multiband uncertainty in robust stochastic optimization in order to achieve adaptability in RO through SP analysis for the optimal operation of energy-efficient building systems. This new method is designed to overcome the drawback of partial protection for the random outcomes in SP as well as the conservativeness of the solution in RO. The original uncertainty range of each random variable is partitioned into multiple sub-bands with the scenarios as the nominal value for each band. The uncertain variables can be immunized through discretized scenarios with partitioned uncertainty bands, the range of which can be adjusted by the parameter of robustness. If the number of scenarios decreases, the uncertainty band for each scenario could be enlarged; if the number of scenarios increases, then the individual uncertainty band will shrink.

Our work differs from other methods in two apparently significant aspects. First, our approach offers flexible adaptability for decision variables through the adjustable multiband uncertainty on the basis of the multi-stage scenario tree. Secondly, the generated formulas can either be flexibly adapted to the particular instance of multi-stage SP when the individual uncertainty band shrinks to empty; or drop to the category of RO when no more than one scenario is considered. Therefore, the proposed approach is at



www.manaraa.com

least as adaptive as SP, or as robust as RO. With fewer scenarios than in SP, the RSO approach takes into account all possible outcomes of uncertainties by considering the uncertainty sub-band for each scenario. Therefore, it is more robust than SP which merely considers the exact discrete scenarios. Meanwhile, it's more flexible than the RO as the decision variables can be adapted to the stochastic process of uncertainties in the structure of multi-stage scenario tree. It would be superior to a substitution of the random parameters by single worst estimates as in RO or discretized scenarios as in SP.

The main contributions in this chapter are summarized as follows,

- A robust stochastic optimization model is formulated by introducing penalty terms in constraints, which in turn reflects the cost volatility due to the uncertain solar power generations, electric and thermal loads. The tractable form of the RSO model is achieved by the strong dual theory.
- The multiband uncertainty set is established on the basis of the multi-stage scenario tree so that the combination of all the individual uncertainty sub-bands can cover the complete uncertainty set. The robustness can be adjusted by the budget of uncertainty parameter.
- With the uncovering of the uncertainties, the status variables for the energy output direction of electric grid, operation status of CHP, and charging/ discharging status of the battery can be adaptable based on the multi-stage scenario tree. The adaptability can be flexibly achieved through the adjustable multiband uncertainty.
- With the realization of the uncertainty, the solution for the power dispatch from electric grid and CHP as well as state of charge of the battery are



www.manaraa.com

adjustable in real time, which can be realized through re-running the optimization problem with the already known status variables for the specific scenario.

The rest of the chapter is organized as follows: section 6.2 discusses the construction of multiband uncertainty as well as the modeling and solution of the proposed robust stochastic method. Section 6.3 presents its application to energy-efficient building system. Section 6.4 shows the results of multiband uncertainty set necessary for the case study. Simulation results are analyzed in section 6.5 to validate the performance of the proposed RSO model. Finally, concluding remarks are drawn in section 6.6.

## 6.1 Robust stochastic problem with multiband uncertainty

To improve the robustness of the stochastic solutions and reduce the computation burden at the same time, a RSO model is proposed to combine both multi-stage SP model and RO-based model. In this RSO model, it is straightforward to minimize the expected cost of worst-case scenarios at each stage. This model applies a penalty term in constraints if the scenario at time *t* is bearing an uncertainty band. Besides, the strong dual theory is used to determine the tractable form of the corresponding min-max problem.

### 6.1.1 Construction of the multiband uncertainty

The formulation of the multi-stage SP is the foundation of the proposed RSO model, a general multi-stage SP model is presented in section 2.1, which will facilitate the introduction to the RSO model here. Once the multi-stage scenario tree is generated, the uncertain characteristics will be represented by the limited number of scenarios,



www.manaraa.com

where the stochastic feature ensures that the status variables for the energy output direction of electric grid, operation status of CHP, and charging/ discharging status of the battery can be adapted according to the multi-stage scenario tree. However, the discretized scenarios may deviate from the realized data. In order to protect the operation of energy-efficient building against the uncertainties, scenarios $v_{tj} = (P_{sol,tj}, P_{nc,tj}, H_{nc,tj})$ in electric balance (3.21) and thermal balance (3.22) are modeled as asymmetric and bounded variables $\tilde{v}_{tj} = (\tilde{P}_{sol,tj}, \tilde{P}_{nc,tj}, \tilde{H}_{nc,tj})$, which take values in

$$\begin{bmatrix} \tilde{P}_{sol,tj} \\ \tilde{P}_{nc,tj} \\ \tilde{H}_{nc,tj} \end{bmatrix} = \begin{bmatrix} P_{sol,tj} \\ P_{nc,tj} \\ H_{nc,tj} \end{bmatrix} + \begin{bmatrix} \Delta P_{sol,tj} \\ \Delta P_{nc,tj} \\ \Delta H_{nc,tj} \end{bmatrix} \tag{6.1}$$

$$\begin{bmatrix} \hat{P}^{l}_{sol,tj} \\ \hat{P}^{l}_{nc,tj} \\ \hat{H}^{l}_{nc,tj} \end{bmatrix} \leq \begin{bmatrix} \Delta P_{sol,tj} \\ \Delta P_{nc,tj} \\ \Delta H_{nc,tj} \end{bmatrix} \leq \begin{bmatrix} \hat{P}^{u}_{sol,tj} \\ \hat{P}^{u}_{nc,tj} \\ \hat{H}^{u}_{nc,tj} \end{bmatrix} \tag{6.2}$$

We introduce the concept of multiband uncertainty range through the partition of the entire uncertain feasible set $[y^l_{kt}, y^u_{kt}]$ at time stage $t$ for the uncertainty $k$, which refers to $(P_{sol,t}, P_{nc,t}, H_{nc,t})$. The lower and upper bounds can either be pre-defined, or obtained from the range of generated scenarios before the reduction. It turns out to be necessary to sort the total $J_t$ scenarios in the sequence as (6.3),

$$y^l_{kt} \leq y_{kt,1} \leq \cdots y_{kt,j-1} \leq y_{kt,j} \leq y_{kt,j+1} \cdots \leq y_{kt,J_t} \leq y^u_{kt} \tag{6.3}$$

The individual uncertainty band should cover the range between two adjacent scenarios. It will be determined by the distance of the nearest scenarios. For example, the right hand side $\hat{y}^u_{kt,j}$ of the uncertainty band is half of the distance between the scenario $j$



www.manaraa.com

and its nearest upper scenario *j+1* in (6.4); the left hand side $\hat{y}^{l}_{kt,j}$ of the uncertainty band is half of the distance between the scenario *j* and its nearest lower scenario *j-1* in (6.5).

$$\hat{y}^{u}_{kt,j} = (y_{kt,j+1} - y_{kt,j})/2 \tag{6.4}$$

$$\hat{y}^{l}_{kt,j} = (y_{kt,j-1} - y_{kt,j})/2 \tag{6.5}$$

Specifically, for the scenario $J_t$ closest to the upper bound $y^{u}_{kt}$ at time *t*, the right hand side $\hat{y}^{u}_{kt,J_t}$ of the uncertainty band is the distance between the scenario $J_t$ and the upper bound in (6.6). For the scenario closest to the lower bound $y^{l}_{kt}$, the left hand side $\hat{y}^{l}_{kt,1}$ of the uncertainty band is the difference between the scenario and the lower bound in (6.7).

$$\hat{y}^{u}_{kt,J_t} = y^{u}_{kt} - y_{kt,J_t} \tag{6.6}$$

$$\hat{y}^{l}_{kt,1} = y^{l}_{kt} - y_{kt,1} \tag{6.7}$$

Therefore, the partitioned uncertainty band $Z_{kt,j}$ for the uncertainty *k* for scenario *j* at time stage *t* is defined as $[y^{l}_{kt,j}, y^{u}_{kt,j}]$, with the scenario *j* at time stage *t* as the nominal value for each individual uncertainty band of the uncertainty *k*,

$$Z_{kt,j} = \{\tilde{y}_{kt,j} \in [y_{kt,j} + \hat{y}^{l}_{kt,j}, y_{kt,j} + \hat{y}^{u}_{kt,j}] \,\big|\, \hat{y}^{u}_{kt,j} \geq 0, \hat{y}^{l}_{kt,j} \leq 0\} \tag{6.8}$$

The overall uncertainty set $Z_{kt}$ which consists of $J_t$ bands is as below.

$$Z_{kt} = Z_{kt,1} \cup \cdots \cup Z_{kt,J_t} \tag{6.9}$$

By defining the lower and upper scaled deviations $\eta^{l}_{ktj}, \eta^{u}_{ktj}$, the uncertainty band $Z_{kt,j}$ can be expressed as,



www.manaraa.com

$$Z_{kt,j} = \{\tilde{y}_{kt,j} = y_{kt,j} + \hat{y}^{l}_{kt,j}\eta^{l}_{kt,j} + \hat{y}^{u}_{kt,j}\eta^{u}_{kt,j} \,\big|\, 0 \le \eta^{u}_{kt,j}, \eta^{l}_{kt,j} \le 1\} \tag{6.10}$$

It's unlikely that all of the entries in $y_{kt,j}$ will change, so we can control the total scaled variations of $y_{kt,j}$ by introducing the budget parameter $\Gamma_{tj}$ as follows,

$$\sum\nolimits_{k \in |I_{tj}|} (\eta^{u}_{kt,j} + \eta^{l}_{kt,j}) \le \Gamma_{tj} \tag{6.11}$$

The uncertainty band (6.10) can then be adjusted through the budget of robustness $\Gamma_{tj}$ within the interval $[0, |I_{tj}|]$, where $|I_{tj}|$ indicates the number of coefficients in a certain constraint for scenario *j* at time stage *t* subject to uncertain parameters. When $\Gamma_{tj} = 0$, the scenario at time *t* is bearing no uncertainty band; However, when $\Gamma_{tj} = |I_{tj}|$, then the scenario will reach its worst value of the individual uncertainty band $Z_{kt,j}$ in which it falls; Otherwise, if $\Gamma_{tj} < |I_{tj}|$, only part of the uncertainty band $Z_{kt,j}$ will be covered.

If the history until stage *r* is $\xi_R$, and the space of possible outcomes at stage *r*+1 is $\Omega_{r+1}(\xi_R)$, the feasible region is therefore established with adjustable multiband uncertainty.

$$\omega_{r+1} \in \Omega_{r+1}(\xi_R) \tag{6.12}$$

$$\Omega_{r+1}(\xi_R) = Z_{kr,j} = \{\tilde{y}_{kt,j} = y_{kt,j} + \hat{y}^{l}_{kt,j}\eta^{l}_{kt,j} + \hat{y}^{u}_{kt,j}\eta^{u}_{kt,j}, \textstyle\sum_{k \in |I_{tj}|} (\eta^{u}_{kt,j} + \eta^{l}_{kt,j}) \le \Gamma_{tj} \,|\, t = 1,..,r\} \tag{6.13}$$

### 6.1.2 RSO model and solution

With the feasible region (6.12)-(6.13) for the uncertain loads and intermittent solar power output, the RSO model can then be proposed for the operation problem of energy-efficient building, where uncertainties reside in the electric and thermal balance



www.manaraa.com

constraint (3.21)-(3.22). Therefore, it is assumed that the uncertain parameter exist in the coefficient of the constraints in recursive equations. The equivalence of the static and adaptive robust model with constraint-wise uncertainty therefore ensures that the solutions for the power dispatch from electric grid and CHP as well as charging/ discharging rate of the battery are adjustable in real time.

Because the decision $x_{r-1}$ is already known at stage *r*, so the uncertainty exists in the right-hand side of the constraint (2.25). Each scenario in the RSO problem attains the highest possible value of the uncertainty band in which it falls, and then the robust counterpart is defined as

$$Q_r(x_{r-1}) = Min \quad c_r x_r + E[Q_{r+1}(x_r)] \tag{6.14}$$

$$s.t. \qquad W_r x_r = \underset{\omega_{r+1} \in \Omega_{r+1}(\xi_R)}{Max} \quad h_r(\xi_R) - T_{r-1} x_{r-1}, x_r \in X_r \tag{6.15}$$

Assume the distribution of the random event $w_{r+1}$ is discrete with a probability $\rho_{w_{r+1}}$, then the recursive equation (6.14)-(6.15) at stage *r* is,

$$Q_r(x_{r-1}) = Min \quad c_r x_r + \sum \rho_{w_{r+1}} Q_{r+1}(x_r) \tag{6.16}$$

$$s.t. \qquad W_{rj} x_{rj} = \underset{y_{kt,j} \in Z_{kt,j}}{Max} \; h_{rj}(\{y_{kt,j} \,|\, t = 1, \cdots, r; k = 1, \cdots, |I_{tj}|\}) - T_{r-1,j} x_{r-1,j}, \quad x_{rj} \in X_{rj}, \quad j = 1, \ldots, J_r \tag{6.17}$$

The idea of the RSO approach is to compute optimal solutions for each scenario that retain feasibility for all possible realizations of uncertainties within the partitioned uncertainty band $Z_{kt,j}$. In order to reduce the complexity of the description for the dualization of the RSO model, the right hand side of (6.17) can be defined as



www.manaraa.com

$$Max\sum_{t=1}^{r} b_{tj} = \underset{y_{kt,j}\in Z_{kt,j}}{Max}\ h_{rj}(\{y_{kt,j}\}) - T_{r-1,j}x_{r-1,j}, t=1,\cdots,r; k=1,\cdots,\left|I_{tj}\right| \quad (6.18)$$

Then, the RSO problem can be described as

$$Q_r(x_{r-1}) = Min \quad c_r x_r + \sum \rho_{w_{r+1}} Q_{r+1}(x_r) \quad (6.19)$$

*s.t.*

$$W_{rj}x_{rj} = Max \quad \sum_{t=1}^{r} b_{tj} \quad (6.20)$$

$$l_{rj} \le x_{rj} \le u_{rj}\ ,\ j=1,\ldots,J_t \quad (6.21)$$

With the scaled deviations as defined in (6.10), we consider the following problem:

$$Q_r(x_{r-1}) = Min \quad c_r x_r + \sum \rho_{w_{r+1}} Q_{r+1}(x_r) \quad (6.22)$$

*s.t.*

$$W_{rj}x_{rj} = \sum_{t=1}^{r}\sum_{k} b_{kt,j} + Max\sum_{t=1}^{r}\sum_{k\in\left|I_{tj}\right|}(\hat{b}^{l}_{kt,j}\eta^{l}_{kt,j} + \hat{b}^{u}_{kt,j}\eta^{u}_{kt,j}) \quad (6.23)$$

$$l_{rj} \le x_{rj} \le u_{rj} \quad (6.24)$$

$$\sum_{k\in\left|I_{tj}\right|}(\eta^{u}_{kt,j} + \eta^{l}_{kt,j}) \le \Gamma_{tj} \quad (6.25)$$

$$0 \le \eta^{u}_{kt,j}, \eta^{l}_{kt,j} \le 1 \quad (6.26)$$

Thus, the auxiliary problem which needs to be solved at time stage *t* is,

$$Max \quad \sum_{k\in\left|I_{tj}\right|}(\hat{b}^{l}_{kt,j}\eta^{l}_{kt,j} + \hat{b}^{u}_{kt,j}\eta^{u}_{kt,j}) \text{ subject to (6.25)-(6.26).} \quad (6.27)$$

In order to make this bi-level min-max model computationally tractable, this maximization problem is then be represented as a minimization problem through strong duality theory since the feasible set is nonempty and bounded. The dual of problem (6.27) is shown as problem (6.28)-(6.31),



www.manaraa.com

$$Min \quad \lambda_{tj}\Gamma_{tj} + \sum_{k\in|I_{tj}|}(\pi^{u}_{kt,j} + \pi^{l}_{kt,j}) \tag{6.28}$$

*s.t.*

$$\lambda_{tj} + \pi^{u}_{kt,j} \geq \hat{b}^{u}_{kt,j} \tag{6.29}$$

$$\lambda_{tj} + \pi^{l}_{kt,j} \geq \hat{b}^{l}_{kt,j} \tag{6.30}$$

$$\lambda_{tj},\ \pi^{u}_{kt,j}, \pi^{l}_{kt,j} \geq 0, \forall t, k \in \left|J_{tj}\right| \tag{6.31}$$

Where $\lambda_{tj}, \pi^{u}_{kt,j}, \pi^{l}_{kt,j}$ are the dual decision variables.

By considering the multiband uncertainty set $Z_{kt,j}$ and incorporating the formulations (6.28)-(6.31) into the original problem (6.18)-(6.21), the uncertain linear programming problem (6.22)-(6.26) has the following robust linear counterpart:

*RSO (LPz)*:

$$Q_r(x_{r-1}) = Min \quad c_r x_r + \sum \rho_{w_{r+1}} Q_{r+1}(x_r) \tag{6.32}$$

*s.t.*

$$W_{rj}x_{rj} = \sum_t [\sum_k b_{kt,j} + \lambda_{tj}\Gamma_{tj} + \sum_{k\in|I_{tj}|}(\pi^{u}_{kt,j} + \pi^{l}_{kt,j})] \tag{6.33}$$

$$\lambda_{tj} + \pi^{u}_{kt,j} \geq \hat{b}^{u}_{kt,j}, \lambda_{tj} + \pi^{l}_{kt,j} \geq \hat{b}^{l}_{kt,j} \tag{6.34}$$

$$\lambda_{tj},\ \pi^{u}_{kt,j}, \pi^{l}_{kt,j} \geq 0 \tag{6.35}$$

$$l_{rj} \leq x_{rj} \leq u_{rj}, \forall r, k \in \left|I_{tj}\right| \tag{6.36}$$

Hence, the RSO problem (6.16)-(6.17) can be rewritten in the form of a single large-scale linear programming problem (6.32)-(6.36), which can also be extended to mixed integer linear programming problem. Apparently, the RSO model can be regarded as a combination of SP problems under multiband uncertainty sets.



www.manaraa.com

$$RSO(LP_Z) = SP(LP_{Z_{kt,1}} \cup \cdots \cup LP_{Z_{kt,J_t}}) \tag{6.37}$$

If the uncertainty feasible region $Z_{kt,j}$ for each scenario drops to empty, then we have

$$\lim_{Z_{kt,j} \to \varnothing} RSO(LP_Z) = SP(LP) \tag{6.38}$$

Similarly, the RSO model can also be viewed as the expected value of the RO models for all the scenarios.

$$RSO(LP_Z) = E[RO(LP_1 \cup \cdots \cup LP_{J_t})] \tag{6.39}$$

If the number of scenarios becomes one, then the RSO model will be

$$\lim_{J_t=1,t=1,\cdots,T} RSO(LP_Z) = RO(LP) \tag{6.40}$$

The combination of all the sub uncertainty bands can cover the overall uncertainty set as in the RO model. However, there is a trade-off between the number of scenarios and the range of the individual uncertainty band. If there are more scenarios, then the partitioned uncertainty set will be narrowed down. If the number of scenarios decreases, then the uncertainty range would be enlarged. The number of scenarios will determine the flexibility of the RSO model. The more scenarios are considered, the more flexible the RSO approach becomes compared with the RO model. The advantage of the RSO model over the RO model is that one can increase the number of scenarios in order to increase the flexibility. In other words, it overcomes the conservativeness in the RO model by introducing the idea of scenarios from the traditional SP method. The loss of information with limited scenarios in the SP model can be overcome by incorporating the additional



www.manaraa.com

information in the individual uncertainty band for each scenario, therefore protecting uncertainties in the RSO model.

## 6.2 Robust stochastic formulation

In order to apply the proposed RSO model to the operation of energy-efficient building, the uncertainties are defined as in (6.41)-(6.43) for solar power generation, electric and thermal loads, respectively.

$$\tilde{P}_{sol,tj} = P_{sol,tj} + \eta^{u}_{s,tj}\hat{P}^{u}_{sol,tj} + \eta^{l}_{s,tj}\hat{P}^{l}_{sol,tj} \tag{6.41}$$

$$\tilde{P}_{load,tj} = P_{load,tj} + \eta^{u}_{p,tj}\hat{P}^{u}_{load,tj} + \eta^{l}_{p,tj}\hat{P}^{l}_{load,tj} \tag{6.42}$$

$$\tilde{H}_{load,tj} = H_{load,tj} + \eta^{u}_{h,tj}\hat{H}^{u}_{load,tj} + \eta^{l}_{h}\hat{H}^{l}_{load} \tag{6.43}$$

The relative and scaled deviations should meet the following requirements,

$$\hat{P}^{u}_{load,tj}, \hat{P}^{u}_{sol,tj}, \hat{H}^{u}_{load,tj} \geq 0\,,\ \hat{P}^{l}_{load,tj}, \hat{P}^{l}_{sol,tj}, \hat{H}^{l}_{load,tj} \leq 0 \tag{6.44}$$

$$0 \leq \eta^{u}_{p,tj}, \eta^{l}_{p,tj}, \eta^{u}_{s,tj}, \eta^{l}_{s,tj}, \eta^{u}_{h,tj}, \eta^{l}_{h,tj} \leq 1 \tag{6.45}$$

For both electric and thermal loads, the worst case occurs when the increase in the electric and thermal loads reach the maximum value; but for the solar power output, its worst case happens when the maximum decrease in solar power generation arrives. The robust counterpart of multi-stage SP model with multiband uncertainty set is described as

$$Q_t = Min \quad [C_{gf,t} \cdot P_{gf,tj} + C_{gt,t} \cdot P_{gt,tj} + C_{gas,t} \cdot (F_{chp,tj} + F_{boil,tj})] + E[Q_{t+1}] \tag{6.46}$$

*s.t.*

$$\eta^{u}_{p,tj} + \eta^{l}_{p,tj} + \eta^{u}_{s,tj} + \eta^{l}_{s,tj} \leq \Gamma_{1,tj} \tag{6.47}$$

$$\eta^{u}_{h,tj} + \eta^{l}_{h,tj} \leq \Gamma_{2,tj} \tag{6.48}$$



www.manaraa.com

$$P_{gf,tj} - P_{gt,tj} + P_{chp,tj} - P_{bc,tj} + P_{bd,tj} = \max\{\tilde{P}_{load,tj} - \tilde{P}_{sol,tj}\} \tag{6.49}$$

$$\eta_{hc}(H_{chp,tj} + H_{boi,tj}) = H_{load,tj} + H_{exh,tj} + \max\{\tilde{H}_{load,tj}\} \tag{6.50}$$

and constraints (4.4)-(4.18).

To get the tractable form of the above RSO problem with the dualization method as introduced in the previous section, the dual form of constraints (6.47)-(6.50) can be reformulated as the following equivalent linear formulation,

$$s.t. \quad P_{gf,tj} - P_{gt,tj} + P_{chp,tj} - P_{bc,tj} + P_{bd,tj} = P_{load,tj} - P_{sol,tj} + \lambda_{1,tj}\Gamma_{1,tj} + \pi^u_{11,tj} + \pi^l_{11,tj} + \pi^u_{12,tj} + \pi^l_{12,tj} \tag{6.51}$$

$$\eta_{hc}(H_{chp,tj} + H_{boi,tj}) = H_{load,tj} + H_{exh,tj} + \lambda_{2,tj}\Gamma_{2,tj} + \pi^u_{21,tj} + \pi^l_{21,tj} \tag{6.52}$$

$$\lambda_{1,tj} + \pi^u_{11,,tj} \geq \hat{p}^u_{load,tj} \tag{6.53}$$

$$\lambda_{1,tj} + \pi^l_{11,tj} \geq \hat{p}^l_{load,tj} \tag{6.54}$$

$$\lambda_{1,tj} + \pi^u_{12,tj} \geq -\hat{p}^u_{sol,tj}, \lambda_{1,tj} + \pi^l_{12,tj} \geq -\hat{p}^l_{sol,tj} \tag{6.55}$$

$$\lambda_{2,tj} + \pi^u_{21,tj} \geq \hat{H}^u_{load,tj} \tag{6.56}$$

$$\lambda_{2,tj} + \pi^l_{21,tj} \geq \hat{H}^l_{load,tj} \tag{6.57}$$

$$\lambda_{1,tj},\ \pi^u_{11,tj}, \pi^l_{11,tj}, \pi^u_{12,tj}, \pi^l_{12,tj}, \lambda_{2,tj}, \pi^u_{21,tj}, \pi^l_{21,tj} \geq 0 \tag{6.58}$$

The stochastic feature of RSO ensures that the energy output direction of electric grid, operation status of CHP, and charging/ discharging status of the battery can be adapted according to the multi-stage scenario tree, while the robust feature of RSO allows



www.manaraa.com

that the power dispatch from electric grid and CHP as well as charging/ discharging rate of the battery are adjustable in real time.

### 6.3 Multiband uncertainty set

Uncertainties involving in both generation and demand sides are considered at the same time. Nine scenarios are generated through the multi-stage scenario tree generation and backward reduction technique. Therefore, the single uncertainty band is partitioned into 9 sub-bands.

In RSO, each scenario is associated with an individual uncertainty band at a certain stage. Table 6.1 shows the worst-case hours (WCHs) in RSO. For the electric loads and solar power generation, WCH appears in different scenarios. Subtracting the solar power generation from the electric loads, the net power demand only reaches its worst value in RSO at hours listed in Table 6.1. It can be observed that the worst net power demand appears at hours when both the electric loads and solar power generation reach their worst value at the same time, or when the worst electric loads happen during the period without solar power generation. For each scenario in RSO, the worst case of thermal loads will only be at a few hours. Because the worst case occurs each hour in RO, then the RSO model is much more flexible and less conservative.



www.manaraa.com

Table 6.1 Hours with worst case in RSO

| Scenarios | Solar power supply | Electric loads | Net power demand | Thermal loads |
|---|---|---|---|---|
| $S_1$ | 6,12 | 1,3,5,8,9,12,16,20 | (1,3),12,20 | 1,3 |
| $S_2$ | 6,8,11,17 | 1,3,5,17 | (1,3),17 | 1,3,15,19 |
| $S_3$ | 9 | 1,6,7,13,18 | (1) | 1,2,5,6,18,23 |
| $S_4$ | 5 | 1,2,4,19 | (1,2,4),19 | 1,4,7,9,14 |
| $S_5$ | -- | 1,6 | (1) | 1,2,5,6,16 |
| $S_6$ | -- | 1,6,14,22-24 | (1), 22-24 | 1,2,5,6,20 |
| $S_7$ | 5,14 | 1,2,4 | (1,2,4) | 1,4,8,10,12,17,22,24 |
| $S_8$ | 5,16 | 1,2,4,10,11,15,21 | (1,2,4),21 | 1,4,11,21 |
| $S_9$ | 6,7,10,13,15,18 | 1,3,5 | (1,3) | 1,3,13 |

Note: () means hours without solar power output.

### 6.3.1 Electric loads

Figure 6.1 represents the partitioning of the single uncertainty set for electric loads. Figure 6.2 shows robust scenarios are usually more conservative where the worst case of the uncertainty is considered at each hour. Figure 6.3 compares the worst-case scenarios in RSO with that in RO for electric loads.

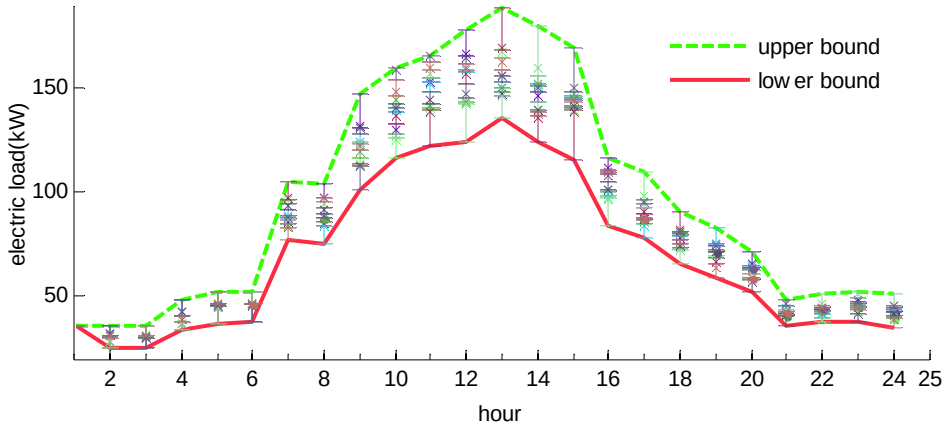


Figure 6.1 The multiband uncertainty set for electric loads



www.manaraa.com

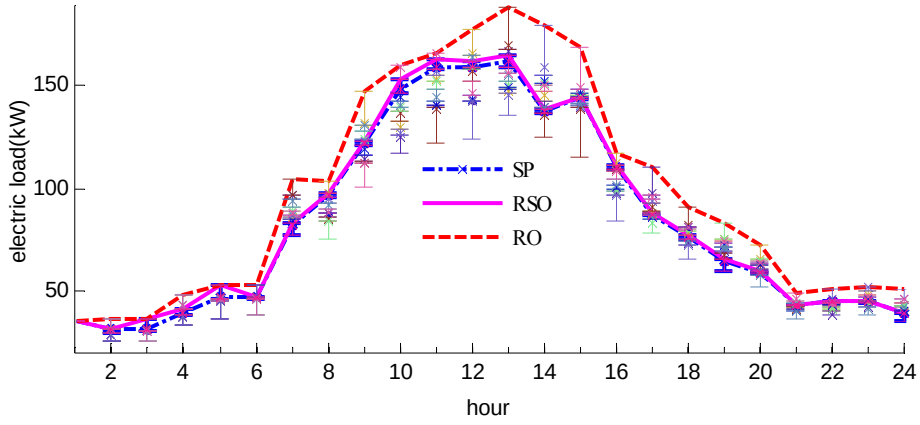


Figure 6.2 The multiband uncertainty set for electric loads ($S_9$: RO & RSO)

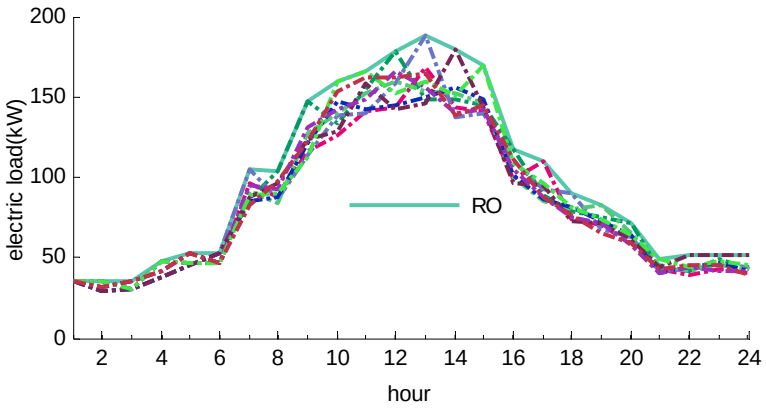


Figure 6.3 Uncertain electric loads (RO & RSO)

### 6.3.2 Solar energy

Figure 6.4 represents the individual uncertainty sets for solar power generation. While Figure 6.5 compares scenarios in both RO and RSO. Figure 6.6 shows all of the scenarios in RSO compared with the worst case in RO.



www.manaraa.com

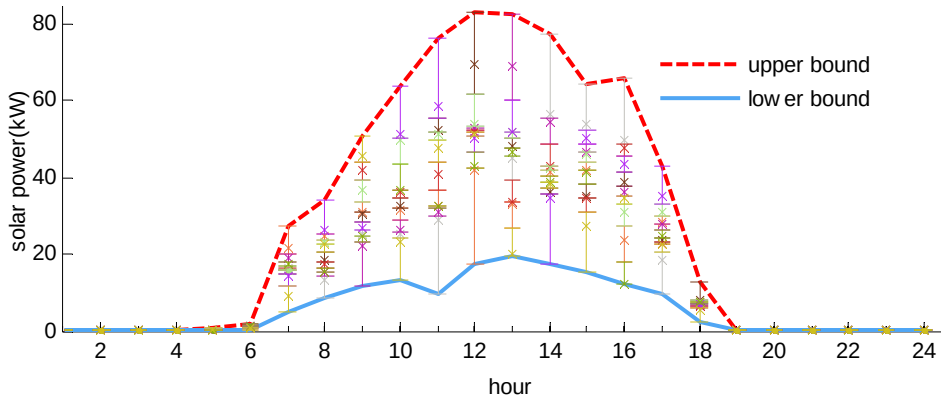


Figure 6.4 The multiband uncertainty set for solar energy ($S_9$)

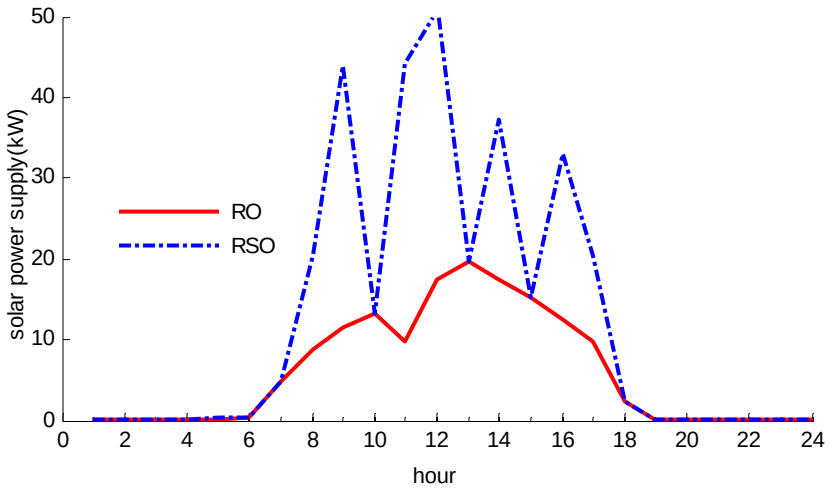


Figure 6.5 Solar energy ($S_9$: RO & RSO)



www.manaraa.com

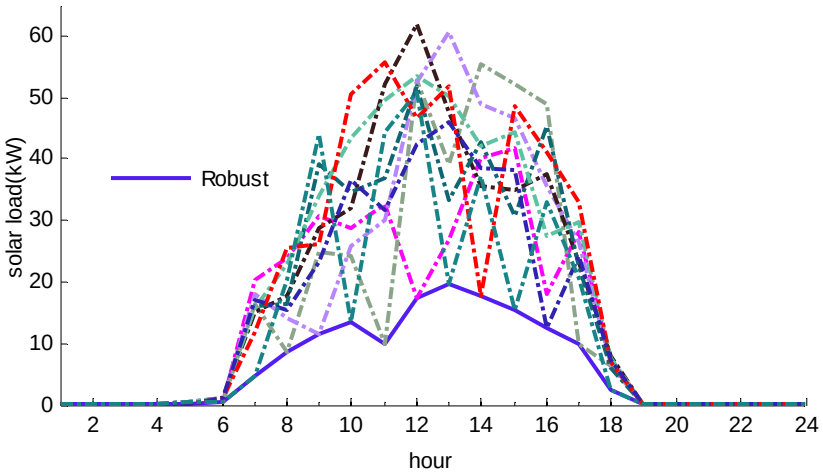


Figure 6.6 Solar energy (RO & RSO)

### 6.3.3 Net power demand

Both the electric demand and solar power generation have a combined effect on the electric power supply for the building energy system. Figure 6.7 shows the uncertain power demand both in SP and RSO. Apparently, the RSO model has higher electric loads and lower solar power generation due to the consideration of the partitioned uncertainty set for each scenario in RSO. Therefore, the net power demand in RSO is always higher than that in the corresponding scenario of the SP model, because the net power demand reflects the total change of both electric loads and solar power generation.



www.manaraa.com

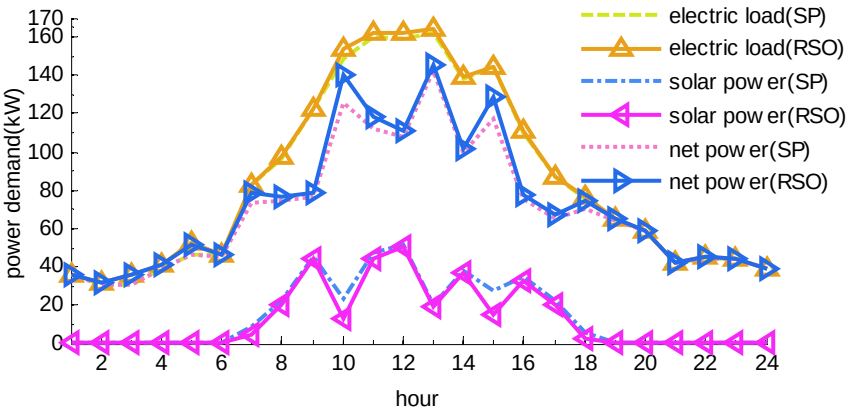


Figure 6.7 Uncertain power demand ($S_9$: SP & RSO)

Figure 6.8 compares the scenarios in RO and RSO for net power demand, Figure 6.9 shows that the net power demand is always higher in RSO than that in the corresponding scenario of the SP model due to the overall impact of uncertainties. Figure 6.10 makes a comparison of the scenarios in RSO with the single worst case in RO.

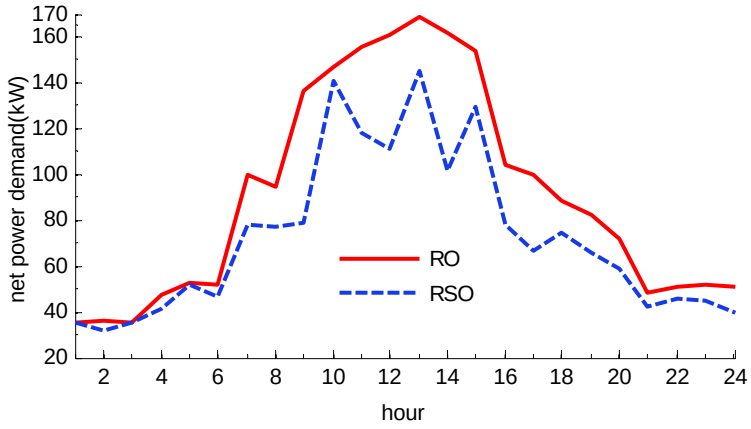


Figure 6.8 Net power demand ($S_9$: RO & RSO)



www.manaraa.com

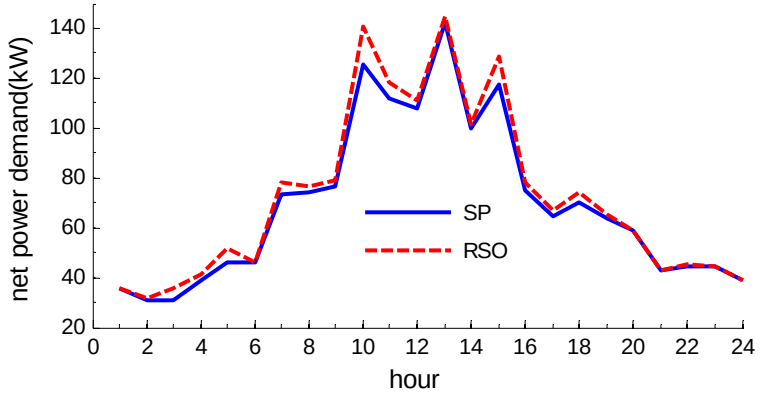


Figure 6.9 Net power demand ($S_9$: SP & RSO)

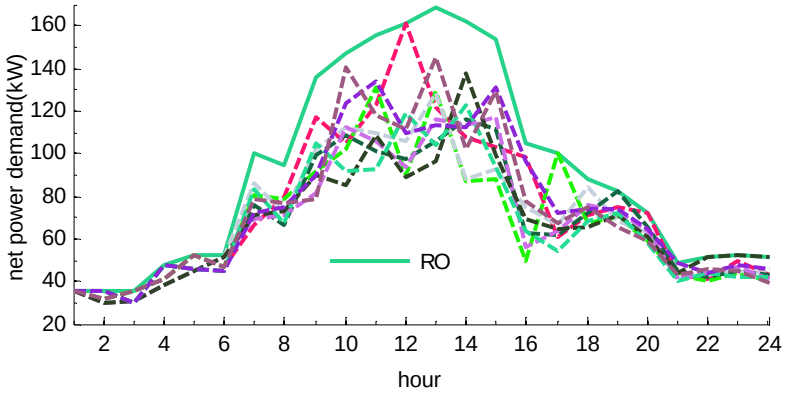


Figure 6.10 Net power demand (RO & RSO)

### 6.3.4 Thermal loads

Figure 6.11 partitions the uncertainty set for thermal loads. Figure 6.12 compares the scenarios in both RO and RSO. From Figure 6.13 we can see that for each scenario in the RSO case, the worst case of thermal loads will only be at a few hours.



www.manaraa.com

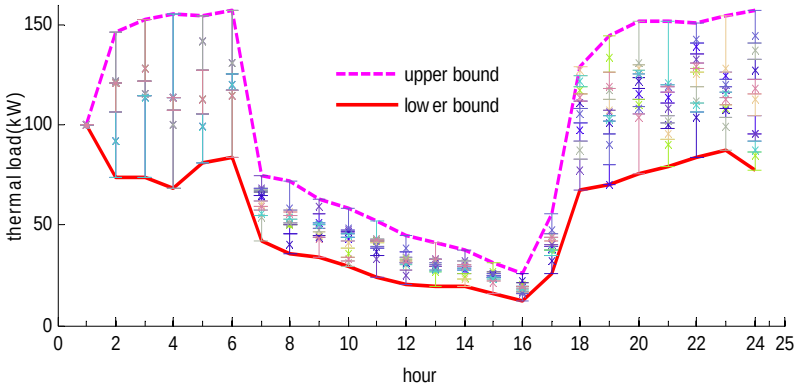


Figure 6.11 The multiband uncertainty set for thermal loads

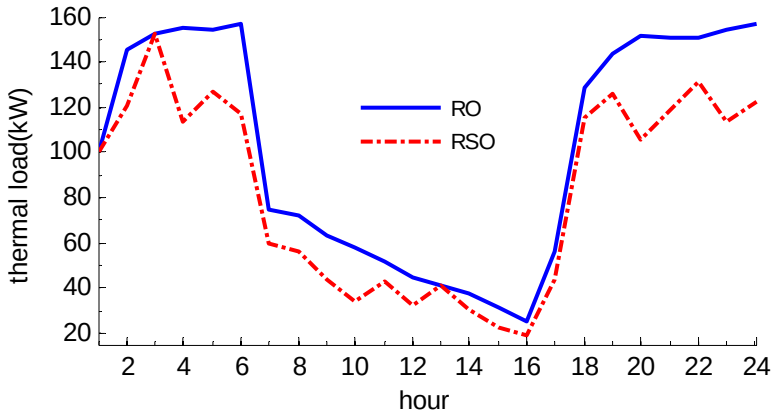


Figure 6.12 Thermal loads ($S_9$: RO & RSO)



www.manaraa.com

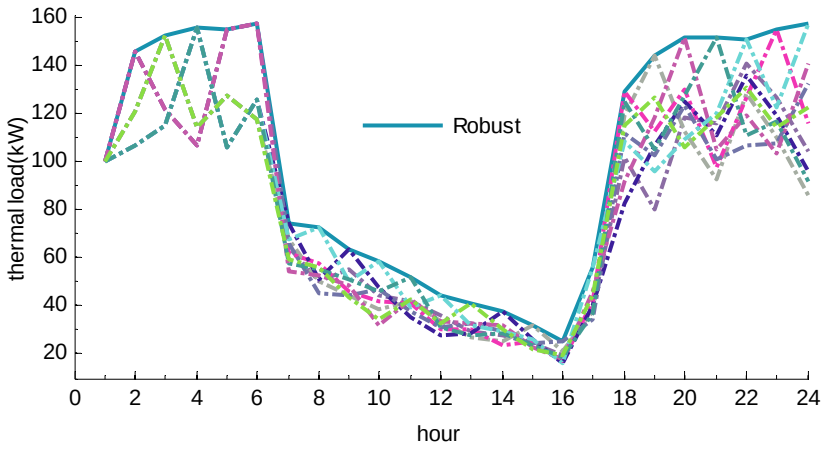


Figure 6.13 Thermal loads (RO & RSO)

### 6.3.5 Adjustment of uncertainty set range

In RSO, the budget of robustness is used to adjust the individual uncertainty range of different scenarios for each uncertainty. In this case, the uncertain electric loads and solar power generation are fixed by $\Gamma_1=2$, so that the worst case for the net power demand won't be changed.

From Figure 6.14, with the change of the robustness $\Gamma_2$, the uncertain feasible region for each scenario of thermal loads will be flexibly adjusted to protect the uncertainty. Correspondingly, the uncertainty band for electric loads and solar power generation can also be changed through the robustness $\Gamma_1$ elastically.



www.manaraa.com

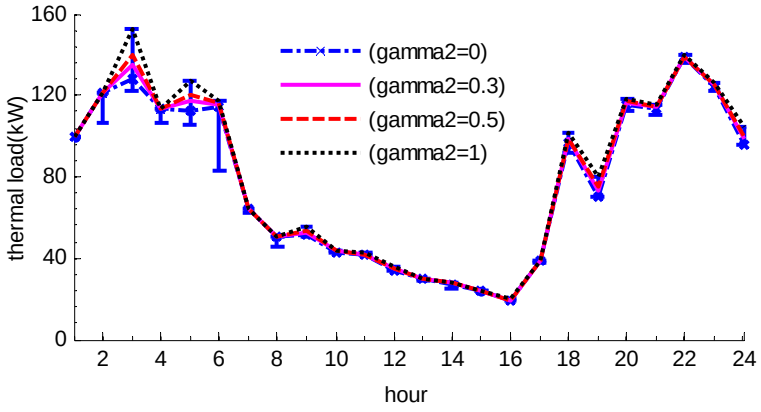


Figure 6.14 Influence of robustness on the uncertainty set of thermal loads scenario

## 6.4 Case study

The performance of the proposed RSO model will be investigated through the following three cases,

Case 1: Compare RO with RSO;

Case 2: Compare SP with RSO;

Case 3: Study the effectiveness of the budget of robustness.

### 6.4.1 RO vs RSO models

#### 6.4.1.1 Power supply

In Figure 6.15, the grid power in the robust case is higher than that in the scenarios of the RSO model for most hours. For example in Table 6.2, in $S_2$ of RSO model, the grid power would be higher at hours 17&21. In $S_9$ of RSO model as shown in Figure 6.16, the grid power would be higher at hours 10&18.



www.manaraa.com

Table 6.2 Hours with higher grid power in RSO model compared with RO

| Scenarios | Hours with higher grid power | Surplus grid power (kW) |
|---|---|---|
| $S_1$ | 21 | 4.5705 |
| $S_2$ | 17 | 1.4763 |
| | 21 | 4.9901 |
| $S_3$ | 3 | 13.4284 |
| | 6 | 29.3669 |
| | 21 | 3.8629 |
| $S_4$ | 6 | 16.0356 |
| | 21 | 4.6846 |
| $S_5$ | 3 | 13.4284 |
| | 6 | 29.3669 |
| | 21 | 0.3511 |
| $S_6$ | 3 | 13.4284 |
| | 6 | 29.3669 |
| | 21 | 5.8178 |
| $S_7$ | 6 | 16.0356 |
| $S_8$ | 6 | 16.0356 |
| $S_9$ | 10 | 2.8784 |
| | 18 | 1.3299 |



www.manaraa.com

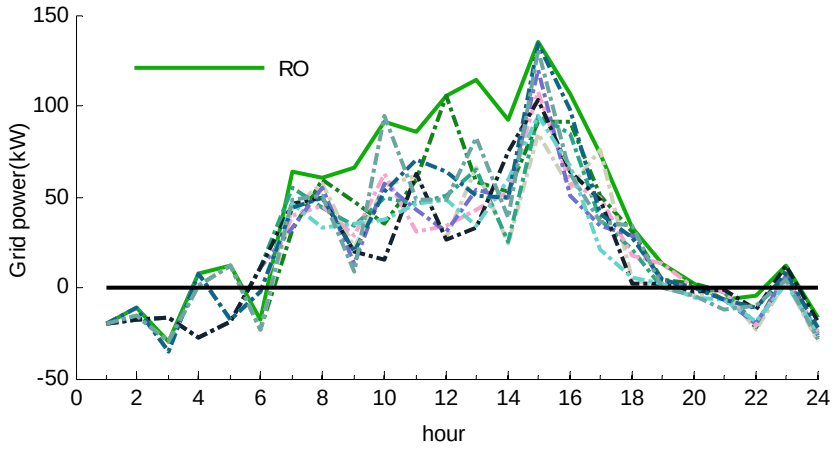


Figure 6.15 Grid power supply (RO & RSO)

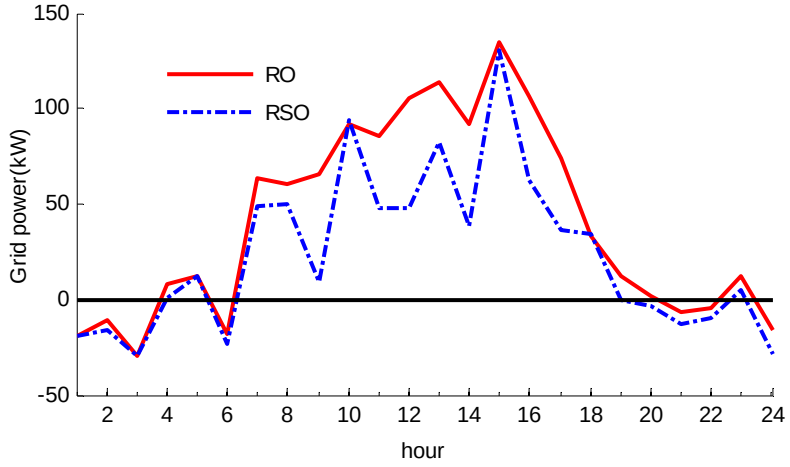


Figure 6.16 Grid power supply ($S_9$: RO & RSO)

In Figure 6.17, the power from battery is fluctuating in both cases due to its charge and discharge behavior. For scenarios 1, 2, 9 (Figure 6.18), the power from battery is the same as that in the robust case during hours 1-9; for scenarios 4, 7, 8, the battery has the same power output during hours 1-3. While for other scenarios, the charging and discharging status are very different in both cases.



www.manaraa.com

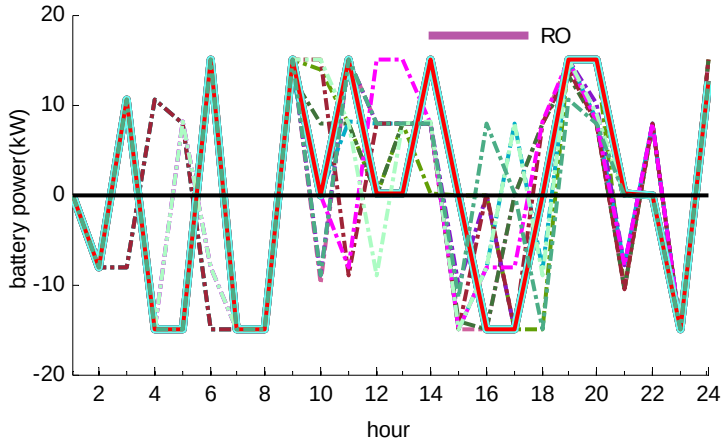


Figure 6.17 Power supply from battery (RO & RSO)

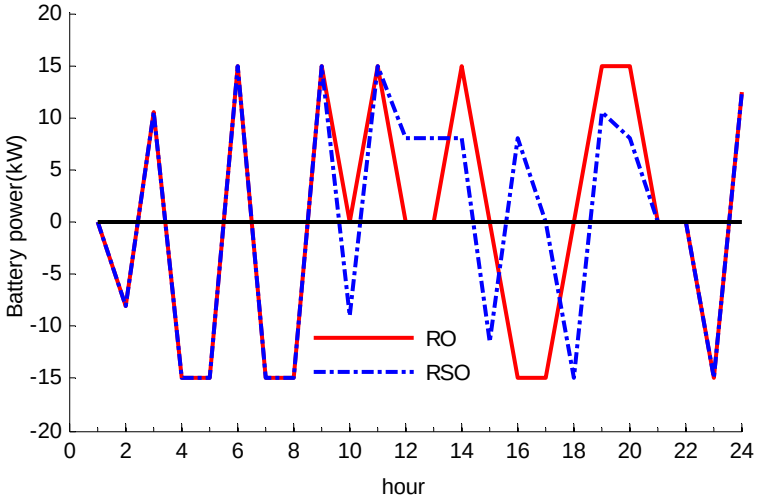


Figure 6.18 Battery power supply ($S_9$: RO & RSO)

The power from grid and battery (Figure 6.19) as well as from the CHP (Figure 6.21, Figure 6.22) is almost higher in RO than that in RSO, which can be explained from Table 6.1 that the net power demand in RO is higher except when the worst case happens in both models at the same time. The same total power output from all sources is required in both RSO and RO when the worst net power demand happens. In Table 6.3, CHP has



www.manaraa.com

lower power output at hour 17 of scenario 2 in RSO than in RO, so the grid and battery power is higher correspondingly (Figure 6.19).

For hours 1-6, 9-14, 18-24, the CHP unit constantly provides 55kW for electric demand either in all scenarios of RSO or in RO. But for hours 7-8, 15-17, the power output from the CHP unit is different as shown in Table 6.3. Usually, RSO has the lower CHP power output at hours without the worst net power demand, or equal to that in RO at hours with the worst net power demand. However, at hour 7 of scenario 2 and 7 in RSO, there are higher power output from CHP than in RO, which will coordinate with grid and battery to supply the uncertain net power demand.

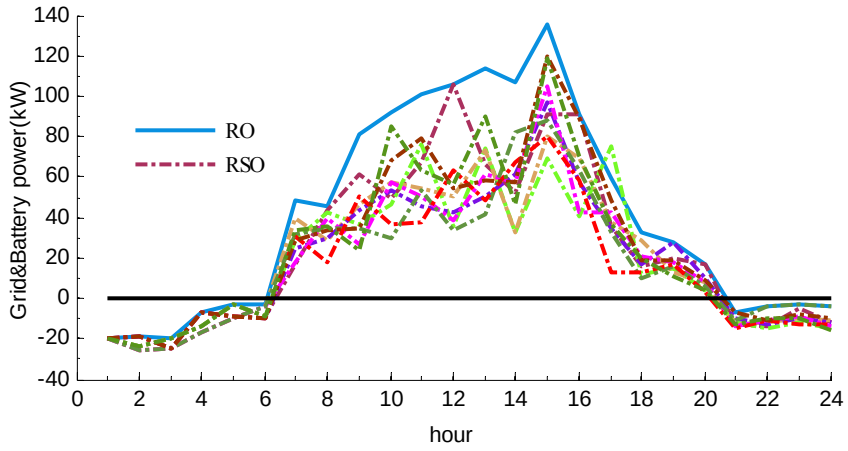


Figure 6.19 Power supply from grid and battery (RO & RSO)



www.manaraa.com

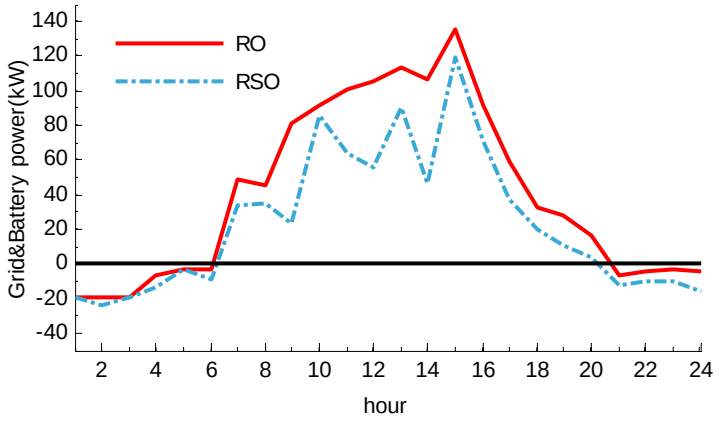


Figure 6.20 Power supply from grid and battery ($S_9$: RO & RSO)

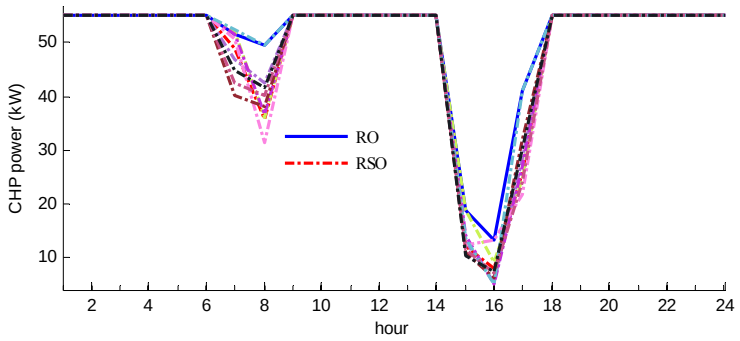


Figure 6.21 Power supply from CHP (RO & RSO)

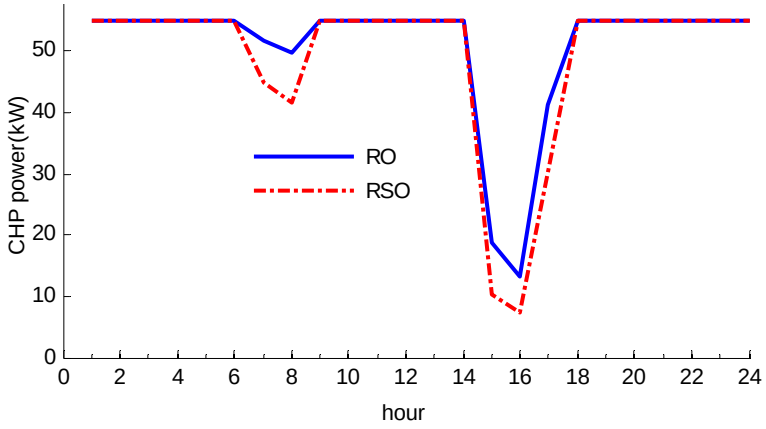


Figure 6.22 Power supply from CHP ($S_9$: RO & RSO)



www.manaraa.com

Table 6.3 Hours with different CHP power in RSO and RO

| Model \ Hour | | $H_7$ | $H_8$ | $H_{15}$ | $H_{16}$ | $H_{17}$ |
|---|---|---|---|---|---|---|
| RO | | 51.59 | 49.62 | 18.74 | 13.12 | 41.10 |
| RSO | $S_1$ | 48.96 | 35.90 | 12.09 | 7.88 | 25.85 |
| | $S_2$ | **52.04** | 36.17 | **18.74** | 9.08 | *24.63* |
| | $S_3$ | 46.86 | 42.54 | 12.86 | 5.19 | 28.52 |
| | $S_4$ | **51.59** | 36.63 | 14.11 | 5.00 | 26.91 |
| | $S_5$ | 50.60 | 31.50 | 12.33 | **13.12** | 21.68 |
| | $S_6$ | 40.17 | 38.09 | 10.86 | 6.20 | 32.03 |
| | $S_7$ | **52.38** | **49.62** | 13.46 | 5.00 | **41.10** |
| | $S_8$ | 42.62 | 40.22 | 11.48 | 7.06 | 24.06 |
| | $S_9$ | 44.71 | 41.54 | 10.18 | 7.36 | 30.28 |

#### 6.4.1.2 Thermal supply

In Figure 6.23, the thermal output from the boiler in RSO is always lower than or equal to that in RO. For hours 7-17, 1) at hour 7 of scenario 4 and hour 8 of scenario 7 with the worst thermal demand in RSO (Table 6.4), boiler output is the same as in RO, which also applies to CHP; 2) otherwise, boiler has no thermal output in both RSO and RO and therefore, the thermal loads will be covered totally by CHP.

Similar to CHP power supply, the CHP unit constantly provides 70.79 kW for thermal demand either in all scenarios of RSO or in RO for hours 1-6, 9-14, 18-24 (Figure 6.25). The higher thermal output from CHP at hour 7 of scenario 2 and 7 in RSO is due to the zero output from boiler.



www.manaraa.com

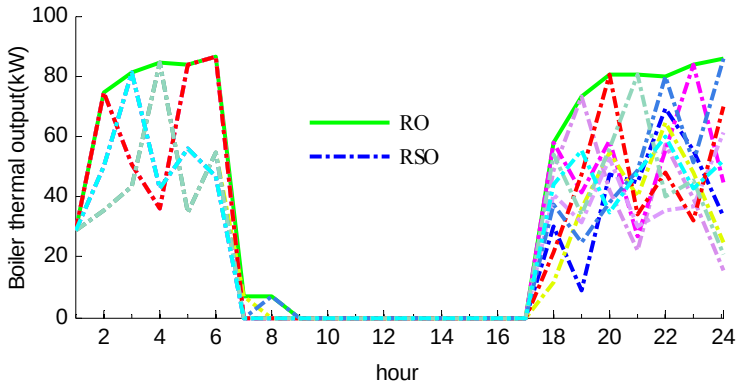


Figure 6.23 Boiler thermal output (RO & RSO)

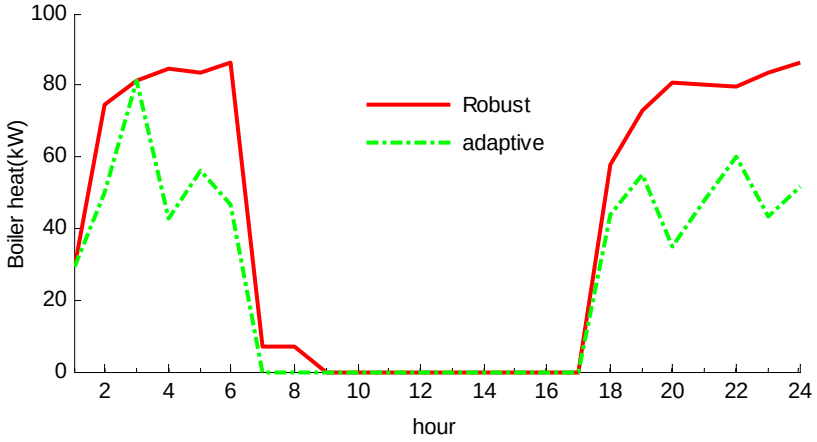


Figure 6.24 Boiler thermal output ($S_9$: RO & RSO)



www.manaraa.com

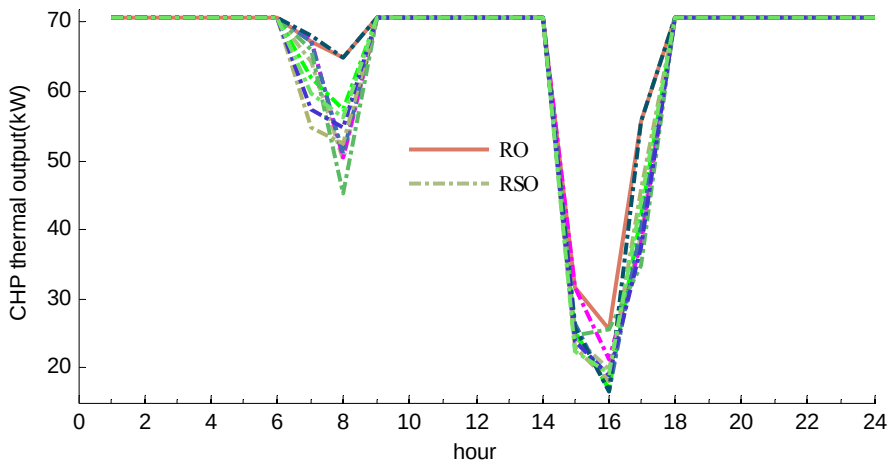


Figure 6.25 CHP thermal output (RO & RSO)

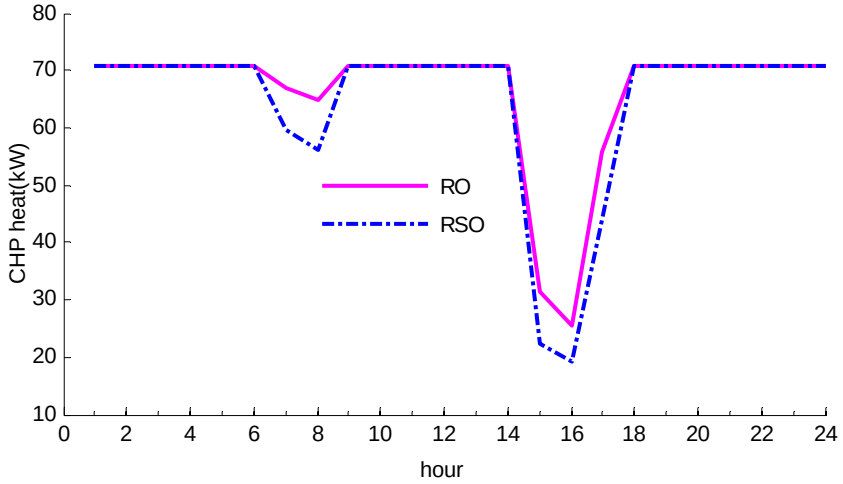


Figure 6.26 CHP thermal output ($S_9$: RO & RSO)



www.manaraa.com

Table 6.4 Hours with variable CHP thermal supply

| Model \ Hour | | $H_7$ | $H_8$ | $H_{15}$ | $H_{16}$ | $H_{17}$ |
|---|---|---|---|---|---|---|
| RO | | 67.10 | 64.97 | 31.55 | 25.47 | 55.76 |
| RSO | $S_1$ | 64.26 | 50.13 | 24.36 | 19.81 | 39.24 |
| | $S_2$ | **67.59** | 50.42 | **31.55** | 21.10 | 37.93 |
| | $S_3$ | 61.99 | 57.31 | 25.19 | 16.89 | 42.14 |
| | $S_4$ | **67.10** | 50.91 | 26.54 | 16.68 | 40.40 |
| | $S_5$ | 66.03 | 45.36 | 24.62 | **25.47** | 34.74 |
| | $S_6$ | 54.74 | 52.50 | 23.03 | 17.99 | 45.93 |
| | $S_7$ | **67.96** | **64.97** | 25.84 | 16.68 | **55.76** |
| | $S_8$ | 57.39 | 54.80 | 23.70 | 18.92 | 37.31 |
| | $S_9$ | 59.65 | 56.23 | 22.29 | 19.25 | 44.04 |

There is extra thermal supply from the CHP in both RO and RSO during hours 9-14 when the energy price from the grid is relatively high (Table 6.4). For other hours, the total thermal supply is just sufficient to meet the thermal demand which is higher in RO (Figure 6.27).

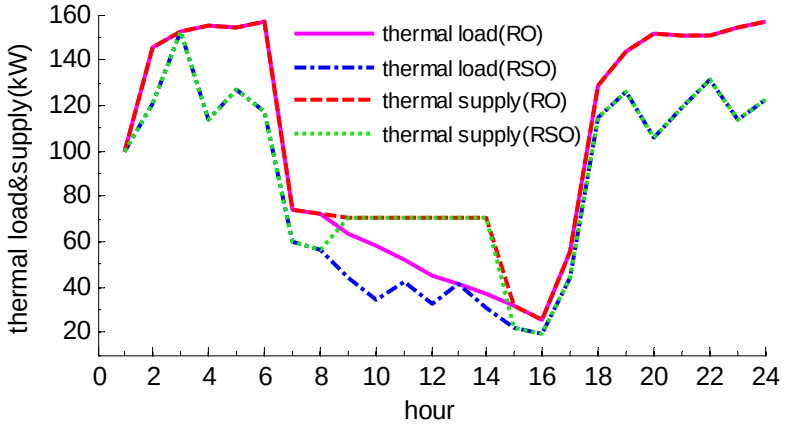


Figure 6.27 Thermal loads and supply ($S_9$: RO & RSO)



www.manaraa.com

### 6.4.2 SP vs RSO models

#### 6.4.2.1 Power supply

In Figure 6.28, the grid power in the adaptive case is always higher than that in the stochastic case because each scenario is considered with an uncertainty range in the RSO case.

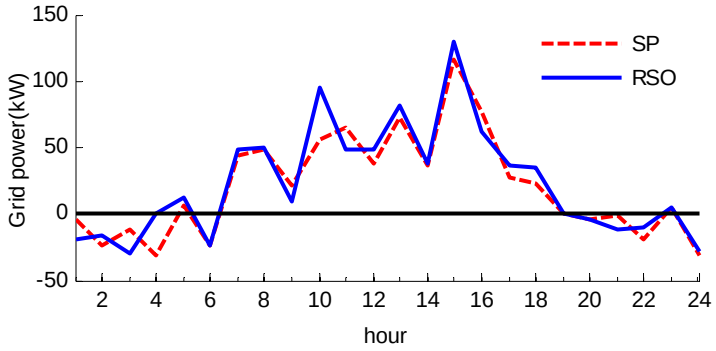


Figure 6.28 Power supply from grid ($S_9$: SP & RSO)

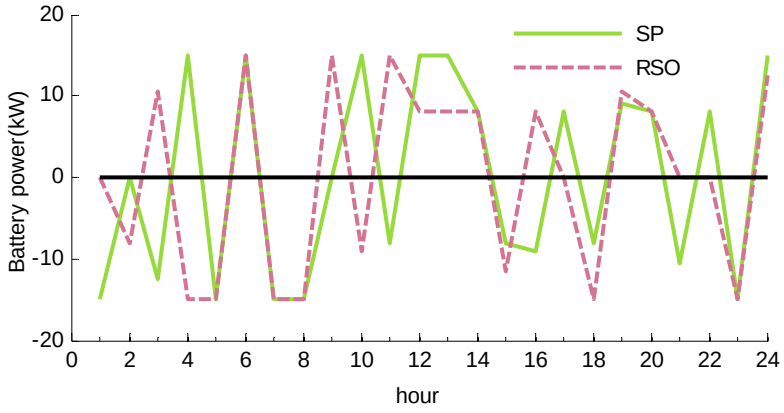


Figure 6.29 Power supply from battery ($S_9$: SP & RSO)



www.manaraa.com

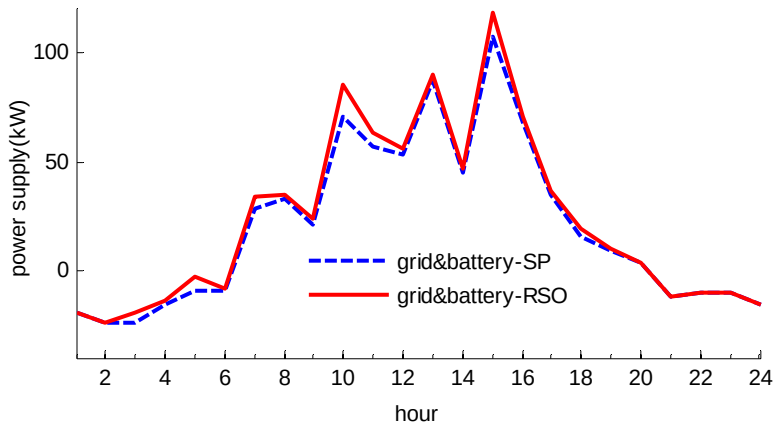


Figure 6.30 Power supply from grid& battery ($S_9$: SP & RSO)

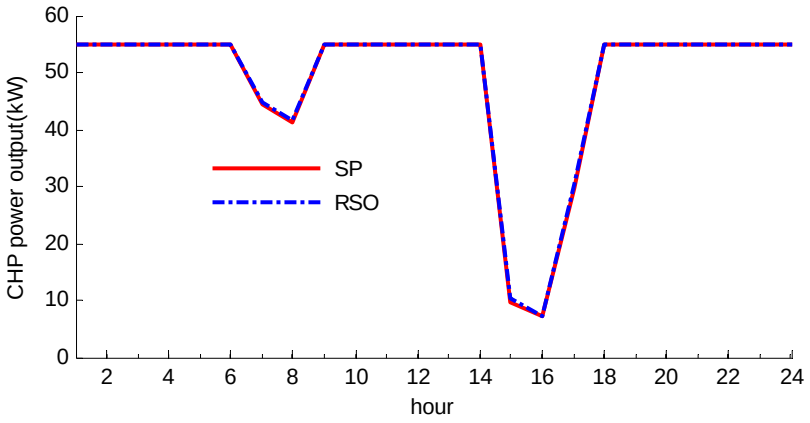


Figure 6.31 Power supply from CHP ($S_9$: SP & RSO)

In Figure 6.32, the power from the electric grid and battery in RSO is always higher than that in SP. But the individual power either from the electric grid or the battery doesn't possess such property as a result of the influence of the charging and discharging behavior of the battery. When the CHP unit in RSO supplies power less than (e.g. hour 7 of scenario 4) or equal to (e.g. scenario 9) that in SP, the extra power demand due to the uncertainty band will be taken over by the grid and battery; otherwise (e.g. hour 7-8 of scenario 8), the



www.manaraa.com

grid, battery, as well as the CHP will coordinate to supply the extra power demand at the same time.

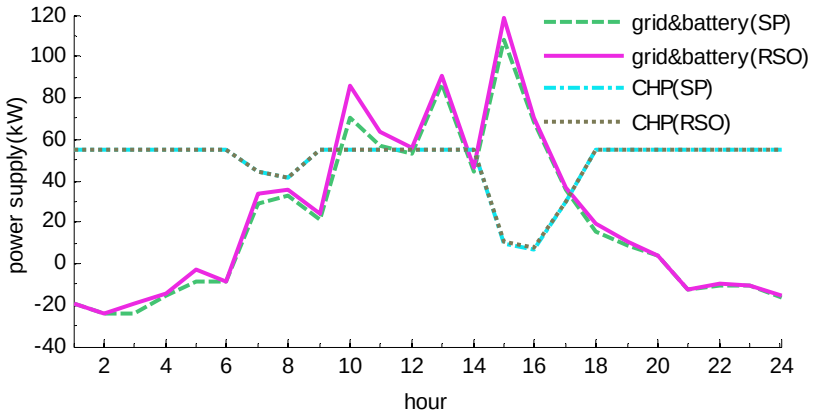


Figure 6.32 Power supply ($S_9$: SP & RSO)

### 6.4.2.2 Thermal supply

For each scenario, the power output of the CHP (e.g. scenario 9 in Figure 6.32) is the same in both RSO and SP during hours 1-6, 9-14, 19-24, so is the thermal output (e.g. scenario 9 in Figure 6.33). For other hours in RSO except hour 7 of scenario 4, the thermal output of the CHP is higher than that of the corresponding scenario in SP due to its contribution in supplying the uncertain demand associated with the uncertainty band in RSO, so is the CHP power output.

Besides, both in SP and RSO, there is extra thermal output from the CHP during hours 9-14, which is exhausted to keep the operating cost minimum for the building. In addition, there is no output from the boiler during hours 7-17 in both models, except at hour 7 of scenario 4 and at hour 8 of scenario 7 in RSO, and therefore the CHP is responsible for the thermal demand in both models. Otherwise, the boiler will take over the



www.manaraa.com

extra thermal demand introduced by the individual uncertainty band in RSO due to the constant CHP thermal output during hours 1-6 and 18-24, excluding hour 18 of scenario 4 where CHP contributes to part of the extra thermal demand.

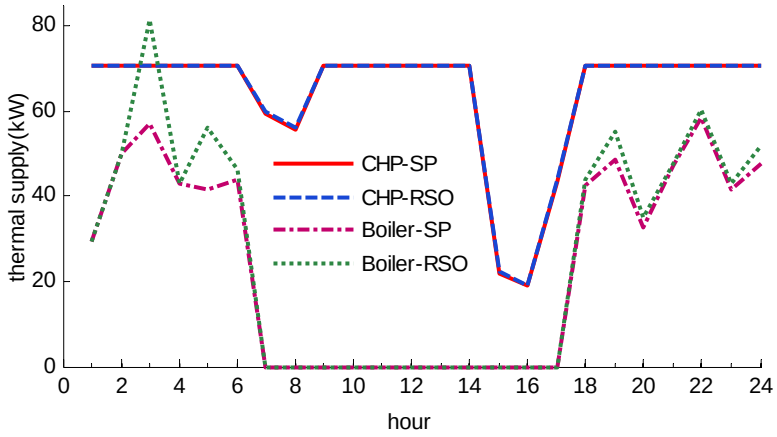


Figure 6.33 Thermal supply from CHP and boiler ($S_9$: SP & RSO)

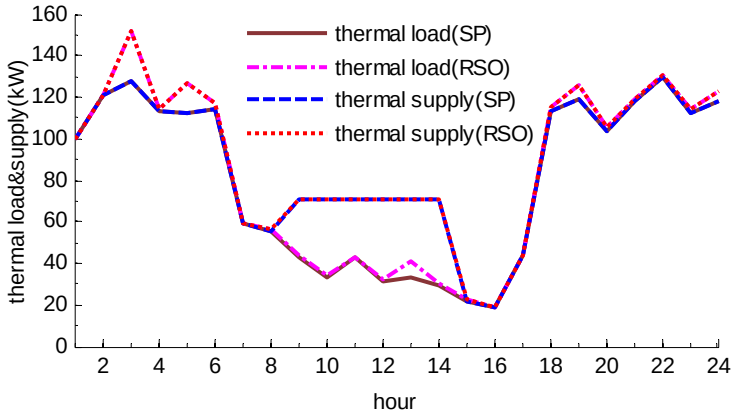


Figure 6.34 Comparison of thermal loads and supply ($S_9$: SP & RSO)



www.manaraa.com

### 6.4.3 Effectiveness of the budget of robustness

In RSO, the budget of robustness is used to adjust the individual uncertainty range of different scenarios for each uncertainty. The uncertain electric loads and solar power generation are fixed by $\Gamma_1$=2, so that the worst case for the net power demand won't be changed. The total power supply from the electric grid and battery is influenced by the power output of the CHP. The change of $\Gamma_2$ would lead to the adjustment of power output from CHP unit corresponding to the altering thermal loads. With the change of the robustness $\Gamma_2$, the uncertain feasible region for each scenario will be flexibly adjusted to protect the uncertainty. With the change of the robustness $\Gamma_2$, the uncertain feasible region for thermal loads can be flexibly adjusted to protect the uncertainty. Correspondingly, the uncertainty band for electric loads and solar power generation can also be changed through the robustness $\Gamma_1$ elastically.

Figure 6.35, Figure 6.36, the total power supply from the electric grid and battery is influenced by the power output of the CHP because the uncertain electric loads and solar power generation are fixed by $\Gamma_1$=2.

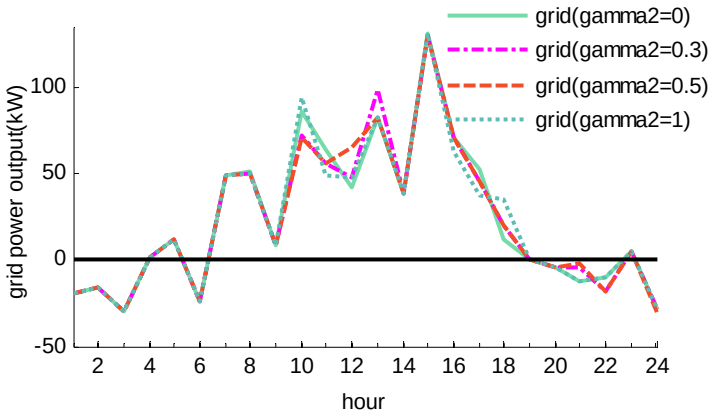


Figure 6.35 Influence of robustness on grid power supply



www.manaraa.com

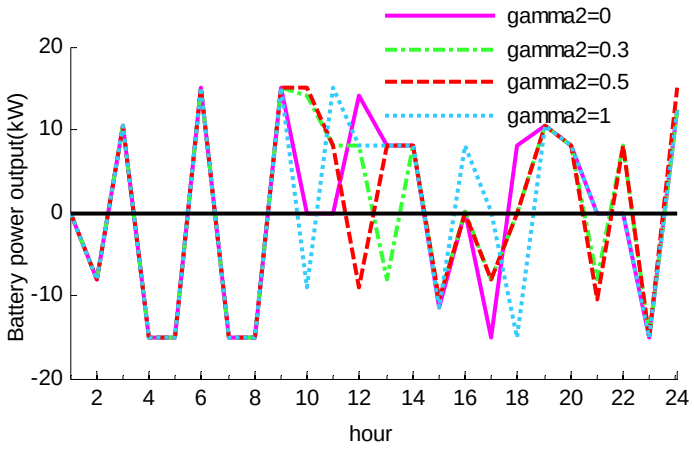


Figure 6.36 Influence of robustness on battery power supply ($S_9$)



www.manaraa.com

Table 6.5 Hours with different power output from grid & battery

| Scenarios | power output(kW) / $\Gamma_2$ | Hours with different power output from grid & battery | | | | |
|---|---|---|---|---|---|---|
| | | $H_7$ | $H_8$ | $H_{15}$ | $H_{16}$ | $H_{17}$ |
| $S_1$ | 0 | 17.3705 | 43.8894 | 91.1640 | 91.1787 | 35.9500 |
| | 0.3 | 17.2992 | 43.8753 | 91.1464 | 91.0789 | 35.7486 |
| | 0.5 | 17.2517 | 43.8659 | 91.1348 | 91.0123 | 35.6144 |
| | 1 | 17.1328 | 43.8424 | 91.1056 | 90.8459 | 35.2787 |
| $S_2$ | 0 | 28.4712 | 42.8145 | 73.8773 | 41.2148 | 76.0508 |
| | 0.3 | 28.4601 | 42.7476 | 72.6110 | 40.9571 | 75.8866 |
| | 0.5 | 28.4528 | 42.7030 | 71.7667 | 40.7853 | 75.7771 |
| | 1 | 28.4344 | 42.5914 | 69.6561 | 40.3559 | 75.5034 |
| $S_3$ | 0 | 41.4691 | 29.7973 | 80.2055 | 69.4387 | 38.8338 |
| | 0.3 | 40.9122 | 29.6251 | 80.1017 | 69.4330 | 38.4693 |
| | 0.5 | 40.5409 | 29.5103 | 80.0325 | 69.3801 | 38.2264 |
| | 1 | 39.6127 | 29.2234 | 79.8594 | 69.2476 | 37.6189 |
| $S_4$ | 0 | 23.4240 | 29.9274 | 97.7901 | $H_{17}$: 34.8984 | $H_{18}$: 17.5829 |
| | 0.3 | 21.7548 | 29.8582 | 97.6690 | 34.7804 | 17.3180 |
| | 0.5 | 27.2954 | 29.8121 | 97.5882 | 34.7018 | 17.3180 |
| | 1 | 24.5135 | 29.6968 | 97.3864 | 34.5051 | 17.3180 |
| $S_5$ | 0 | 19.6915 | 44.4057 | 105.2512 | 45.8059 | 44.5426 |
| | 0.3 | 19.2703 | 43.0991 | 105.1963 | 44.8499 | 43.8368 |
| | 0.5 | 18.9895 | 42.2280 | 105.1596 | 44.2126 | 43.3664 |
| | 1 | 18.2876 | 40.0502 | 105.0680 | 42.6193 | 42.1902 |
| $S_6$ | 0 | 31.9899 | 36.0411 | 88.5775 | 63.9414 | 34.1173 |
| | 0.3 | 31.7909 | 35.6712 | 88.5527 | 63.7173 | 33.7583 |
| | 0.5 | 31.6582 | 35.4246 | 88.5362 | 63.5678 | 33.5189 |
| | 1 | 31.3265 | 34.8081 | 88.4950 | 63.1943 | 32.9205 |
| $S_7$ | 0 | 31.0331 | 24.3262 | 80.1232 | | 20.9497 |
| | 0.3 | 30.9434 | 20.3790 | 80.0478 | | 18.5852 |
| | 0.5 | 30.8836 | 17.7475 | 79.9976 | | 17.0089 |
| | 1 | 30.7341 | 17.8221 | 79.8720 | | 13.0680 |
| $S_8$ | 0 | 30.8365 | 35.0614 | 119.8849 | 89.4895 | 48.4109 |
| | 0.3 | 30.3010 | 34.7935 | 119.7217 | 89.4552 | 48.4043 |
| | 0.5 | 29.9440 | 34.6149 | 119.6129 | 89.4323 | 48.3999 |
| | 1 | 29.0516 | 34.1684 | 119.3409 | 89.3750 | 48.3889 |
| $S_9$ | 0 | 33.9766 | 35.7120 | 119.5050 | 70.9369 | 37.3501 |
| | 0.3 | 33.8854 | 35.5839 | 119.3264 | 70.8809 | 37.1859 |
| | 0.5 | 33.8246 | 35.4985 | 119.2073 | 70.8436 | 37.0764 |
| | 1 | 33.6727 | 35.2849 | 118.9097 | 70.7503 | 36.8028 |



www.manaraa.com

It is observed from Table 6.7 that the power output from CHP increases and that from the grid and battery decreases accordingly. For other hours when the power output from CHP doesn't change with the varying budget of robustness, the boiler supplies the extra thermal loads.

From Figure 6.37, with the increase of the robustness $\Gamma_2$, the thermal loads will increase correspondingly. During hours 9-14 in Figure 6.39, the total thermal output from the CHP and boiler unit will not change with the adjustment of the robustness. The thermal output from the CHP increases with the robustness at hours 7-8&15-17 for scenarios 1-3, 5-6, 8-9, and at hours 1-8,15,17-18 for scenario 4, at hours 7-8, 15,17 for scenario 7, while the boiler will increase the thermal output with the increase of the robustness except hours 9-14 when the thermal loads are totally supplied by CHP.

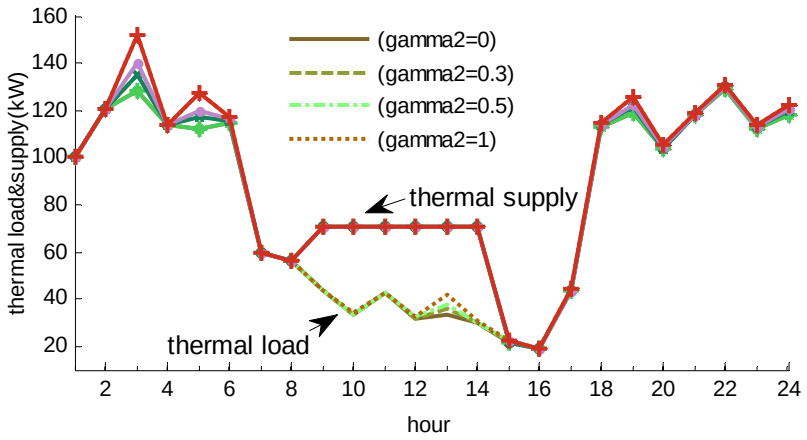


Figure 6.37 Influence of robustness on thermal loads and supply ($S_9$)



www.manaraa.com

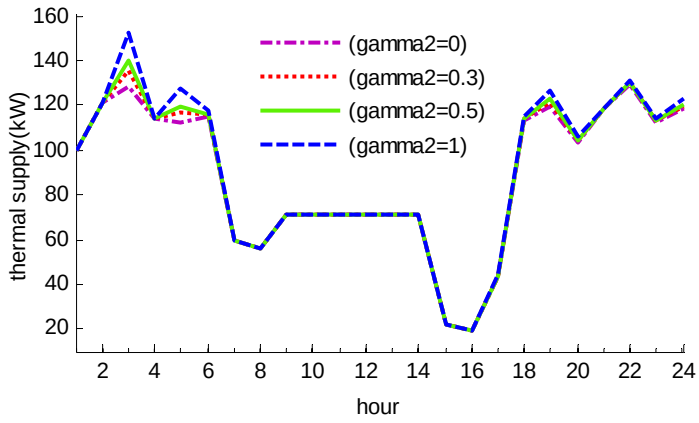


Figure 6.38 Influence of robustness on thermal supply ($S_9$)

When the boiler is out of operation during hours 7-8 and 15-17, the CHP unit takes over the extra thermal demand introduced due to the enlarging uncertainty band with the increase of $\Gamma_2$.

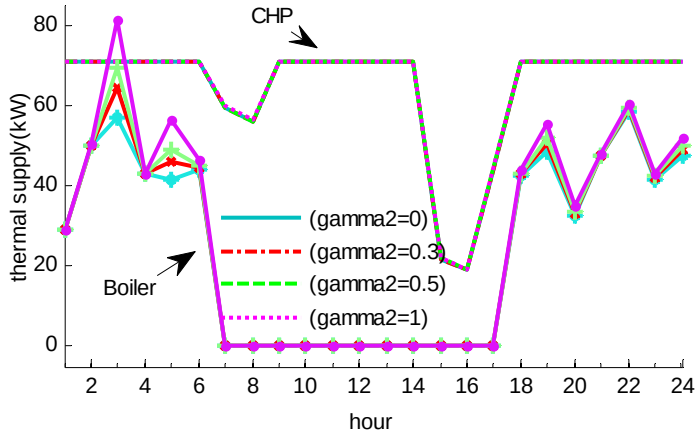


Figure 6.39 Influence of robustness on thermal supply from CHP and boiler



www.manaraa.com

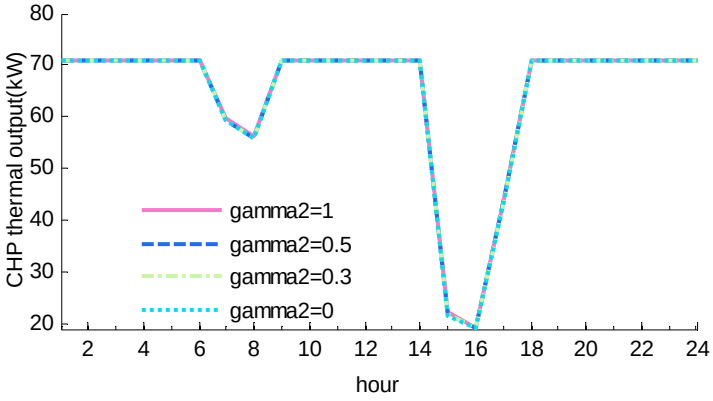


Figure 6.40 Influence of robustness on thermal supply from CHP ($S_9$)

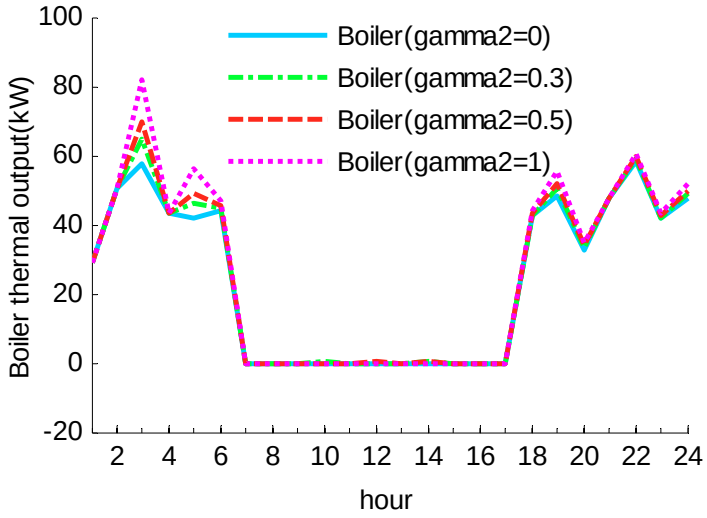


Figure 6.41 Influence of robustness on thermal supply from boiler ($S_9$)



www.manaraa.com

Table 6.6 Hours with different thermal output from CHP

| Scenarios | CHP thermal output(kW) / $\Gamma_2$ | Hours with different thermal output from CHP | | | | |
|---|---|---|---|---|---|---|
| | | $H_7$ | $H_8$ | $H_{15}$ | $H_{16}$ | $H_{17}$ |
| $S_1$ | 0 | 64.0023 | 50.0791 | 24.2932 | 19.4480 | 38.5192 |
| | 0.3 | 64.0794 | 50.0944 | 24.3122 | 19.5560 | 38.7372 |
| | 0.5 | 64.1308 | 50.1045 | 24.3248 | 19.6281 | 38.8825 |
| | 1 | 64.2594 | 50.1299 | 24.3564 | 19.8082 | 39.2457 |
| $S_2$ | 0 | 67.5551 | 50.1807 | 26.9824 | 20.1683 | 37.3344 |
| | 0.3 | 67.5670 | 50.2531 | 28.3528 | 20.4472 | 37.5121 |
| | 0.5 | 67.5750 | 50.3014 | 29.2664 | 20.6331 | 37.6306 |
| | 1 | 67.5949 | 50.4221 | 31.5504 | 21.0978 | 37.9268 |
| $S_3$ | 0 | 59.9844 | 56.6886 | 24.8161 | 16.6860 | 40.8234 |
| | 0.3 | 60.5871 | 56.8749 | 24.9285 | 16.6921 | 41.2178 |
| | 0.5 | 60.9888 | 56.9991 | 25.0034 | 16.7494 | 41.4807 |
| | 1 | 61.9933 | 57.3096 | 25.1906 | 16.8928 | 42.1381 |
| $S_4$ | 0 | 68.2818 | 50.6635 | 26.1087 | H17: 39.9722 | H18: 70.50728 |
| | 0.3 | 70.0881 | 50.7384 | 26.2398 | 40.0999 | 70.7940 |
| | 0.5 | 64.0923 | 50.7883 | 26.3272 | 40.1850 | 70.7940 |
| | 1 | 67.1028 | 50.9131 | 26.5456 | 40.3978 | 70.7940 |
| $S_5$ | 0 | 64.5165 | 40.6524 | 24.4195 | 22.0273 | 32.1955 |
| | 0.3 | 64.9723 | 42.0664 | 24.4790 | 23.0619 | 32.9592 |
| | 0.5 | 65.2762 | 43.0097 | 24.5187 | 23.7516 | 33.4683 |
| | 1 | 66.0358 | 45.3658 | 24.6178 | 25.4758 | 34.7412 |
| $S_6$ | 0 | 54.0278 | 51.1627 | 22.9375 | 17.1794 | 44.637 |
| | 0.3 | 54.2431 | 51.5630 | 22.9643 | 17.4220 | 45.0259 |
| | 0.5 | 54.3867 | 51.8299 | 22.9821 | 17.5837 | 45.2849 |
| | 1 | 54.7457 | 52.4971 | 23.0268 | 17.9879 | 45.9325 |
| $S_7$ | 0 | 67.6347 | 57.9306 | 25.5652 | | 47.2276 |
| | 0.3 | 67.7318 | 62.2022 | 25.6467 | | 49.7863 |
| | 0.5 | 67.7965 | 65.0498 | 25.7010 | | 51.4922 |
| | 1 | 67.9582 | 64.9691 | 25.8369 | | 55.7568 |
| $S_8$ | 0 | 55.4636 | 53.8314 | 23.1160 | 18.7964 | 37.2868 |
| | 0.3 | 56.04306 | 54.1214 | 23.2926 | 18.8336 | 37.2940 |
| | 0.5 | 56.4294 | 54.3146 | 23.4103 | 18.8584 | 37.2987 |
| | 1 | 57.3951 | 54.7978 | 23.7046 | 18.9203 | 37.3106 |
| $S_9$ | 0 | 59.3267 | 55.7642 | 21.6490 | 19.0442 | 43.4528 |
| | 0.3 | 59.4254 | 55.9029 | 21.8423 | 19.1047 | 43.6305 |
| | 0.5 | 59.4911 | 55.9953 | 21.9712 | 19.1451 | 43.7489 |
| | 1 | 59.6556 | 56.2264 | 22.2933 | 19.2461 | 44.0451 |



www.manaraa.com

Table 6.7 Comparison of power change in $S_9$ (kW)

| Budget of robustness ($\Gamma_2$) | Power output / Energy resource | Hour | | | | |
|---|---|---|---|---|---|---|
| | | $H_7$ | $H_8$ | $H_{15}$ | $H_{16}$ | $H_{17}$ |
| 0 | CHP | 59.33 | 55.76 | 21.65 | 19.04 | 43.45 |
| | Grid & battery | 33.98 | 35.71 | 119.51 | 70.94 | 37.35 |
| 0.3 | CHP | 59.42 | 55.90 | 21.84 | 19.10 | 43.63 |
| | Grid&battery | 33.88 | 35.58 | 119.33 | 70.88 | 37.18 |
| 0.5 | CHP | 59.49 | 55.99 | 21.97 | 19.14 | 43.75 |
| | Grid&battery | 33.82 | 35.50 | 119.21 | 70.84 | 37.08 |
| 1 | CHP | 59.65 | 56.23 | 22.29 | 19.25 | 44.04 |
| | Grid&battery | 33.67 | 35.28 | 118.91 | 70.75 | 36.80 |

## 6.5 Conclusion

In order to relieve the computational burden in power systems operations with the renewable penetration and inaccurate loads forecast, this chapter presented an innovative robust stochastic optimization model. The proposed approach not only overcomes the conservativeness in the robust model, but also circumvents the curse of dimensionality in the stochastic model. This method is different from other adaptive robust models in that it offers full adaptability for decision variables through the partition of the uncertain feasible region. Moreover, it does not require large number of scenarios but can protect uncertainties through the scenarios with each of them bearing an individual uncertainty band. The structure of the RSO model is designed to increase the adaptability while keeping the model computationally tractable. The numerical results showed the flexibility of the proposed method in dealing with uncertainty-related optimization problems.



www.manaraa.com

# CHAPTER VII

# CONCLUSION

## 7.1 Contributions

This dissertation addressed a challenging topic in smart grid-- the optimal operation of energy-efficient building with combined heat and power systems considering uncertainty from intermittent solar power generation and unpredictable energy consumption. The optimal scheduling problem is conducted specifically for individual end consumers with the goal of minimizing the daily operation cost. The scheduling of both controllable electric and thermal loads is optimized through mixed integer linear programming and could be realized through smart meters. The uncertainty modeling strategies are key to formulating different optimization models under uncertainty.

In chapter II, the optimization methods under uncertainty has been reviewed, including multi-stage stochastic programming, robust optimization. The modeling of uncertainty is also described, followed by the introduction of multivariate auto-regressive moving average time series model, which is used to forecast the daily energy consumption and solar power production.

In chapter III, in order to achieve maxima cost savings and reduce energy consumption overall, increase energy efficiency, in turn reducing emission of greenhouse gases, deterministic optimization of building energy consumption is formulated at the whole-building level to cover sub-systems such as HVAC, lighting, on-site generation



www.manaraa.com

and storage. The hybrid energy system model is proposed which consists of cogeneration system and PV solar system.

In chapter IV, the stochastic optimal operation of building energy system is investigated. Case studies are conducted including 1) the impact of CHP on energy supply. With the introducing of CHP system, the expected energy expenses could be effectively reduced by 17.6%. CHP is playing an important role in power supply through the collaborative operation with electric grid and battery. Meanwhile it cooperates with boiler unit in order to provide cost-effective thermal supply. The amount of energy production of CHP system depends on the relative price of electricity from the electric grid compared with that of natural gas. It constantly produces thermal power as much as 74 kW per hour when electricity from the grid is relatively high. Moreover, it decreases the thermal output when the thermal demand is relatively low.

2) the impact of battery on energy supply from CHP system and electric grid. The operation of battery would influence the power output from electric grid, but have no impact on power output from CHP system since it is determined by the thermal demand. The operation of battery could reduce the expected energy cost by 1.5%.

3) the operation of interruptible electric loads is influenced by electricity price. The consideration of interruptible electric loads increases the expected daily operation cost by 5.6% compared with the case without interruptible electric loads. Power supply from CHP system is not changed. Both the power output from electric grid and battery would be changed accordingly in order to meet the extra operation requirement for interruptible electric loads.



www.manaraa.com

4) the operation of interruptible thermal loads would increase the expected daily operation cost by 3.2% compared with the case without interruptible thermal loads. The scheduling of interruptible thermal loads is influenced by both electricity price and natural gas price. The maximum thermal output from the CHP unit decreases from 74.1 kW per hour to 70.8 kW per hour, while the boiler unit increases its maximum thermal output from under 50 kW per hour to above 100 kW per hour to fulfill the operation requirement for interruptible thermal loads.

Meanwhile, this chapter presented a very interesting hybrid approach combining multi-stage stochastic programming and rolling scheduling method for the optimal operation of energy-efficient buildings. This chapter successfully applied the hybrid approach to the optimal operation of energy-efficient building systems.

In chapter V, the robust formulation of the optimal operation of building energy systems was proposed with the consideration of uncertainty from electric and thermal loads, as well as solar power production. Case studies are conducted including 1) the influence of uncertain electric grid and solar power generation. The uncertainty in electric loads increases the daily cost by 4.98%, while the consideration of uncertainty in both electric loads and solar power would increase the daily cost by 12.13%.

2) The effect of battery in risk alleviation of energy supply against uncertainty. The total operating cost is reduced by 3.69% in deterministic case and by 3.23% in robust case. It shows that the battery is effective in coordinating with the electric grid to meet the uncertain power demand.

3) The influence of CHP system. Due to the response of the CHP to both uncertain electric and thermal energy requests, the total operating cost is reduced by



www.manaraa.com

18.38% in deterministic case and by 17.08% in robust case. It is reported that the CHP is effective in coordinating with the grid and battery in supplying uncertain power demand. Meanwhile, the CHP is also an economic way to meet the uncertain power demand.

4) The adjustment of robustness. The daily operation cost would be changed with the adjustment of the robustness parameter. When no protection is taken against uncertainties in the electric loads and solar power generation, the operation cost reaches $ 172.3 per day. When the protection against uncertainties in the electric loads and solar power generation are fully ensured, the operation cost reaches $ 195.6 per day, increased by 13.52%.

In chapter VI, the novel robust stochastic method was proposed to solve the curse of dimension problem in stochastic programming, overcoming the conservativeness of robust optimization at the same time. The proposed approach offers flexible adaptability for decision variables through the adjustable multiband uncertainty on the basis of the multi-stage scenario tree. The generated formulas can either be flexibly adapted to the particular instance of multi-stage SP when the individual uncertainty band shrinks to empty; or drop to the category of RO when no more than one scenario is considered. The proposed framework is at least as adaptive as SP, or as robust as RO. With fewer scenarios than in SP, the RSO approach takes into account all possible outcomes of uncertainties by considering the uncertainty sub-band for each scenario. Therefore, it is more robust than SP which merely considers the exact discrete scenarios. Meanwhile, it's more flexible than the RO as the decision variables can be adapted to the stochastic process of uncertainties in the structure of multi-stage scenario tree. It would be superior



www.manaraa.com

to a substitution of the random parameters by single worst estimates as in RO or discretized scenarios as in SP.

## 7.2 Suggestions for Further research

Based on the research work conducted in this dissertation, potential research focus could be in the following areas:

- Incorporate the price-responsive demand response into the optimal operation of building systems by taking into account of the elastic price information.
- Consider the consumers' comfort in the building with the application of thermostat devices.
- Apply the stochastic and robust optimization method to other power system related optimization problem, such as power flow, state estimation, security constrained unit commitment, system-of-system based power issues.
- Optimization of energy consumption at multi-building level is important in the future since micro-grid is widely developed in the world where on-site generation and co-generation can supply efficient energy for the multi-building system.
- Advanced decomposition algorithm is essential to solve the optimization problem of building energy system with disturbance from occupants' activities, price of electricity and other primary sources of energy, and outdoor weather conditions.



www.manaraa.com

REFERENCES


[1] Z. Zhu, J. Tang, S. Lambotharan, W. Chin, and Z. Fan, "An Integer Linear Programming Based Optimization for Home Demand-Side Management in Smart Grid," Innovative Smart Grid Technologies (ISGT), Jan. 2012, Washington, DC.

[2] Green Life Energy Solutions LLP, "Solar PV Rooftop Solutions," available at http://www.gles.in/solarpvrooftopsolution.html

[3] K. F. Rautenbach, "Characterization of a solar roof tile (SunSlates$^{TM}$)," Master thesis, University of Stellenbosch, Dec. 2008.

[4] Mississippi Cooling, Heating, and Power (micro-CHP) and Bio-fuel Center, "Micro-Cooling, Heating, and Power (m-CHP) Instructional Module," Supported by United States Department of Energy, 2005.

[5] S. Boljevic and B. Noel, "Impact of Combined Heat and Power Plant on Thermal and Electrical Energy Supply for Small and Medium Size Enterprises, " 42nd International Univ. Eng. Conf. *(*UPEC*)*, pp. 35-39, Brighton, UK, Sep. 2007.

[6] R. Jablko, C. Saniter, R. Hanitsch, and S. Holler, "Technical and Economical Comparison of micro CHP systems," Intl. Conf. on Future Power systems, pp. 1-6, Nov. 2005.

[7] S. M. Sadeghzadeh, "An Integrated Method for Decentralized Combined Heat and Power Planning," IEEE EUROCON Conf., pp. 486-493, 2009, St.–Petersburg, Russia.

[8] U.S. Combined Heat and Power Association, "National CHP Roadmap: Doubling Combined Heat and Power Capacity in the United States by 2010," Washington, D.C., USA, 1998.

[9] A. Rong and R. Lahdelma, "Optimal Operation of Combined Heat and Power Based Power Systems in Liberalized Power Markets," available at http://www.eolss.net/Sample-Chapters/C05/E6-39-14-00.pdf, 2013.

[10] L. Perez-Lombard, J. Ortiz, and C. Pout, "A Review on Buildings Energy Consumption Information," Energy and Buildings, vol. 40, no. 3, pp, 394-398, 2008.




www.manaraa.com

[11] S. Herzog, D. Atabay, H. Jungwirth, and V. Mikulovic, "Self-Adapting Building Models for Model Predictive Control," *13th Conf. of Intl. Building Performance Simulation Association*, Chambery, France, Aug. 2013.

[12] J. F. Martins, J. A. Oliveira-Lima, V. Delgado-Gomes, R. Lopes, D. Silva, S. Vieira, and C. Lima, "Smart Homes and Smart Buildings," 13th Biennial Baltic Electronics Conf. (BEC), Tallinn, Estonia, Oct. 3-5, 2012.

[13] V. Hartkopf, V. Loftness, A. Mahdavi, S. Lee, and J. Shankavaram, "An Integrated Approach to Design and Engineering of Intelligent Buildings-The Intelligent Workplace at Carnegie Mellon University," Automation in Construction, vol. 6, pp, 401-415, 1997.

[14] A. Mohamed and M. T. Khan, "A Review of Electrical Energy Management Techniques: Supply and Consumer Side (Industries)," Journal of Energy in Southern Africa, vol. 20, no. 3, Aug. 2009, pp, 14-21, available at http://www.erc.uct.ac.za/jesa/volume20/20-3jesa-mohamed.pdf

[15] A. Zipperer, P. A. Aloise-Young, S. Suryanarayanan, D. Zimmerle, R. Roche, L. Earle, D. Christensen, and P. Bauleo, "Electric Energy Management in the Smart Home: Perspectives on Enabling Technologies and Consumer Behavior, " Proceedings of the IEEE, Aug. 2013.

[16] D. Sheflin and J. Eaton, "Energy Efficiency and Smart Grid: Discussion Topics, " Honeywell, December, 2010.

[17] T. T. Kim and H. V. Poor, "Scheduling Power Consumption with Price Uncertainty," IEEE Trans. on smart grid, vol. 2, no. 3, Sep. 2011, pp, 519-527.

[18] M. Rahimiyan, L. Baringo, and A. J. Conejo, "Energy Management of A Cluster of Interconnected Price-Responsive Demands, " IEEE Trans. on Power Systems, vol. 29, no. 2, pp, 645-655, March 2014.

[19] Hai-Yun Helen Xing, "Building Load Control and Optimization," Doctor Dissertation, Massachusetts Institute of Technology (MIT), 2004.

[20] Z. Chen, L. Wu, and Y. Fu, "Real-Time Price-Based Demand Response Management for Residential Appliances via Stochastic and Robust Optimization," IEEE Trans. on Smart Grid, vol. 3, no. 4, pp. 1822-1831, Dec. 2012.

[21] P. Du and N. Lu, "Appliance Commitment for Household Load Scheduling," IEEE Trans. on Smart Grid, Vol. 2, No. 2, pp, 411-419, June 2011.

[22] P. Samadi, H. Mohsenian-Rad, Vincent W. S. Wong, and R. Schober, "Tackling The Load Uncertainty Challenges for Energy Consumption Scheduling in Smart Grid," IEEE Trans. on Smart Grid, vol. 4, no. 2, pp, 1007-1016, June 2013.



www.manaraa.com

[23] X. Guan, Z. Xu, and Q. Jia, "Energy-Efficient Buildings Facilitated by Microgrid," IEEE Trans. on Smart Grid, Vol. 1, No. 3, pp. 243-252, Dec. 2010.

[24] B. Sun, P. B. Luh, Q. Jia, Z. Jiang, F. Wang, and C. Song, "An Integrated Control of Shading Blinds, Natural Ventilation, and HVAC Systems for Energy Saving and Human Comfort," 6th annual IEEE Conf. on Automation Science and Engineering, Toronto, Ontario, Canada, Aug. 21-24, 2010.

[25] C. Chang, W. Fu, "Stochastic Multi-objective Generation Dispatch of Combined Heat and Power Systems," IEE Proc.-Gener. Trans. Distr., Vol. 145, No. 5, September 1998.

[26] U.S. Department of Energy, "Benefits of Demand Response in Electricity Markets and Recommendations for Achieving Them," A Report to the United States Congress, Feb. 2006.

[27] M. Muratori, B. A. Schuelke-Leech, G. Rizzoni, "Role of Residential Demand Response in Modern Electricity Markets," Renewable and Sustainable Energy Reviews, vol. 33, pp, 546-553, 2014.

[28] K. Dietrich, J. M. Latorre, L. Olmos, A. Ramos, "Demand Response and Its Sensitivity to Participation Rates and Elasticities," 8th International Conf. on the European Energy Market (EEM), pp, 711-716, May 25-27, 2011, Zagreb, Croatia.

[29] L. Xie (project leader), "Quantifying Benefits of Demand Response and Look-ahead Dispatch in Systems with Variable Resources (Markets Project M-26)," PSERC report, Sep. 2013.

[30] K. Dietrich, J. M. Latorre, L. Olmos, and A. Ramos, "Demand Response in An Isolated System with High Wind Integration," IEEE Trans. on Power systems, vol. 27, No. 1, pp, 20-29, Feb. 2012.

[31] T. Weng, B. Balaji, S. Dutta, R. Gupta, and Y. Agarwal, "Managing Plug-Loads for Demand Response within Buildings," Proceedings of the Third ACM Workshop on Embedded Sensing Systems for Energy-Efficiency in Buildings (BuildSys '11), pp, 13-18, 2011.

[32] C. Zhao, J. Wang, J. P. Watson, and Y. Guan, "Multi-Stage Robust Unit Commitment Considering Wind and Demand Response Uncertainties," IEEE Trans. on Power Systems, vol. 28, no. 3, pp, 2708-2717, Aug. 2013.

[33] L. Qian, Y. Zhang, J. Huang, and Y. Wu, "Demand Response Management Via Real-Time Electricity Price Control in Smart Grids," IEEE Journal on Selected Areas in Communications, vol. 31, no. 7, pp, 1268-1280, Jul. 2013.



www.manaraa.com

[34] D. Li, S. K. Jayaweera, O. Lavrova, and R. Jordan, "Load Management for Price-Based Demand Response Scheduling-A Block Scheduling Model," Jan. 2011, available at http://www.ece.unm.edu/cisl/publication/SGC/conf_2011_04_01.pdf

[35] N. Li, L. Chen, and S. H. Low, "Optimal Demand Response Based on Utility Maximization in Power Networks," IEEE Power and Energy Society General Meeting, San Diego, CA, July 24-29, 2011.

[36] M. Alizadeh, Y. Xiao, A. Scaglione, M. Van Der Schaar, "Incentive Design for Direct Load Control Programs," Oct. 2013. Available at http://arxiv.org/pdf/1310.0402.pdf

[37] William W. Hogan, "Providing Incentives for Efficient Demand Response," Oct. 29, 2009, available at http://www.hks.harvard.edu/fs/whogan/Hogan_Demand_Response_102909.pdf

[38] Public Utility Commission, "Demand Response Programs for Oregon Utilities," May 2003. Available at http://www.nwcouncil.org/media/4523/drrptfin.pdf

[39] F. A. Wolak, "Residential Customer Response to Real-Time Pricing: The Anaheim Critical-Peak Pricing Experiment," May 24, 2006. Available at http://web.stanford.edu/group/fwolak/cgi-bin/sites/default/files/files/Residential%20Customer%20Response%20to%20Real-Time%20Pricing,%20The%20Anaheim%20Critical-Peak%20Pricing%20Experiment_May%202006_Wolak.pdf

[40] "ComEd RRTP Program Overview," ComEd, 2012, available at https://rrtp.comed.com/about/

[41] Casey Laughman (ed), "2 FM Quick Reads on Demand-Response," Building Operating Management, available at http://www.facilitiesnet.com/facilitiesmanagement/tip/The-Risks-and-Benefits-of-DemandResponse-Programs--23122

[42] United States Government Accountability Office (GAO), "Consumers Could Benefit from Demand Programs, But Challenges Remain," Electricity Markets, Aug. 2004, available at http://www.gao.gov/assets/250/243580.pdf .

[43] Federal Energy Regulatory Commission, "Assessment of Demand Response & Advanced Metering," Staff Report, Aug. 2006, revised Dec. 2008, available at http://www.ferc.gov/legal/staff-reports/demand-response.pdf

[44] PJM Interconnecion, "2012 Economic Demand Response Performance Report: Analysis of Economic DR Participation in the PJM Wholesale Energy Market After The Implementation of Order 745," available at http://www.pjm.com/~/media/markets-ops/dsr/economic-dr-performance-report-analysis-of-activity-after-implementation-of-745.ashx



www.manaraa.com

[45] "Real-time hourly prices in The ComEd Residential Real Time Pricing (RRTP) program," available at https://rrtp.comed.com/live-prices/?date=20140910

[46] "5 minute pricing in The ComEd Residential Real Time Pricing (RRTP) program," available at https://rrtp.comed.com/live-prices/five-minute-prices/

[47] J. R. Birge and Francois Louveaux, "Introduction to Stochastic Programming," New York: Springer-Verlag, 2011.

[48] S. W. Wallace and W. T. Ziemba (eds.), "Applications of Stochastic Programming," SIAM Mathematical Programming Series on Optimization, SIAM, Philadelphia, 2005.

[49] G. Barbarosoglu and Y. Arda, "A Two-Stage Stochastic Programming Framework for Transportation Planning in Disaster Response," Journal of the Operational Research Society, vol. 55, pp, 43-53, 2004.

[50] D. Barro and E. Canestrelli, "A Decomposition Approach in Multistage Stochastic Programming," available at http://www.unive.it/media/allegato/DIP/Economia/Rendiconti-ex-matematica-app/rendiconti-2005/Barro-Canestrelli.pdf

[51] Willem K. Klein Haneveld, "Chapter 3: Duality in Stochastic Linear and Dynamic Programming, " vol. 274 of lecture notes in Econ. and Math. Systems, 1986.

[52] C. C. Caroe and R. Schultz, "Dual Decomposition in Stochastic Integer Programming," Operations Research Letters, vol. 24, no. 1-2, pp, 37-45, Feb. 1999.

[53] A. M. Alonso and C. Garcia-Martos, "Time Series Analysis: Forecasting with ARIMA Models, " Jun.-Jul. 2012, available at http://www.etsii.upm.es/ingor/estadistica/Carol/TSAtema7petten.pdf .

[54] J. Contreras, R. Espinola, F. J. Nogales, and A. J. Conejo, "ARIMA Models to Predict Next-Day Electricity Prices, " IEEE Trans. on Power Systems, vol. 18, No. 3, pp, 1014-1020, Aug. 2003.

[55] F. J. Nogales, J. Contreras, A. J. Conejo, and R. Espinola, "Forecasting Next-Day Electricity Prices by Time Series Models, " IEEE Trans. on Power System, vol. 17, no. 2, pp, 342-348, May 2002.

[56] G. Gross and F. D. Galiana, "Short-Term Load Forecasting, " Proc. IEEE, vol. 75, no. 12, pp. 1558–1573, Dec. 1987.

[57] M. T. Hagan and S. M. Behr, "The Time Series Approach to Short Term Load Forecasting, " IEEE Trans. on Power System, vol. 2, pp. 785–791, Aug. 1987.



www.manaraa.com

[58] Giebel, G., Brownsword, R., and Kariniotakis, G., 2003, "The State-of-the-art in Short-Term Prediction of Wind Power, A Literature Overview," Project Anemos, Contract No. ENK5-CT-2002-00665, http://anemos.cma.fr

[59] G. Kariniotakis, P. Pinson, N. Siebert, G. Giebel, and R. Barthelmie, "The State of the Art in Short-Term Prediction of Wind Power: A Literature Overview," 2004, available at http://www.risoe.dk/rispubl/VEA/veapdf/ANEMOS_giebel.pdf

[60] L. Soder, "Simulation of Wind Speed Forecast Errors for Operation Planning of Multi-Area Power Systems, " 8th Intl. Conf. on Probabilistic Methods Applied to Power Systems, Iowa State Univ., Iowa, Sep. 2004.

[61] A. Boone, "Simulation of Short-term Wind Speed Forecast Errors Using a Multi-variable ARMA (1,1) Time-series Model", Master Thesis, Royal Institute of Technology, Sweden, 2005.

[62] F. Furini, M. Laguna, and M. Samorani, "Minimax Robust Unit Commitment Problem with Demand and Market Price Uncertainty, " Oct. 19, 2012, available at http://www.optimization-online.org/DB_HTML/2012/10/3646.html

[63] N. Menemenlis, M. Huneault, and A. Robitaille, "Thoughts on Power System Flexibility Quantification for the Short-Term Horizon," IEEE Power and Energy Society General Meeting. pp. 1-8, 2011.

[64] R. Barth, L. Soder, C. Weber, H. Brand, and D. J. Swider, "Methodology of the Scenario Tree Tool," Institute of Energy Economics and the Rational Use of Energy, University of Stuttgart, Jan. 2006.

[65] A. Ben-Tal, A. Goryashko, E. Guslitzer, and A. Nemirovski. "Adjustable Robust Solutions of Uncertain Linear Programs," Math Program Ser A, Vol. 99, pp, 351-376, 2004.

[66] A. Ben-Tal, L. EI Ghaoui, and A. Nemirovski, "Robust Optimization," Princeton University Press, 2009.

[67] R. Jiang, J. Wang, and Y. Guan, "Robust Unit Commitment with Wind Power and Pumped Storage Hydro," IEEE Trans. on Power Systems, vol. 27, no. 2, pp, 800-810, 2012.

[68] D. Bertsimas, E. Litvinov, X. Sun, J. Zhao, and T. Zhen, "Adaptive Robust Optimization for the Security Constrained Unit Commit Problem," IEEE Trans. on Power Systems, Vol. 28, No. 1, pp, 52-63, 2013.

[69] M. Hoffman, T. U. Daim, "Building Energy Efficiency Technology Roadmaps: A Case of Bonneville Power Administration (BPA),"Technology Management for the Global Future (PICMET), vol. 3, pp, 1503-1527, July 2006.



www.manaraa.com

[70] D. P. Kaundinya, P. Balachandra, and N. H. Ravindranath, "Grid-Connected Versus Stand-Alone Energy Systems for Decentralized Power-A Review of Literature," Renewable and Sustainable Energy Reviews, vol. 13, pp, 2041-2050, 2009.

[71] World Bank, "District Energy- A Smart Option for Cities," May 29, 2013, available at blogs.worldbank.org

[72] M. A. Eltawil and Z. Zhao, "Grid-Connected Photovoltaic Power Systems: Technical and Potential Problems- a Review, " Renewable and Sustainable Energy Reviews, vol. 14, pp, 112-129, 2010.

[73] I. A. H. Haris, "Grid-Connected and Building Integrated Photovoltaic: Application Status & Prospect for Malaysia, " available at http://www.mbam.org.my/mbam/images/MBJ3Q06%28pdf%29/@BIPVHadri.pdf

[74] S. Chowdhury, M. Al-Amin, S. Sanjari, S. Tasnim, and M. Ahmad, "Performance Parameter Analysis of Grid Connected Building Integrated Photovoltaic Application in Bangladesh," IEEE Intl. Conf. on Informatics, Electronics & Vision (ICIEV), pp, 870-875, May 18-19, 2012, Dhaka.

[75] B. Fry, "Simulation of Grid-Tied Building Integrated Photovoltaic Systems," Master's Thesis, University of Wisconsin-Madison, 1998.

[76] U.S. Department of Energy (DOE), "Buildings Share of U.S. Primary Energy Consumption, "available at http://buildingsdatabook.eren.doe.gov/TableView.aspx?table=1.1.3

[77] Z. Ma and S. Wang, "Building energy research in Hong Kong: A Review, " Renewable and Sustainable Energy Reviews, Vol. 13, Issue 8, pp. 1870-1883, Oct. 2009.

[78] J. L. Snowdon, "IBM Smarter Energy Management Systems for Intelligent Buildings," Jun. 2009, available at http://citris-uc.org/files/Snowden%20IBM%20Research%20061009.pdf.

[79] H. Michaels and K. Donnelly, "Architecting the Consumer Side of the Grid for Energy Efficiency," MIT-IPC-Energy innovation working paper 11-003, Jun. 30, 2011, available at web.mit.edu/ipc/www.

[80] L. Kuznia, B. Zeng, G. Centeno, and Z. Miao, "Stochastic Optimization for Power System Configuration with Renewable Energy in Remote Areas", Annals of Operations Research, March 2012.

[81] C. Abbey and G. Joos, "A Stochastic Optimization Approach to Rating of Energy Storage Systems in Wind-Diesel Isolated Grids," IEEE Trans. on Power Systems, Vol. 24, No. 1, Feb. 2009.



www.manaraa.com

[82] J. kondoh, "A Direct Load Management Scheme to Control Appliances and EVs While Considering End Users Comfort, " Grid-Interop, Nov. 17-19, 2009, Denver, CO, available at http://www.gridwiseac.org/pdfs/forum_papers09/kondoh.pdf

[83] J. Wong, Y. S. Lim, J. Tang, and E. Morris, "Grid-Connected Photovoltaic System in Malaysia: A Review, " Renewable and Sustainable Energy Reviews, Vol. 29, pp, 535-545, 2014.

[84] M. Prodanovic, T.Gafurov, and M.B.Tellez, "A Demand Based Approach to Optimization of Energy Supply Mix for Smart Buildings," Proc. Innovative Smart Grid Tech., Washington, D.C., USA, 2012.

[85] P. Meibom, H. V. Larsen, R. Barth, H. Brand, C. Weber, and O. Woll, "WILMAR Joint Market Model, Documentation," Riso National Lab., Denmark, Jan. 2006.



www.manaraa.com